INVESTIGATION INTO THE IMPROVEMENT OF MOS_2 FUNCTIONALIZATION, SMALL MOLECULE TRANSISTORS, AND 2D PEROVSKITES

ELIZABETH AUDREY KEENAN

A dissertation submitted to the faculty at the University of North Carolina at Chapel Hill in partial fulfillment of the requirements for the degree of Doctor of Philosophy in the Department of Chemistry.

Chapel Hill
2018

Approved By:

Wei You

Scott Warren

Frank Leibfarth

Joanna Atkin

Matthew Lockett

ABSTRACT

Elizabeth Audrey Keenan: Investigation into the improvement of MoS_2 functionalization, Small Molecule Transistors, and 2D Perovskites
(Under the direction of Wei You)

Many types of materials make up the world, and one subset of these materials are colloquially called 2D. This dissertation encompasses a range of very thin materials and looks for ways to study their properties. First, a functionalization method for MoS_2 is presented. By using chemical vapor deposition, MoS_2 is able to be functionalized with various organic monolayers that do not harm the underlying electronic properties. Next, a study is presented on how new derivatives of TES-ADT can be used in OFETs. By working on improving the film quality, the electronic properties of these materials can be improved. Lastly, a different method for the preparation of 2D mixed perovskites is presented. Using the melt infiltration approach, different layer numbers of mixed perovskites can be prepared. This approach gives a way to look at and study the formation of mixed perovskites over time.

TABLE OF CONTENTS

LIST OF FIGURES

LIST OF TABLES

Chapter 1: Thin Film Materials

The electronic world is booming. The size of a typical electronic device has shrunk from the size of a room to something that can fit in your hand in the span of decades. One reason that our world has been able to achieve this great feat is the power of computers has consistently increased over the past 50 years. This gradual increase was predicted all the way back in 1965 by Gordon E. Moore, and is commonly known as Moore's Law. He predicted this increase in power would give rise to "handy home computers" that would be available to the public and that could perform typically laborious functions with ease. Obviously, Moore's prediction was right and we now have powerful computers at our fingertips at all times. Specifically, Moore predicted that the amount of components in an integrated circuit would keep doubling about every 18 months, while things like that size of the circuit and the cost of the circuit would decrease.[1]

Amazingly, this prediction has also held up over time, with computer processors now having billions of components on an integrated circuit. But, even Moore knew that this scientific advancement would take a lot of work from scientists and engineers for generations to come. For example, in order to keep making electrical components like transistors smaller and smaller, a basic understanding of how molecules and materials interact on a microscopic is always necessary. With all the new technological advances in recent history, it is important to take a step back and focus on why electronic materials behave like they do. This question can

help researchers realize how materials can be altered for different purposes and help to expand the knowledge known about all electronic materials.

Organic and Inorganic Semiconducting Materials

Electronic materials can be classified in many different ways based on their atomic makeup (organic, inorganic), their size (2D materials, thin film materials), and their conductivity (semiconductor, metal). Each different material can serve a different purpose but oftentimes different materials compete to serve the same purpose.

2D Materials

Two-dimensional (2D) materials are known for their very small thickness, around 1-2 nm, and for their interesting properties as they are shrunk down into very thin layers. 2D materials are unique because many 2D materials do not behave the same as their bulk material counterparts. The most well-known 2D materials of this century is graphene. Graphene is a 2D material because it consists of a single layer of carbon 1 atom thick. In 2010, Andre Geim and Konstantin Nososelov won the Noble Prize in Physics for their groundbreaking work on two-dimensional graphene (cite). Graphene is a thin, transparent, conductive material that is also very strong and stretchable. Their work on graphene, along with an increased interest from the research community, lead to a race to find and study other 2D materials. One such category of 2D materials is transition metal dichalcogenides (TMDs). This includes materials such as MoS_2, WS_2, and $MoSe_2$.

Even though a vast amount of academic research has gone into graphene, MoS_2 and other 2D materials over the past 10 years, there are still no large commercial products that use

these materials.[2] In order to broaden the potential applications of 2D materials, it is important to understand how the materials can be manipulated.

Organic Semiconductors

Organic semiconducting materials have often been overshadowed by inorganic electronic devices, which are generally more powerful and are more widespread in the electronic devices of today. Even though organic electronics are sometimes seen as the underdog, they still have an important place in many applications. In 2000, the Nobel Prize in Chemistry was given to Alan J. Heeger, Alan G. MacDiarmid, and Hideki Shirakawa for their discovery that plastics (mainly polymers) can be made into electrically conductive materials.[3] This cemented the fact that organic semiconductors have a future in modern electronics and that time and resources need to go into the study and development of organic semiconducting materials.

Over 17 years later, organic semiconductors have a role in everyday life. For example, you can go to Best Buy and buy a TV made with organic light emitting diodes (OLED). Yes, it is very expensive but so were personal computers when they first entered the market. Organic photovoltaics (OPVs) have reached efficiencies as high as 11.5% in recent years (**Figure 1.1**). Even though this is a lower efficiency than the more common single crystalline silicon (25.3%), OPVs are generally more lightweight and cheaper to process compared to silicon photovoltaics. Lastly, organic field-effect transistors (OFETs) have many promising applications in the modern world. For example, their flexibility makes them a good candidate for wearable electronic devices and for chemical and biological sensors.[4] For all these applications, new materials and

better understanding of organic semiconductors will help drive commercial success of these products and lead to the integration of organic semiconductors in everyday life.

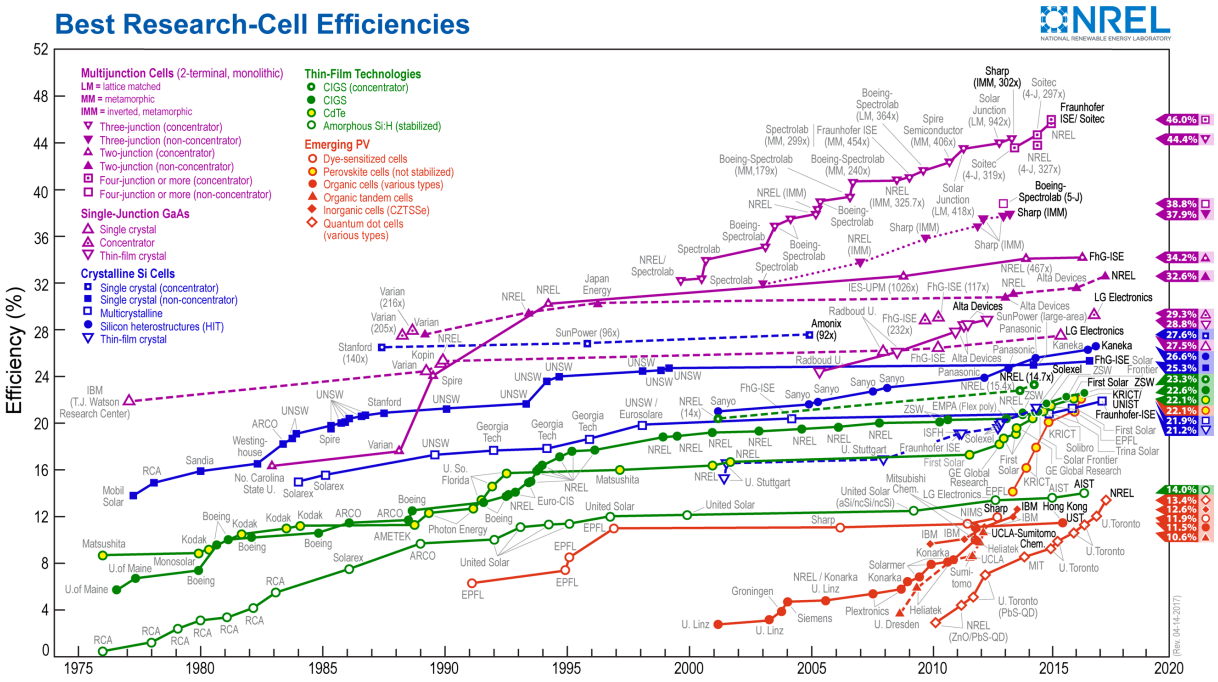

Figure 1.1: Historic Solar Cell Efficiencies

This graph shows how the efficiency of solar cells has been increasing over time. Specifically, the efficiency of perovskite cells has drastically increased in only a few years. This plot is courtesy of the National Renewable Energy Laboratory, Golden, CO.

Organic-Inorganic Hybrid Perovskites

In the world of solar cells, no other material has improved in efficiency as quickly as organic-inorganic hybrid perovskites. The most common perovskite solar cell, based on the methylammonium lead iodide ($MAPbI_3$) perovskite, has gone from an efficiency of a few percent to over 22.1% in the matter of years (**Figure 1.1**). Because of this, perovskites have garnered much interest in the research community. The problem with making perovskite solar cells is that the perovskite material is not very stable in the long term when exposed to air, water, and light. Therefore, studying the properties of $MAPbI_3$ perovskites as well as other perovskite compositions will help to overcome this obstacle.

Dissertation Overview

This dissertation will focus on the characterization and understanding of both inorganic and organic materials on a microscopic level. Studying how materials interact with one another helps to elucidate why materials behave as they do. Herein, I will discuss three separate thin film electronic materials. First, I will present the functionalization of thin film MoS_2 with organic molecules and the mechanism of functionalization. Second, I will present the electronic properties of new derivatives of a common organic electronic material, TES-ADT. Lastly, I will discuss a non-conventional method to fabricate mixed cation organic-inorganic hybrid perovskites and how this method helps to study how the different components of mixed perovskites interact and how to control film formation.

REFERENCES

(1) Moore, G. E. Creaming More Components onto Integrated Circuits. *Electronics* **1965**, *38* (8), 114–117.

(2) Park, S. The Puzzle of Graphene Commercialization. *Nat. Rev. Mater.* **2016**, *1* (11), 16085.

(3) The Royal Swedish Academy of Sciences. The Nobel Prize in Chemistry 2000 https://www.nobelprize.org/nobel_prizes/chemistry/laureates/2000/press.html.

(4) Zaki, T. Short-Channel Organic Thin-Film Transistors. **2015**, 5–32.

Chapter 2: Surface Functionalization of Molybdenum Disulfide with Organic Molecules by Chemical Vapor Deposition

Transition metal dichalcogenides (TMDs) have emerged as one of the leading groups of two-dimensional (2D) materials because of their fascinating electronic and optical properties.[1] One such material, molybdenum disulfide (MoS_2), is of particular interest because of its transition from an indirect (1.2 eV) to direct (1.8 eV) band gap material as it changes from bulk to monolayer form.[2] Furthermore, it has been reported that monolayer MoS_2 based field-effect transistors can produce high mobility (~200 $cm^2/(V\ s)$) and good on/off current ratios (>10^7).[3] Thus, MoS_2 has been studied for use in applications such as transistors,[4] sensors,[5] phot ovolatics,[6] and spintronics[7]. For example, with its thinness, flexibility, and good electronic properties, MoS_2 is an ideal candidate for future biological technology applications, such as the detection of biomolecules,[8] where silicon based electronic devices currently dominate but lack the flexibility that MoS_2 electronic devices could provide. Typically, such biological arrays use silicon surfaces functionalized with aminosilane molecules to facilitate the immobilization of biologically active molecules. Being able to mirror this procedure to MoS_2 requires the ability to covalently functionalize the surface of MoS_2. Recent reviews of 2D material functionalization have shown the interest and the potential for greater understanding of different ways to functionalization MoS_2 and it's possible applications[9–11].

With the great potential for use of MoS_2 in many different areas, there is a need to discover new ways to alter its electronic and optical properties, as well as improve its

versatility. One possibility to do this is to chemically modify the surface of MoS_2. Herein, I present a versatile method to functionalize the surface of MoS_2 with an organic molecule. In order to do this successfully, a few crucial steps are needed. This entails first developing a method to deposit an organic molecule, specifically an organosilane, on the surface of MoS_2. Then, it is necessary to study how this molecule effects the properties of MoS_2. Finally, a bonding motif is presented.

Molybdenum Disulfide Background

While applications for bulk MoS_2 have been around for decades[12–14], the discovery of the interesting properties of MoS_2 as the layer number is decreased is more recent. In 2010, Mak, et. al. reported how the optical and electronic properties of MoS_2 change with decreasing thickness.[2] In doing so, they outlined a few important intrinsic properties of monolayer MoS_2. This sparked a boom in the interest of MoS_2 and other thin film TMDs. Following, I will outline the basic structure and properties of thin layer MoS_2, along with preparation techniques.

Structure of MoS_2

A monolayer of MoS_2 consists of three atomic layers: a hexagonal layer of molybdenum sandwiched between two hexagonal layers of sulfur. Each molybdenum is covalently bonded to six sulfur atoms and the crystal structure has two possible phases. The first phase is referred to as 2H and the atoms are in a trigonal prismatic structure. This phase is the thermodynamically favored phase and is most common. The second phase is the 1T phase, where the atoms are arranged in an octahedral structure. This work only deals with the 2H phase, because it is the more thermodynamically stable phase.

Bulk MoS_2 consists of many of these layers stacked upon each other which are held together by weak van der Waals interactions between S atoms. Since van der Waals forces are weaker than the covalent bonds that hold together a monolayer, the bulk material is easily exfoliated into monolayers. A monolayer of MoS_2 is around 0.8 nm thick (**Figure 2.1**).

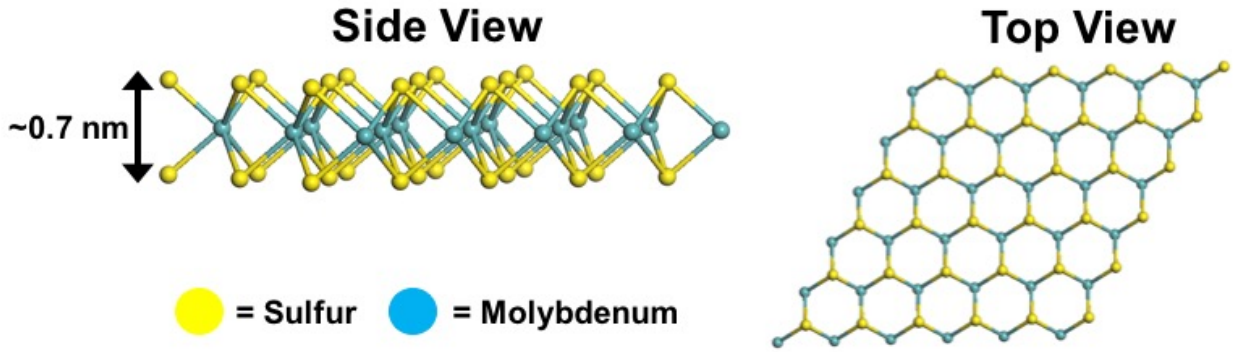

Figure 2.1: Structure of MoS_2
The side view and top view of the MoS_2 crystal structure.

Preparation of MoS_2

Since MoS_2 natural occurs in its bulk form, there are two common practices to prepare MoS_2 as a 2D or thin film. First, the bulk form can be exfoliated in thin layers. This is done in two main ways, liquid exfoliation and mechanical exfoliation. For liquid exfoliation, bulk MoS_2 is suspended in a liquid and then sonicated. In doing this, the bulk MoS_2 is broken up into thin layers and these layers can be separated based on the layer number.[15] In mechanical exfoliation, the scotch tape method is used.[2] Here, a piece of tape is used to peel off a single layer of MoS_2 from the bulk form. For both of these methods, only small areas of MoS_2 can be reliably produced.

The second method to produce thin films of MoS_2 is to grow the MoS_2 on a substrate. One way to do this is to used chemical vapor deposition (CVD). In this method, MoS_2 is grown at high temperatures from precursor material such as $MoCl_5$ and sulfur method. In doing so, thin

films of MoS_2 are able to be grown on multiple different substrates and these films can even be transferred to other substrates. For this study, the MoS_2 was prepared by Cao, et.al. using a CVD method that they created.[16] With this method, centimeter sized films are able to be created and the exact layer number of these films can be controlled.

Organosilane Functionalization

Organosilanes are a class of self-assembled monolayers (SAMs) commonly used to create thin films on silicon oxide (SiO_2). These thin films are very stable because of the covalent bond between the molecule and the surface and therefore can greatly alter the substrate properties.[17]

For this study, we turned to using silanes for modification of the MoS_2 surface. The advantages of this material included the known ability to attach to various oxide surfaces through siloxane linkages and the ability to form covalent bonds between adjacent silane molecules, generating stability across the silane film and the ability to perform further modification without harming the monolayer.[17] In addition, various end groups such as vinyl, carboxylic acid, methyl ester and many more can be incorporated into silane functionalization, allowing for a large possibility for future applications ranging from biological arrays to photolithography.[17] Further, SAMs of organosilanes have been shown to alter the electronic properties of graphene.[18] This sparked interest in using these molecules to chemically functionalize MoS_2. In particular, aminosilanes were investigated because the free amino group can be used for further chemical modification.[19]

One way to modify a SiO_2 surface with an aminosilane is to use a CVD process. In this process, the SiO_2 surface is cleaned and activated to create a uniform hydroxyl layer. Next, the

aminosilane and SiO_2 substrate are placed in a CVD chamber, where a vacuum is pulled and the temperature is raised. This allows for the aminosilane molecules to vaporize and react with the hydroxyl-terminated SiO_2 surface via a silanization reaction where the hydroxyl groups displace the alkoxy groups of the aminosilane and form a covalent Si-O-Si linkage.[20] When this reaction is done with a trioxysilane, the molecules cross-link with each other to form a stable monolayer. This works very well on SiO_2 because SiO_2 can have a hydroxyl-terminated surface. The main obstacle to converting this procedure to functionalize MoS_2 with an organosilane is there is no easy way to create a hydroxyl-terminated surface on MoS_2.

Even though organosilane SAM formation works the best on a hydroxyl-terminated surface, there have been reports of organosilane SAM formation on surfaces such as gold, which does not readily form a hydroxyl-terminated surface.[21] For example, Finlea et. al. reported the formation of an octyltrichlorosilane (OTS) monolayer on the surface of gold. This is done by using UV ozone (UVO) treatment to form a hydrophilic AuO_x layer on the gold substrate. Water is then spin-coated on the surface to form a thin water layer. When the organosilane is deposited, the water layer helps attract the organosilane molecule and promotes cross-linking at the surface. In this process, only some OTS molecules individually link to the surface, while all molecules covalently cross-link to create a 2D network.[22] This is called 2D self-polymerization, and bonding of every silane molecule to the surface is not necessary to create a fully functionalized film[18]. In this regard, materials that do not contain a large number of bonding sites can still be functionalized with a silane molecule. Thus, the native vacancies of MoS_2 provide a way to link silane molecules to the surface and a starting point for covalent surface functionalization.

Characterization of MoS_2 Properties

MoS_2 has many defining characteristics that can help in its identification. Many of these characteristics are dependent on the layer number, which helps to differentiate between bulk, few layer, and monolayer MoS_2. First, 1 layer of MoS_2 is around 0.69 nm thick. This thickness can be measured with an atomic force microscopy (AFM). The thickness of few layer MoS_2 is additive, which bilayer MoS_2 having a thickness of 1.4 nm. This is one quick and easy way to determine the thickness and layer number of a thin film of MoS_2.

Raman spectroscopy is a useful way to characterize MoS_2 because both monolayer and bulk MoS_2 show Raman active peaks. The two main peaks, E_{2g} and A_{1g}, occur around 378.5 and 400.2 cm^{-1}, respectively, in bulk MoS_2. These peaks also appear in monolayer MoS_2 but will generally appear closer together. The distance between these two peaks corresponds to the layer number of MoS_2.[23,24] The distance between the two Raman active peaks increases as the layer number increases. The peak distance is often used to identify the layer number of a given film of MoS_2.

MoS_2 also possesses unique photoluminescence properties. Because of the change from an indirect to a direct band gap as layer number decreases, the PL peaks also shift. Monolayer MoS_2 has only one PL peak at 1.9 eV. As the layer number increases, another peak appears around 1.6 eV[2]. This peak decreases with layer number until it reaches 1.3 eV in bulk MoS_2. The lowest energy PL peak can be used to help characterize the layer number of MoS_2.

Lastly, XPS can be used to characterize MoS_2. Monolayer MoS_2 has a Mo 3d doublet and a S 2p doublet when characterized with XPS. Changes in the binding energy of these peaks of the appearance of difference doublets or different elemental peaks help to show changes in the

oxidation state of the MoS_2 and give insight into any surface functionalization the MoS_2 films may have.

Experimental

Preparation of MoS_2

This study used bilayer MoS_2 made using a CVD process by the Cao group at North Carolina State University, Department of Materials Science and Engineering. In a typical growth process, 5-15 mg of $MoCl_5$ powder and 1 g of sulfur powder was placed in the center of a tube furnace. A sapphire substrate was placed downstream of the powder in the furnace. The furnace was then heated to 850 °C under a constant flow of Ar gas. This produced MoS_2 films on sapphire with a size around 1-2 cm^2.

Chemical Vapor Deposition of Organosilanes

For the chemical vapor deposition, the MoS_2 and 1 mL of 3-aminopropyltrimethoxysilane (APTMS) were placed in a desiccator. A vacuum was pulled until the pressure equaled ~1 torr. The desiccator was closed and then left for 1 hour. After, the sample was placed in an oven at 200 ˚C for 30 minutes to anneal the monolayer. **Figure 2.2** shows a schematic representation of this process.

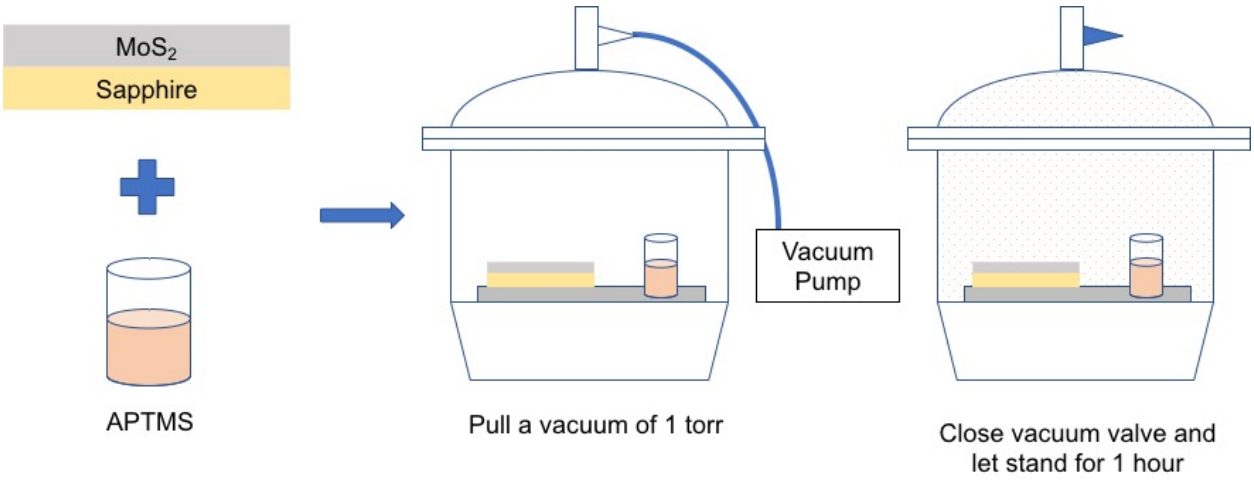

Figure 2.2: Chemical Vapor Deposition of APTMS

This figures shows a representation of the homemade CVD setup. The MoS_2 is placed in a desiccator with a vial of the silane molecule. After pulling a vacuum, the substrate is let to react for the desired amount of time.

Characterization

X-ray photoelectron spectroscopy (XPS) was done on a Kratos Axis Ultra DLD X-ray Photoelectron Spectrometer with a monochromatic Al K alpha source. All spectra were calibrated to the C 1s peak (284.6 eV). Raman spectroscopy and photoluminescence spectroscopy were done using a Renishaw inVia confocal Raman microscope with a 514 nm laser. Spectroscopic Ellipsometry was done using a J. A. Woollam Variable Angle Spectroscopic Ellipsometer. A spectral range of 425-900 nm was used with an angle of incidence of 70˚. The data was analyzed using the J. A. Woollam WVASE software

Results and Discussion

The first goal of this study is to develop a method to chemically functionalize the surface of MoS_2. In order to systematically and successfully complete this task, a few key points will be addressed:

1. Characterization of bilayer MoS_2.
2. Development of a method to consistently deposit APTMS on a surface.
3. Verification this method deposits APTMS on the surface of MoS_2.

The main idea of this study was to find a way to functionalize the surface of MoS_2 with some kind of organic molecule. When starting, a few things were taken into consideration. First, what layer number of MoS_2 should be used? If monolayer MoS_2 was chosen, the worry was that the functionalization process may harm the MoS_2 structure and leave no MoS_2 in the end. Therefore, bilayer MoS_2 was chosen. If the functionalization did harm the top layer of the bilayer MoS_2, there would still be a second layer of MoS_2 that could benefit from the functionalization. (Spoiler alert: no harm was done to the MoS_2 structure in the making of this dissertation.)

Next, I chose 3-aminopropyltrimethoxysilane (APTMS) as the model compound to functionalize the MoS2. The structure of APTMS is shown in **Figure 2.3**. A commercially available liquid, APTMS has an amino end group that can be easily identified with XPS, and aminosilanes are commonly used for different surface reactions.[19]

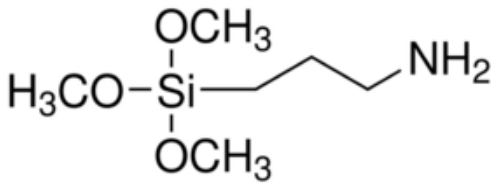

Figure 2.3: Chemical Structure of APTMS

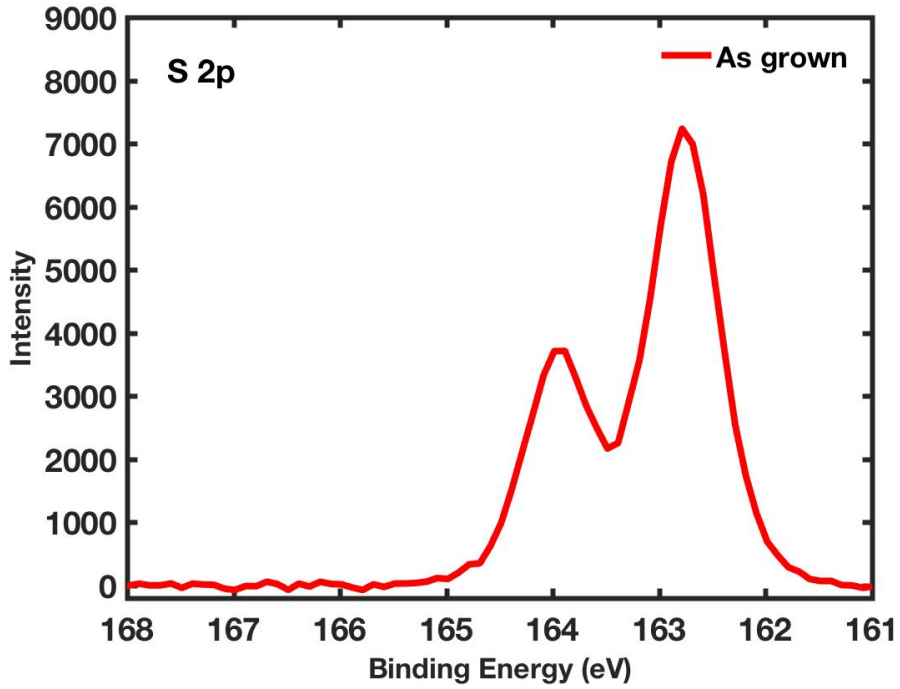

Figure 2.5: XPS Spectrum of S 2p region of as grown MoS_2

The S 2p spectrum of MoS_2 shows a single S 2p doublet, which is normal for MoS_2. This also shows that there is no oxidation of the MoS_2.

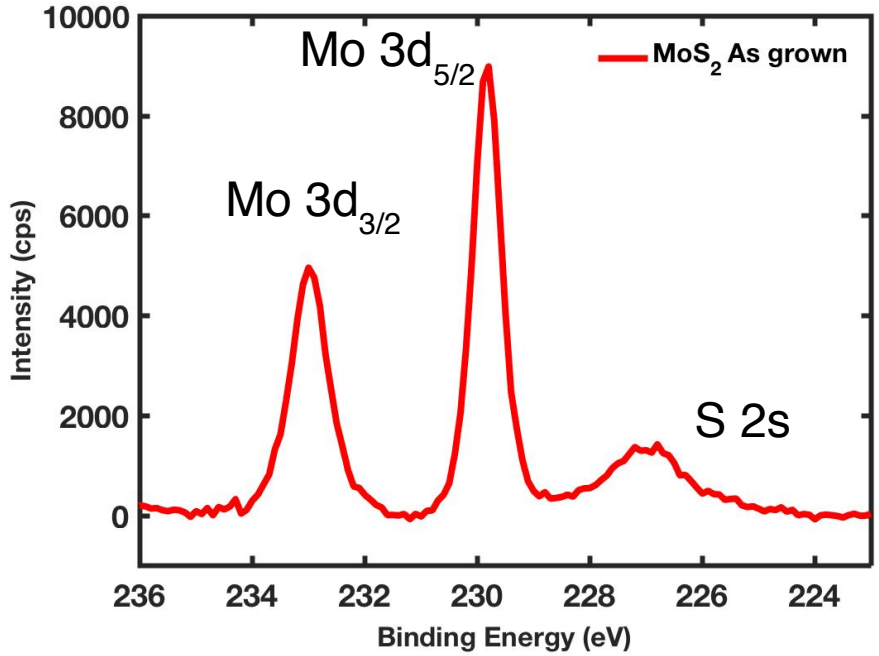

Figure 2.4: XPS Spectrum of Mo 3d region of as grown MoS_2

The Mo 3d XPS spectrum of MoS_2 shows the characteristic peaks for the Mo atoms. There is also a small S 2s peak from the S atoms of MoS_2.

Characterization of Bilayer MoS_2

XPS of MoS_2

There are two XPS regions that can be used together to identify MoS_2. First, the chemical shift associated with the Mo 3d peak of MoS_2 helps to differentiate MoS_2 from other similar materials, such as molybdenum trioxide (MoO_3). The Mo peak of MoO_3 is shifted to higher binding energies than in MoS_2. Further, seeing two doublets in this region points towards partial oxidation of the MoS_2. The S 2p region of XPS corresponds to the sulfur atoms in MoS_2. Changes in either of these XPS doublets point towards changes in the oxidation state of the Mo or S atoms in the MoS_2. **Figure 2.4** and **Figure 2.5** show the XPS spectra of the as grown MoS_2

The MoS_2 used throughout this study was grown with the abovementioned CVD procedure on a sapphire substrate. Sapphire is a good substrate to use because the lattice is a very close match for the lattice of MoS_2. XPS of the initial CVD grown MoS_2 shows that no oxidation occurred during the preparation of the film and that the film consists of just MoS_2.

Raman Shifts of MoS_2

Raman spectroscopy of MoS_2 gives insight into disorder, strain, and doping of MoS_2.[25] The two characteristic Raman modes of MoS_2 are the out-of-plane A_{1g} and the in-plane E_{2g} vibrational modes. The distance between these two peaks corresponds to the layer number of MoS_2.[23,24] Changes in either peak offers direct evidence to evaluate disruptions in the MoS_2 structure.

This makes Raman spectroscopy a good technique to verify whether a substance is MoS_2 and how many layers it is. In this work, Raman is used to determine if the APTMS causes any change in the structure of MoS_2 and to investigate any new Raman active bonding that may

occur. Using a 514 nm laser, as grown MoS_2 clearly shows both the E_{2g} and the A_{1g} peaks (**Figure 2.6**).

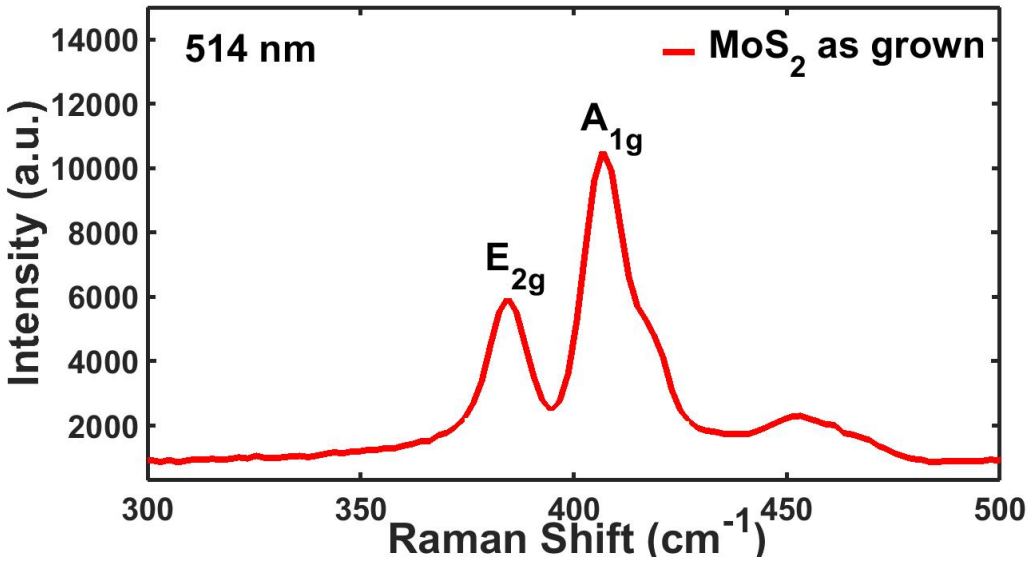

Figure 2.6: Raman Shifts of Bilayer MoS_2

The Raman spectrum of MoS_2 shows the A_{1g} and the E_{2g} MoS_2 peaks. The small peak around 460 cm^{-1} is from the underlying sapphire substrate.

Development of Aminosilane functionalization

There are a few possible ways to perform an organosilane functionalization, with the main options being choosing between a liquid or a vapor deposition process. Now, vapor deposition is generally known to produce a more uniform and reproducible organosilane layer, which made this option stand out as preferable. In doing a chemical vapor deposition process to deposit organosilane layers, the typical procedure requires specialized equipment to control the temperature and pressure. Depending on the organosilane, different temperature and pressure is needed.[20] The problem with this was the current setup of the Wei You lab at UNC did not have any equipment like this. Therefore, in typical grad school fashion, I choose to improvise and create my own custom system to perform CVD of organosilanes. With the

equipment I had on hand, I could either control just the pressure, by using a vacuum desiccator, or just the temperature, by using an oven. Of the two options, the one that would interfere the least with my labmates research was the desiccator, so that is the option I choose.

CVD of APTMS

When first beginning to develop the CVD method for APTMS deposition, I tried the method on bare SiO_2/Si substrates. Silane functionalization on hydroxylated silicon substrates has been frequently reported in literature[19,26,27]. The first few tries in the desiccator yielded very thick and rough films of APTMS that would not be acceptable for functionalized MoS_2 with a thin layer of APTMS. By rethinking my method, I realized that loading desiccator in the ambient environment leads to too much moisture in the air, which causes the APTMS to polymerize quickly in air and creates a thick, rough layer. To counteract this effect, I began to load the desiccator in the glovebox. This reduced the amount of moisture in the desiccator and this greatly helped me to control the process, which I will discuss next.

When developing the CVD method, there were a few variables that needed to be honed to give the desired thickness of 1-2 nm of APTMS. Both the pressure of the desiccator and the length of time of deposition can be easily changed to vary the final silane thickness. One problem that occurred was that the final APTMS thickness was not consistent. **Table 2.1** shows that doing 3 trials with identical time and pressure yields APTMS thicknesses varying from 1 to 5 nm. Reported procedures for CVD functionalization with silane molecules do the functionalization at high temperatures, such as 150 C[27]. Because of this, an anneal step was added after the functionalization to see if it would help improve consistency. As **Table 2.1** shows, even when the samples were of differing thickness before annealing, the thickness after

annealing were much closer and more consistent. Therefore, a 30 min anneal at 200 C was done for all samples. After developing the method using Si/SiO_2 wafers, the method was used to functionalized CVD grown bilayer MoS_2. Since the MoS_2 does not have a hydroxyl functionalization like the SiO_2, steps were tried to optimize the functionalization on MoS_2. Then, the functionalization was verified and the thickness was measured.

Table 2.1: Thickness of APTMS layer before and after annealing

	Thickness Before Anneal (nm)	Thickness After Anneal (nm)
Sample 1	5.19	1.503
Sample 2	2.9	1.59
Sample 3	1.116	1.408

UV Ozone Treatment of MoS_2

To begin the investigation on how to covalently functionalize MoS_2, a method to activate the MoS_2 surface to prepare for APTMS was examined. Taking inspiration from the previous example of aminosilane functionalized gold, UVO treatment was deemed a good starting point. Azcatl *et. al.* reported that 5 minutes of UVO exposure on exfoliated MoS_2 will lead to oxygen functionalization on the surface of MoS_2 and create an S-O bond.[28] Using this result as a starting point, bilayer MoS_2 was exposed to 5 minutes of UVO treatment. Disappointingly, this lengthy time period does not create oxygen functionalization on the surface but instead greatly damages and oxidizes the MoS_2. This can been seen when comparing the Mo 3d XPS peaks of a sample before and after UVO treatment (**Figure 2.7**). The as grown MoS_2, before any treatment, shows the typical peaks seen for MoS_2; mainly Mo^{4+} peaks and also the S 2s peak (**Figure 2.7a**). After UVO treatment, the Mo^{4+} peaks sharply

decrease and a large Mo^{5+} peaks appear (**Figure 2.7b)**. This indicates that the Mo was being oxidized and turned into MoO_3[29]. Also, the S 2s peak almost completely disappears. This indicates that the UVO treatment was much too harsh and converted the MoS_2 into MoO_3 which was not favorable for this project.

Verification of APTMS Functionalization

Next, the APTMS functionalization was done on MoS_2 films with no prior activation of the surface. The characterization of the functionalized films is very important to confirming the

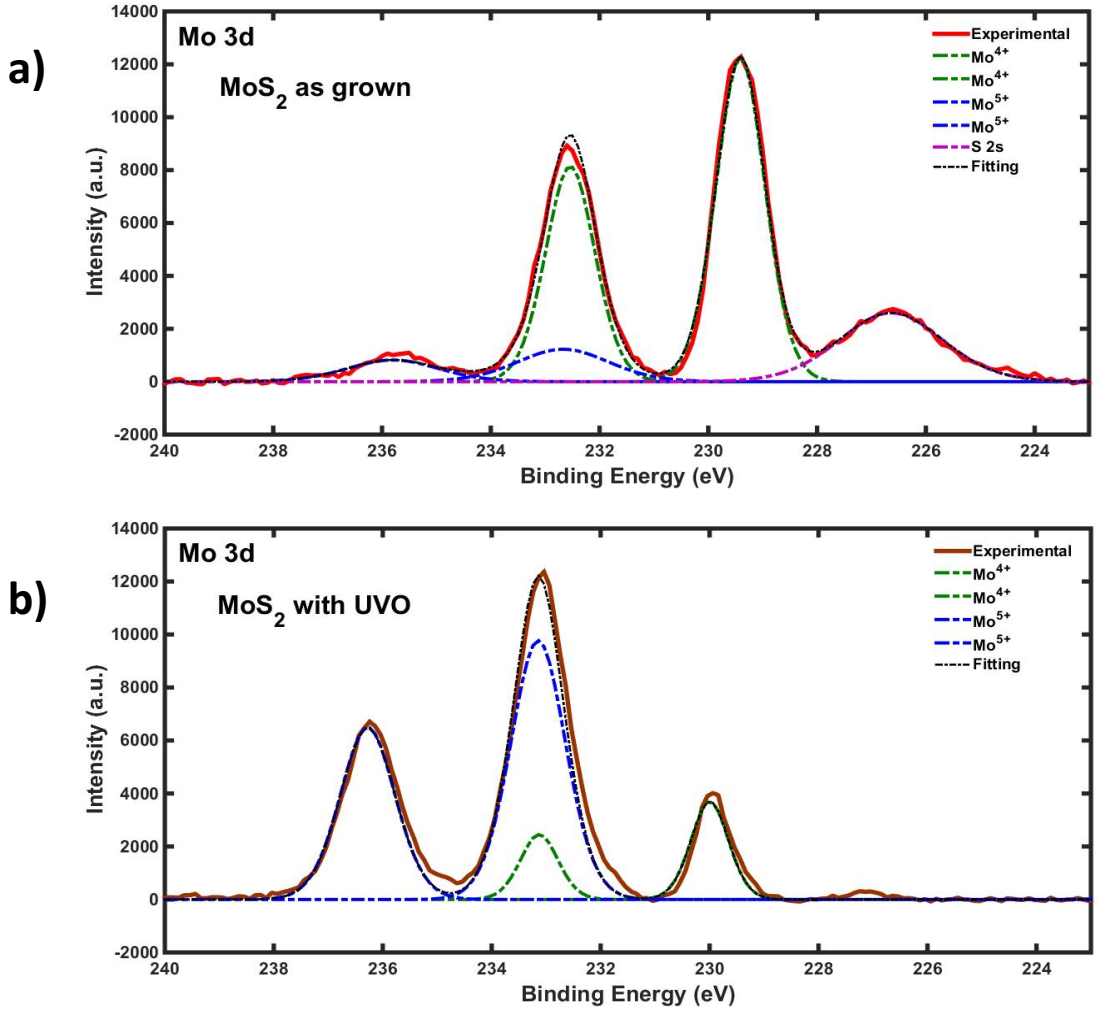

Figure 2.7: Mo 3d XPS Spectra of MoS_2 before and after UV Ozone Treatment

(a) Mo 3d peaks of as grown MoS_2 mostly Mo^{4+} peaks, which is the oxidation state of as grown MoS_2. **(b)** The UVO treatment causes oxidation of the MoS_2 and mostly Mo^{5+} peaks are present.

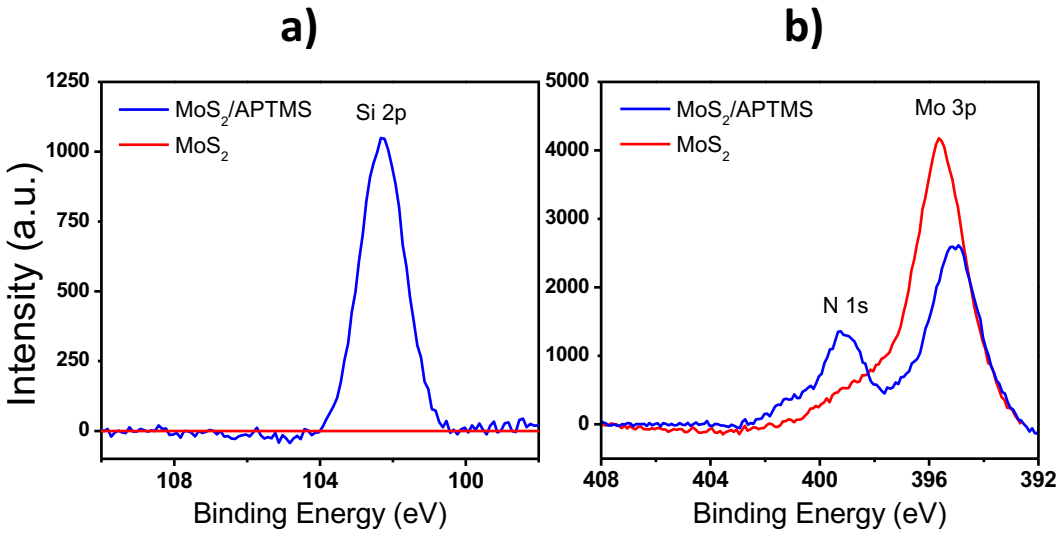

Figure 2.8: XPS Verification of APTMS Deposition

a) Si 2p XPS of MoS2 surface before (red) and after (blue) functionalization with APTMS. b) N 1s XPS of MoS2 surface before (red) and after (blue) functionalization with APTMS. The emergence of the Si 2p and N 1s peak after functionalization shows the presence of APTMS on the MoS2 surface.

presence, bonding, and effect of the APTMS thin layer on the surface of MoS_2. The deposition of an APTMS thin layer was confirmed by examining XPS spectra (**Figure 2.8**). XPS of MoS_2 before functionalization does not have any signal in the range where a Si 2p or a N 1s signal would appear. This was also one reason that APTMS was chosen over silane molecules with a carbon chain or a sulfur end group. The N group is easily identifiable.

Figure 2.8b shows the emergence of a N 1s peak at 399.2 eV, which is only present after the APTMS deposition has taken place, indicating the presence of the $–NH_2$ group of APTMS.[30] The other peak present in **Figure 2.8b** at 395.0 eV corresponds to the Mo 3p peak, and is seen in both samples. The emergence of the N 1s peak clearly shows that an APTMS thin layer is present on the surface of the MoS_2. This is good verification that the CVD method developed is able to deposit the silane molecule on surfaces other than the typical Si/SiO_2 substrate.

Next, looking at the Si 2p XPS spectra can give insight into if the siloxane bonds intrinsic to cross-linking are present. **Figure 2.8a** shows the presence of a Si 2p peak after APTMS deposition. The peak at 102.3 eV corresponds directly to the known siloxane bond peak present in cross-linked APTMS thin layers[30]. The cross-linking of the silane molecules is necessary to form a robust thin layer.

Along with robustness, homogeneity of the APTMS film is crucial for many applications and can ensure that the whole sample behaves the same[27]. Therefore, a very low roughness and consistent monolayer thickness is the goal when depositing APTMS on MoS_2. AFM micrographs of MoS_2 before and after APTMS show that the morphology of the surface slightly changes but that the monolayer is consistent throughout the substrate (**Figure 2.9**).

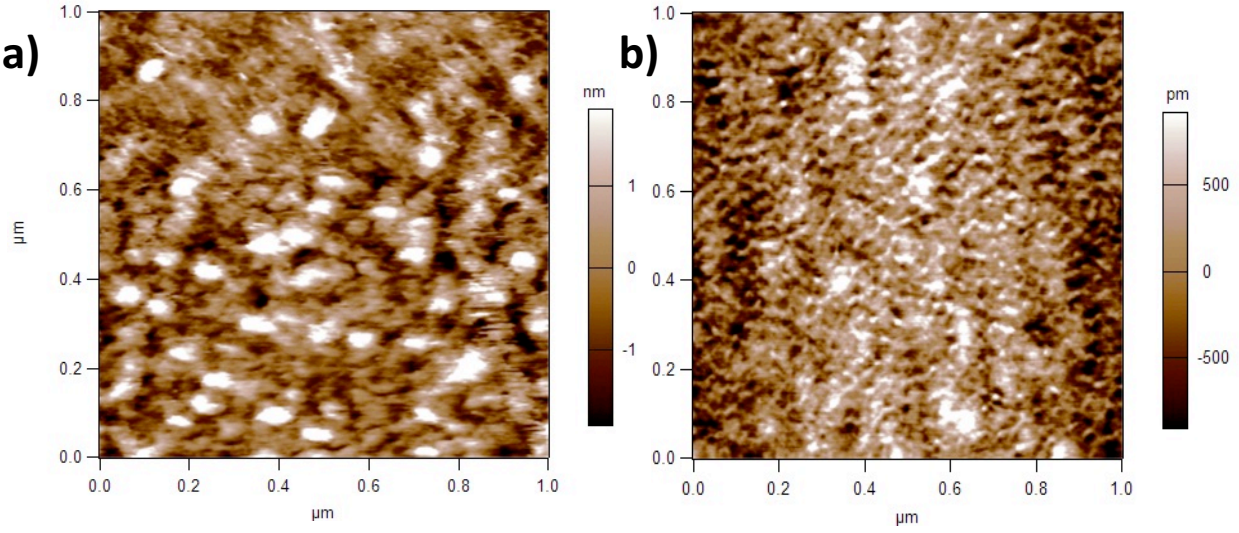

Figure 2.9: AFM of MoS_2 before and after APTMS deposition

a) AFM micrograph of bare MoS_2. b) AFM micrograph of MoS_2 after APTMS deposition

By using the AFM micrographs to calculate the average roughness of MoS_2 before and after deposition (688.1 pm and 463.4 pm, respectively), we find that not only does the film not get any rougher, but it instead has a lower roughness after APTMS deposition (**Table 2.2**). A low

roughness also indicates that the thickness measured for the APTMS layer is the same throughout the sample and that the functionalization creates a continuous uniform layer of APTMS on the surface of MoS_2.

Table 2.2: MoS_2 surface roughness before and after APTMS deposition

	MoS_2 roughness (pm)	**MoS_2/APTMS roughness(pm)**
Area 1	955.5	477.1
Area 2	509.4	466.6
Area 3	599.3	446.4
Average	688.1	463.4

Thickness Measurements

Controlling this thickness of the APTMS monolayer shows if there is one uniform layer of APTMS, or if the molecules have deposited on top of each other. To find the thickness of the APTMS monolayer, two different methods are used. This first method uses XPS to calculate the thickness. By using the attenuation seen in the Mo peaks before and after the addition of APTMS, the thickness can be calculated using equation *(1)*[31]

$$I_{Mo} = I_{Mo}^{\infty} e^{(-d_C/\lambda_C(E_{Mo})\cos\theta)} \qquad (1)$$

where I_{Mo} = intensity of Mo peak after deposition, I_{Mo}^{∞} = intensity of Mo peak before deposition, $\lambda_c(E_{Mo})$ = mean free path of C as a function of Mo kinetic energy, and d_C = thickness of the APTMS layer. In this case, θ = 0˚ because the emission angle of the XPS is 0˚. Two samples were compared: one of as grown MoS_2 and one of MoS_2 with APTMS deposited. First, the intensity of the Mo $3d_{5/2}$ peak is found. For each sample, four spots are analyzed, and

the average intensity is used (Table 3). The mean free path is estimated using literature for carbon. Carbon is chosen because it is assumed to be the material through which the Mo electrons are attenuated. The mean free path literature data[31] is graphed, and the best fit line is used to find the mean free path of carbon at the kinetic energy of the Mo $3d_{5/2}$ peak (Fig. 13). Using equation (1), this gives an APTMS thickness of 1.3 nm.

Table 2.3: Mo $3d_{5/2}$ peak intensity

The intensity of the Mo peak at four different spots on the same sample for as grown MoS_2 and MoS_2 with APTMS.

	Mo Peak Intensity Bare MoS_2	Mo Peak Intensity MoS_2/APTMS
Area 1	15657.7	12224.8
Area 2	16564.0	10537.0
Area 3	16476.8	111156.0
Area 4	16050.5	8714.4
Average	16187.3	10658.1

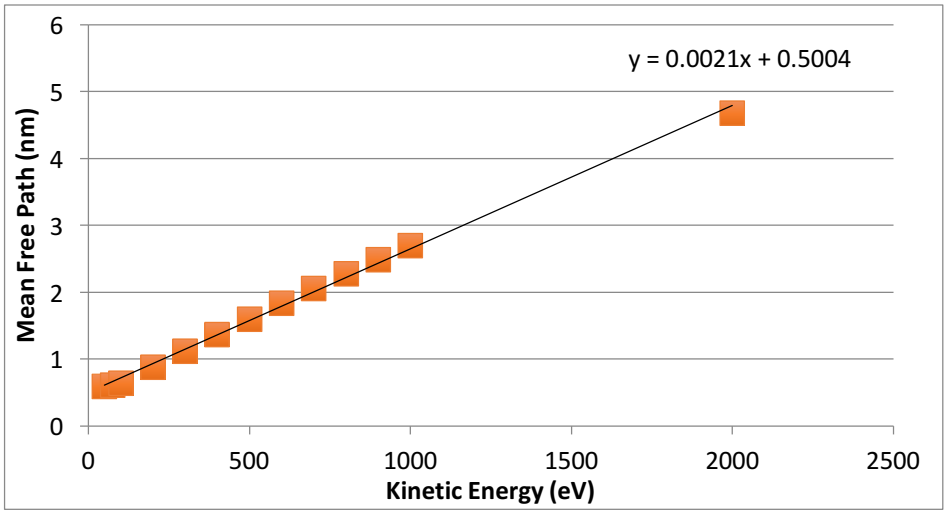

Figure 2.10: Graph of Mean Free Path of Carbon vs. Kinetic Energy

This graph was used to find the mean free path of carbon for the thickness of APTMS on the surface of MoS_2 calculations

Spectroscopic ellipsometry (SE) is used to measure the thickness of APTMS. First, the optical spectra of the as grown MoS_2 are found and fit (Fig. S3). A Tauc-Lorentz oscillation model is needed to fit the optical properties and determine the thickness of the MoS_2 because it is a semiconductor.[32] A two-layer model is used, with the first layer modeled as a sapphire substrate and the second as a Tauc-Lorentz-4. This gives a thickness of 1.3 nm for the as grown MoS_2, which corresponds to bilayer MoS_2. Next, the optical properties of MoS_2 with APTMS are found and fit (Fig. S3). A three-layer model is used. The first two layers are the same as the as grown MoS_2, and the third is a Cauchy fit to model the APTMS layer. This gives an APTMS thickness of 1.3 nm. This number matches the thickness found using XPS. A 1.3 nm layer represents about 2 times a monolayer of APTMS because a monolayer of APTMS has thickness around 0.7 nm.[33] This shows that a very thin layer of APTMS is present on the MoS_2. Further, we know that the layer is uniform based on the AFM roughness data. This leads to the conclusion that the whole substrate has a 1.3 nm layer of APTMS.

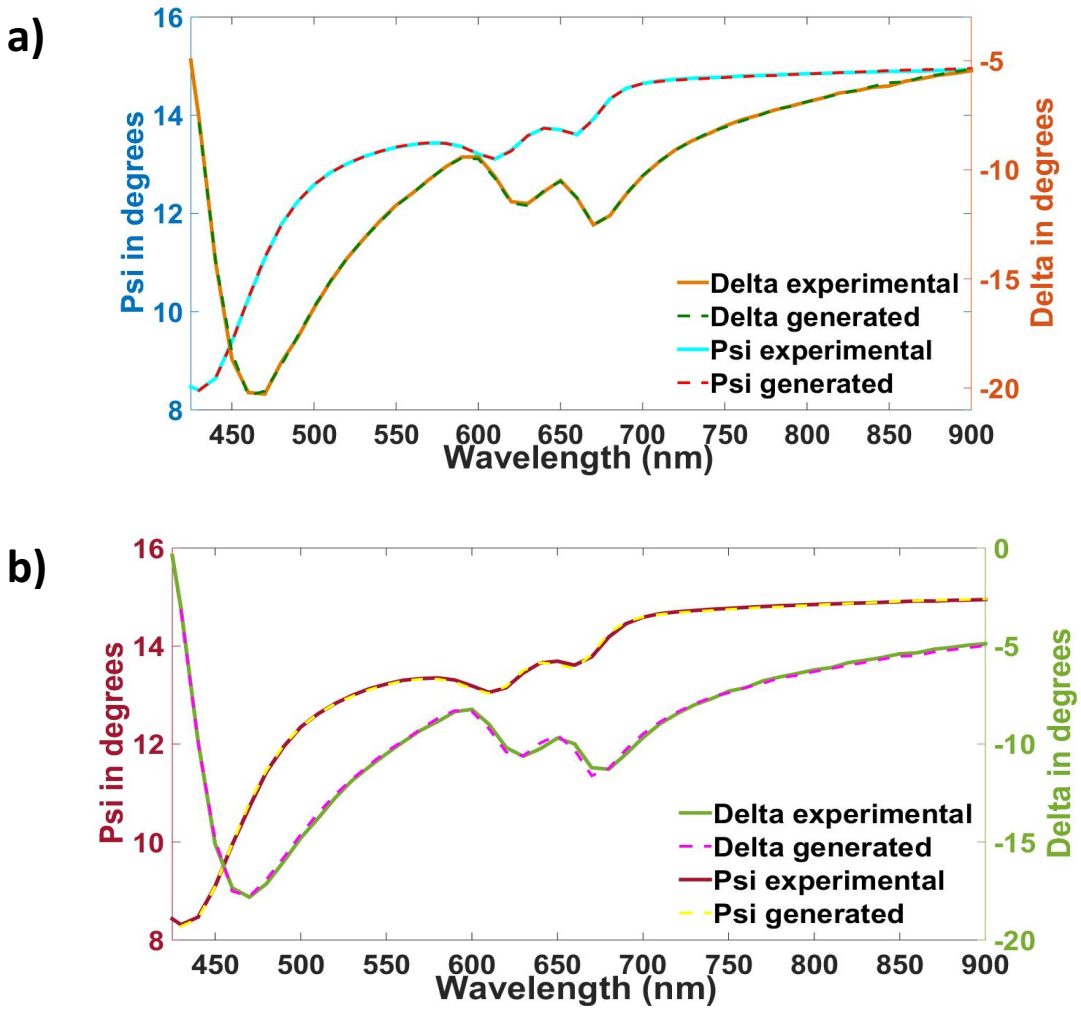

Figure 2.11: Spectroscopic Ellipsometry of MoS_2 before and after APTMS deposition

a) Experimental and generated SE spectra of as grown MoS2. b) Experimental and generated SE spectra of MoS2 with APTMS.

Conclusion

This chapter tells the story of the development of a method to uniformly deposit a thin layer of an organic molecule on top of MoS_2. This method is easy to set up with minimal lab equipment and can be verified by XPS. Further, the method has the potential to be tuned to give different thicknesses of APTMS by changing the deposition time.

The next step in this journey is to look at how the functionalization effects the MoS_2 and how the APTMS and MoS_2 interact. Further, if this method works for APTMS functionalization

on MoS_2, it may be able to move into other organic molecules and even other 2D materials. Since the method is simple and tunable, it has the possibility to be set up in a variety of environments without complicated and expensive equipment, like many commercial CVD setups.

REFERENCES

(1) Wang, Q. H.; Kalantar-Zadeh, K.; Kis, A.; Coleman, J. N.; Strano, M. S. Electronics and Optoelectronics of Two-Dimensional Transition Metal Dichalcogenides. *Nat. Publ. Gr.* **2012**, *7* (11), 699–712.

(2) Mak, K.; Lee, C.; Hone, J.; Shan, J.; Heinz, T. Atomically Thin MoS2: A New Direct-Gap Semiconductor. *Phys. Rev. Lett.* **2010**, *105* (13), 136805.

(3) Yoon, Y.; Ganapathi, K.; Salahuddin, S. How Good Can Monolayer MoS_2 Transistors Be? *Nano Lett.* **2011**, *11* (9), 3768–3773.

(4) Radisavljevic, B.; Radenovic, A.; Brivio, J.; Giacometti, V.; Kis, A. Single-Layer MoS2 Transistors. *Nat. Nanotechnol.* **2011**, *6* (3), 147–150.

(5) Li, H.; Yin, Z.; He, Q.; Li, H.; Huang, X.; Lu, G.; Fam, D. W. H.; Tok, A. I. Y.; Zhang, Q.; Zhang, H. Fabrication of Single- and Multilayer MoS2 Film-Based Field-Effect Transistors for Sensing NO at Room Temperature. *Small* **2012**, *8* (1), 63–67.

(6) Fontana, M.; Deppe, T.; Boyd, A. K.; Rinzan, M.; Liu, A. Y.; Paranjape, M.; Barbara, P. Electron-Hole Transport and Photovoltaic Effect in Gated MoS2 Schottky Junctions. *Sci. Rep.* **2013**, *3*, 1634.

(7) Mak, K. F.; He, K.; Shan, J.; Heinz, T. F. Control of Valley Polarization in Monolayer MoS2 by Optical Helicity. *Nat. Nanotechnol.* **2012**, *7* (8), 494–498.

(8) Zhu, C.; Zeng, Z.; Li, H.; Li, F.; Fan, C.; Zhang, H. Single-Layer MoS2-Based Nanoprobes for Homogeneous Detection of Biomolecules. *J. Am. Chem. Soc.* **2013**, *135* (16), 5998–6001.

(9) Presolski, S.; Pumera, M. Covalent Functionalization of MoS2. *Mater. Today* **2016**, *19* (3), 140–145.

(10) Hirsch, A.; Hauke, F. Post Graphene 2D Chemistry: The Emerging Field of Molybdenum Disulfide and Black Phosphorus Functionalization. *Angew. Chemie Int. Ed.* **2017**, n/a-n/a.

(11) Li, Z.; Wong, S. L. Functionalization of 2D Transition Metal Dichalcogenides for Biomedical Applications. *Mater. Sci. Eng. C* **2017**, *70*, 1095–1106.

(12) Niederhäuser, P.; Hintermann, H. E.; Maillat, M. Moisture-Resistant MoS2-Based Composite Lubricant Films. *Thin Solid Films* **1983**, *108* (2), 209–218.

(13) Winer, W. O. Molybdenum Disulfide as a Lubricant: A Review of the Fundamental Knowledge. *Wear* **1967**, *10* (6), 422–452.

(14) Roberts, E. W. Ultralow Friction Films of MoS2 for Space Applications. *Thin Solid Films* **1989**, *181* (1–2), 461–473.

(15) Coleman, J. N.; Lotya, M.; O'Neill, A.; Bergin, S. D.; King, P. J.; Khan, U.; Young, K.; Gaucher, A.; De, S.; Smith, R. J.; Shvets, I. V; Arora, S. K.; Stanton, G.; Kim, H.-Y.; Lee, K.; Kim, G. T.; Duesberg, G. S.; Hallam, T.; Boland, J. J.; Wang, J. J.; Donegan, J. F.; Grunlan, J. C.; Moriarty, G.; Shmeliov, A.; Nicholls, R. J.; Perkins, J. M.; Grieveson, E. M.; Theuwissen, K.; McComb, D. W.; Nellist, P. D.; Nicolosi, V. Two-Dimensional Nanosheets Produced by Liquid Exfoliation of Layered Materials. *Science* **2011**, *331* (6017), 568–571.

(16) Yu, Y.; Li, C.; Liu, Y.; Su, L.; Zhang, Y.; Cao, L. Controlled Scalable Synthesis of Uniform, High-Quality Monolayer and Few-Layer MoS2 Films. *Sci. Rep.* **2013**, *3* (1), 1866.

(17) Onclin, S.; Ravoo, B. J.; Reinhoudt, D. N. Engineering Silicon Oxide Surfaces Using Self-Assembled Monolayers. *Angew. Chem. Int. Ed. Engl.* **2005**, *44* (39), 6282–6304.

(18) Lee, B.; Chen, Y.; Duerr, F.; Mastrogiovanni, D.; Garfunkel, E.; Andrei, E. Y.; Podzorov, V. Modification of Electronic Properties of Graphene with Self-Assembled Monolayers. *Nano Lett.* **2010**, *10* (7), 2427–2432.

(19) Haensch, C.; Hoeppener, S.; Schubert, U. S. Chemical Modification of Self-Assembled Silane Based Monolayers by Surface Reactions. *Chem. Soc. Rev.* **2010**, *39* (6), 2323–2334.

(20) Zhang, F.; Sautter, K.; Larsen, A. M.; Findley, D. A.; Davis, R. C.; Samha, H.; Linford, M. R. Chemical Vapor Deposition of Three Aminosilanes on Silicon Dioxide: Surface Characterization, Stability, Effects of Silane Concentration, and Cyanine Dye Adsorption. *Langmuir* **2010**, *26* (18), 14648–14654.

(21) Allara, D. L.; Parikh, A. N.; Rondelez, F. Evidence for a Unique Chain Organization in Long Chain Silane Monolayers Deposited on Two Widely Different Solid Substrates. *Langmuir* **1995**, *11* (7), 2357–2360.

(22) Finklea, H. O.; Robinson, L. R.; Blackburn, A.; Richter, B.; Allara, D.; Bright, T. Formation of an Organized Monolayer by Solution Adsorption of Octadecyltrichlorosilane on Gold: Electrochemical Properties and Structural Characterization. *Langmuir* **1986**, *2* (2), 239–244.

(23) Li, H.; Zhang, Q.; Yap, C. C. R.; Tay, B. K.; Edwin, T. H. T.; Olivier, A.; Baillargeat, D. From Bulk to Monolayer MoS2: Evolution of Raman Scattering. *Adv. Funct. Mater.* **2012**, *22* (7), 1385–1390.

(24) Lee, C.; Yan, H.; Brus, L. E.; Heinz, T. F.; Hone, J.; Ryu, S. Anomalous Lattice Vibrations of Single- and Few-Layer MoS2. *ACS Nano* **2010**, *4* (5), 2695–2700.

(25) Pimenta, M. A.; Corro, E. Del; Carvalho, B. R.; Fantini, C.; Malard, L. M. Comparative Study of Raman Spectroscopy in Graphene and MoS2-Type Transition Metal Dichalcogenides. *Acc. Chem. Res.* **2015**, *48* (1), 41–47.

(26) Allara, D. L.; Parikh, A. N.; Rondelez, F. Evidence for a Unique Chain Organization in Long Chain Silane Monolayers Deposited on Two Widely Different Solid Substrates. **1995**, No. 19, 2357–2360.

(27) Zhang, F.; Sautter, K.; Larsen, A. M.; Findley, D. a; Davis, R. C.; Samha, H.; Linford, M. R. Chemical Vapor Deposition of Three Aminosilanes on Silicon Dioxide: Surface Characterization, Stability, Effects of Silane Concentration, and Cyanine Dye Adsorption. *Langmuir* **2010**, *26* (18), 14648–14654.

(28) Azcatl, A.; McDonnell, S.; K. C., S.; Peng, X.; Dong, H.; Qin, X.; Addou, R.; Mordi, G. I.; Lu, N.; Kim, J.; Kim, M. J.; Cho, K.; Wallace, R. M. MoS 2 Functionalization for Ultra-Thin Atomic Layer Deposited Dielectrics. *Appl. Phys. Lett.* **2014**, *104* (11), 111601.

(29) Qin, P.; Fang, G.; Ke, W.; Cheng, F.; Zheng, Q.; Wan, J.; Lei, H.; Zhao, X. In Situ Growth of Double-Layer MoO3/MoS2 Film from MoS2 for Hole-Transport Layers in Organic Solar Cell. *J. Mater. Chem. A* **2014**, *2* (8), 2742.

(30) Jakša, G.; Štefane, B.; Kovač, J. XPS and AFM Characterization of Aminosilanes with Different Numbers of Bonding Sites on a Silicon Wafer. *Surf. Interface Anal.* **2013**, *45* (11–12), 1709–1713.

(31) Cumpson, P. J.; Seah, M. P. Elastic Scattering Corrections in AES and XPS. II. Estimating Attenuation Lengths and Conditions Required for Their Valid Use in Overlayer/Substrate Experiments. *Surf. Interface Anal.* **1997**, *25* (6), 430–446.

(32) Yim, C.; O'Brien, M.; McEvoy, N.; Winters, S.; Mirza, I.; Lunney, J. G.; Duesberg, G. S. Investigation of the Optical Properties of MoS2 Thin Films Using Spectroscopic Ellipsometry. *Appl. Phys. Lett.* **2014**, *104* (10), 103114.

(33) Chauhan, A. K.; Aswal, D. K.; Koiry, S. P.; Gupta, S. K.; Yakhmi, J. V.; Sürgers, C.; Guerin, D.; Lenfant, S.; Vuillaume, D. Self-Assembly of the 3-Aminopropyltrimethoxysilane Multilayers on Si and Hysteretic Current–voltage Characteristics. *Appl. Phys. A* **2007**, *90* (3), 581–589.

Chapter 3: Effects of Functionalization of Molybdenum Disulfide with Organic Molecules

Introduction

Creating a method to produce a functionalized film of MoS_2 was only the first step of the process. The next step was figuring out how the functionalization affected the MoS_2 and if the functionalization method could be done with different aminosilane molecules. It is important to understand how the APTMS interacts with the MoS_2 and what changes the APTMS may cause. To begin, I will introduce some background about different types of MoS_2 functionalization and how it effects the MoS_2 film. Then, I will describe the effect of the APTMS functionalization on MoS_2 and provide a model of the bonding motif. Lastly, I will discuss how the method can be modified for use with different aminosilane molecules.

Examples of MoS_2 Functionalization

When looking into the effect on the MoS_2 and the mechanism of functionalization, I first looked into understanding how different surface functionalization affects MoS_2 and similar materials. The native surface of MoS_2 provides a good starting point for chemical functionalization. Theoretical calculations have shown that it is thermodynamically stable to fill in surface sulfur vacancies with other atoms, such as oxygen.[1] Correspondingly, it has been shown that chemically exfoliated MoS_2 can be functionalized with thiol-terminated ligands in the sulfur vacancies either in solution during the exfoliation process or on chemical vapor deposition (CVD) grown MoS_2.[2–6] It has been reported that MoS_2 can be non-covalently functionalized with carbon nanotubes.[7] Non-covalent methods present interesting ways to tune

the properties of MoS_2 but lack the stability of a covalent functionalizations. Methods that focus only on adding molecules in the sulfur vacancies through a sulfur linkage usually lack the ability to functionalize the entire MoS_2 surface, since sulfur vacancies in MoS_2 are only on the order of 10^{-13} cm^{-2}.[8]

In addition, MoS_2 surface sulfurs can be modified for functionalization. The sulfur layer of MoS_2 can be covalently functionalized by reacting chemically exfoliated MoS_2 with organohalide solutions.[9] In addition, a well-tuned UV-ozone process is capable of inserting oxygens both into defect sites and onto the MoS_2 top sulfur sheet without damaging the overall electronic properties. However, these processes still yield sub-ML functionalization on MoS_2.[1,10] An entire surface functionalization, that is uniform, smooth, and allows for a variety of functional groups to be attached would greatly facilitate the use of MoS_2 in a variety of application spaces.

Furthermore, previous work with graphene functionalized with a monolayer of fluoroalkyltrichlorosilanes to induce a doping effect[11] and with an aminosilane to covalently interface graphene with carbon nanotubes,[12] provides further evidence of the potential applications of covalently functionalizing MoS_2 with silane molecules. Similar methods have been used with varying results to functionalize the surface of MoS_2. For example, Mouri *et. al.* used 2,3,5,6-Tetrafluoro-7,7,8,8-tetracyanoquinodimethane (F_4TCNQ) and Nicotinamide adenine dinucleotide (NADH) to functionalize the surface of monolayer MoS_2.[13] They found that the p-type dopant, F_4TCNQ increased the photoluminescence (PL) intensity of the monolayer MoS_2 while the n-type dopant, NADH, decreased the PL intensity. This shows how some surface functionalization also has an effect on the electronic properties of MoS_2.

Applications of Functionalized Transition Metal Dichalcogenides

Transition metal dichalcogenides (TMDs) are a subset of 2D materials that includes MoS_2. Other materials such as WS_2 and $MoSe_2$ also fall into this category and have similar properties and structures as MoS_2. [14–16] Therefore, many of the possible applications for functionalized MoS_2 are also possible applications for other TMDs and vice versa.[17] While work on the functionalization of TMDs is still mainly focused on methods and the effects on optical and electronic properties, potential applications for these functionalization's have started gaining interest.

Kim *et. al.* reported the preparation of a volatile organic compound sensor using functionalized MoS_2.[18] In this study, the scientists used mercaptoundecanoic acid to functionalize MoS_2 and then use it to create a gas sensor. They reported that different volatile organic compounds, such as toluene, ethanol and acetone, produced different sensor responses. They further present the possibility that this type of gas sensor could gain versatility if other compounds can be used to functionalize the MoS_2.

Jiang *et. al.* reported a simple MoS_2 functionalization with octa-vinyl polyhedral oligomeric silsesquioxanes.[19] By using this functionalized MoS_2 to make a nanoomposite with polyvinyl alcohol (PVA), they can increase both the thermal stability and fire resistance of the PVA.

Results and Discussion

Having achieved a uniform surface functionalization of MoS_2 with APTMS, I next set out to fully characterize the as-functionalized MoS_2, aiming to investigate the impact of the surface-bound silane layer to the intrinsic properties of MoS_2 and probe the formation mechanism of

this silane layer. The latter could include a few possible bonding mechanism of the APTMS molecule to the surface of MoS_2, for example, via –S-O-Si bonding, -Mo-O-Si, or even via $–NH_2$ adsorbed to the surface of MoS2. Nevertheless, a covalent linkage to the surface of MoS_2 provides a unique form of surface functionalization, giving a stable thin layer and providing a different effect compared to a non-covalent surface functionalization.

Raman and Photoluminescence of Functionalized MoS_2

Chapter 2 of this work detailed the creation of a CVD method to functionalize MoS_2 with APTMS and presented a confirmation that the functionalization worked. Now, in Chapter 3, I will focus on the MoS_2 and on how the APTMS interacts with the MoS_2. To begin, I looked at if the functionalization changed or influenced the underlying MoS_2 structure

Raman spectroscopy of MoS_2 gives insight into disorder, strain, and doping of MoS_2.[20] The two characteristic Raman modes of MoS_2 are the out-of-plane A_{1g} and the in-plane E_{2g} vibrational modes. Changes in either mode offer direct evidence to evaluate disruptions in the MoS_2 structure. For example, adsorbed molecules on the surface of MoS_2 have been previously shown to alter the distance between the A_{1g} and E_{2g} Raman peaks by shifting the A_{1g} peak to a lower wavenumber.[21] Further, covalent bonding to the surface sulfur atom of MoS_2 has been shown to split the peak of the A_{1g} mode.[22] Thus, either of these changes in the Raman spectra could point to changes in the A_{1g} out-of-plane vibrational constant of MoS_2.

After APTMS deposition, there is no change in the Raman shift for either mode compared to the native MoS_2 (**Figure 3.1b**). The distance between the A_{1g} and E_{2g} peaks remains the same. An absence of any change in the Raman spectra indicate that the thickness of the MoS_2 layer does not change during functionalization. Therefore, the functionalization does not

harm the MoS_2 or decrease the layer number. This is a promising result for the use of this functionalization in future applications.

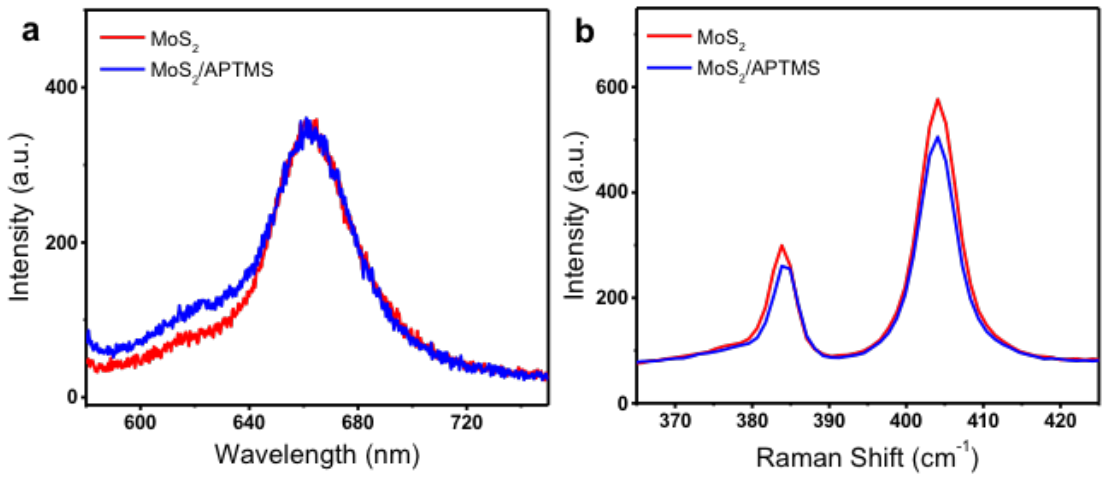

Figure 3.1: Raman and PL of MoS_2 before and after APTMS deposition

a) Photoluminescence spectra of MoS_2 before and after functionalization with APTMS. The exciton peak energy does not shift after functionalization. b) Raman spectra of MoS_2 before and after functionalization, indicating that the layer number or structural integrity is not changed by functionalization.

With no change in the Raman peak shift, a few conclusions can be made about the effects of the APTMS on MoS_2. Since there is no shift in the Raman mode, it is clear that the new method of functionalizing MoS2 with APTMS does not induce a great amount of disorder in the film. Molecules purely adsorbed on the surface of MoS_2 are known to change the A_{1g} peak shift;[23] the absence of any changes leads to the conclusion that the APTMS molecule is not simply adsorbed on the surface sulfur layer.

The Raman spectra indicate that the APTMS layer does not induce any measureable amount of strain on the sample. Lastly, there is no indication that the APTMS is bonded to the sulfur atom, since there is no splitting of the A_{1g} peak. These data support the inference that the APTMS molecule is not simply lying on the MoS_2, adsorbed to the surface or bonded to the

sulfur atom. But, the data in Chapter 2 shows that APTMS is clearly present on the surface. Thus, the next question is: does the $–NH_2$ group directly interact with the surface or is interaction blocked by a cross-linked silane network? This is an important question, because different conformations of the APTMS thin layer will have a different effect on the MoS_2 properties. For example, if the $-NH_2$ moiety of the APTMS layer direct interacts with the MoS_2 surface there will be a shift in the A_{1g} Raman peak. This is seen when MoS_2 is placed on top of a surface that has been functionalized with an aminosilane.[24] In this scenario, the free $–NH_2$ end of the functionalized substrate then is directly touching the MoS_2, which has been reported to increase the photoluminescence intensity at room temperature[25] compared to MoS_2 on a clean, non-functionalized surface. However, for the MoS_2 functionalized with APTMS in this study, we did not observe noticeable change in the photoluminescence intensity after the addition of APTMS, indicating that the $–NH_2$ group is not directly interacting with the surface (**Figure 3.1a**). Further, there is no shift in the photoluminescence peak position. Since the photoluminescence peak position corresponds to the band gap of the MoS_2, no shift indicates that the APTMS functionalization does not have any effect on the MoS_2 band gap. From analyzing both the Raman spectra and the photoluminescence spectra, there is no evidence that the $-NH_2$ group directly interacts with the MoS_2 surface. This leads to the more likely scenario of the silane group directly interacting with the MoS_2 surface and facilitating the functionalization.

Changes in the XPS spectra of functionalized MoS_2

If silane groups directly interact with the MoS_2, there could be some changes in the oxidation state of the Mo or S atoms, which can be probed through XPS. In native MoS_2, the characteristic S 2p region contains only one S 2p doublet, corresponding to the native oxidation

state of sulfur in MoS_2, S^{2-}, whereas the Mo 3d region contains a doublet pertaining to the Mo^{4+} oxidation state. Before functionalization, the MoS_2 bilayer samples possess both the characteristic S 2p and Mo 3d XPS peaks of bilayer MoS_2 (**Figure 3.2**). Similarly, the same S and Mo peaks are seen after functionalization. The presence of the same doublets before and after APTMS deposition confirm that the functionalization does not change the underlying MoS_2 crystal lattice or change the Mo and S native oxidation states. Sulfur oxidation, in the form of an S-O bond, would produce a doublet around 166-168 eV. The absence of any peaks in this region rules out any sulfur oxidation. This conclusion also reiterates the fact that the functionalization method does not harm the underlying MoS_2 structure and does not cause any disorder in the MoS_2.

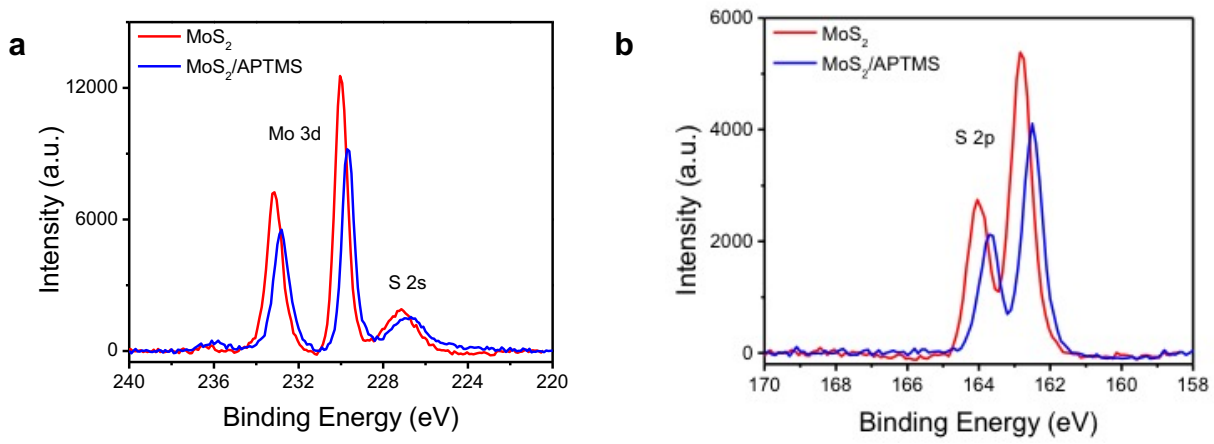

Figure 3.2: XPS Spectra of MoS_2 before and after APTMS deposition

a) Mo 3d XPS spectra of MoS_2 before and after deposition of APTMS shows a 0.3 eV downshift in the peak position b) S 2p XPS spectra of MoS_2 before and after deposition of APTMS shows an equivalent 0.3 eV downshift in the peak position.

Second, oxidation of the native Mo^{4+} to either Mo^{5+} or Mo^{6+} causes the emergence of higher energy doublets in the Mo 3d region. The absence of this shows that Mo is still in the Mo^{4+} state and has not undergone oxidation. This also confirms that the bonding presence in

the final species does not change the original oxidation states of the MoS_2. Furthermore, no changes in the S 2p doublet eliminates the possibility of a covalent bond to the S atom because a S-O, S-Si, or S-N bond would change the oxidation state of the S, subsequently changing the S 2p doublet. This mirrors the previous Raman data conclusion that there is no new bond to the S surface atom. On the other hand, even though there is no change in the Mo 3d doublet, this does not rule out an additional non-sulfur Mo bond. Oxygen bonding to the Mo can maintain the Mo^{4+} oxidation state, as it does in substances such as MoO_2. Similarly, the Mo 3d doublet for MoO_2 appears at nearly the same binding energy as the Mo 3d doublet for MoS_2. Because of this, the O 1s XPS spectra was further analyzed to look at the bonding in the MoS_2 after functionalization. In short, all these results essentially rule out the possible binding mechanisms including –S-O-Si bonding and –Mo ($-S_2$)-O-Si. More importantly, it appears that our new method of surface functionalization of MoS_2 by APTMS can keep the structure of MoS_2 intact and prevent its oxidation, thereby maintaining the native properties of MoS_2.

For native MoS_2 on a sapphire substrate, the bulk of the O 1s peak is attributed to the Al-O bond of the sapphire, with a small peak for C-O organic compounds in the XPS chamber (**Figure 3.3a**). Since the APTMS contains oxygen, we would expect changes to this peak. After functionalization, the shape of the O 1s spectra drastically changes (**Figure 3.3b**). Fitting of the O 1s spectra after functionalization introduces a new oxygen bonding peak at 530.2 eV. There are a few initials possibilities for the identity of this peak, but some can be ruled out based on previous data. First, it has already been determined that there is no S-O bonds present in the sample. Further, literature reports that the Si-O-Si siloxane bond O 1s peak appears at 532 eV.[26]

By ruling out an S-O or Si-O bond, the O 1s peak at 530.2 eV can then be attributed to a Mo-O peak, which has been shown in literature to occur around 530.5 eV.[27]

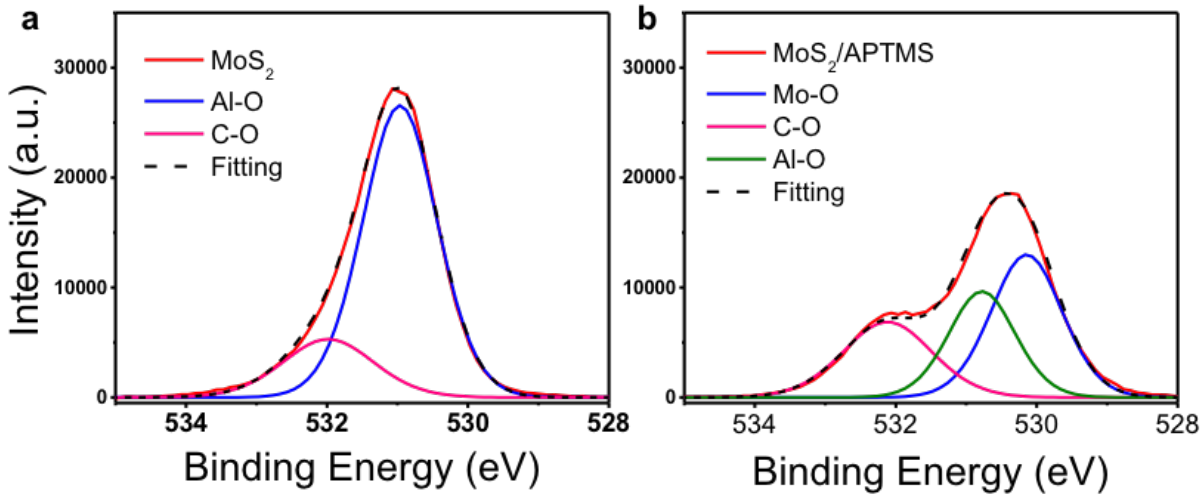

Figure 3.3: O 1s XPS spectra of MoS_2 before and after functionalization

a) O 1s XPS spectrum of MoS_2 before functionalization contains a large peak for the substrate, Al_2O_3. b) O 1s XPS spectrum of MoS_2 after functionalization shows a large change in shape compared to before functionalization. The emergence of an Mo-O peak produces this change.

It has been previously established that oxygen atoms can bond in sulfur *vacancies* on the surface of MoS_2 and it is thermodynamically favorable for the vacancies to be filled with oxygen[1]. In the CVD formation of the APTMS thin layer the vaporized APTMS molecules can bond to a surface through a Si-O-surface bond. Since the APTMS has an available O atom, this O can bond in the vacancies on the MoS_2 surface. This then allows the APTMS to bond in the sulfur vacancies, which produces the Mo-O bond seen in the Mo 3d XPS spectra. These O atoms on the surface provide a way to anchor the APTMS thin layer to the MoS_2, allowing the APTMS molecules to then cross-link to create a covalent APTMS network.

OTS Functionalization of MoS_2

With this type of silane functionalization of MoS_2, the bonding is dependent upon having a silane linkage, not on the end group of the silane molecule. Therefore, the method can be easily transferred to silanes with other end groups as long as the silane is still present to facilitate the bonding to the MoS_2 and the covalent cross-linked network formation. To show this, the molecule octyltricholorsilane (OTS) was used to functionalize MoS_2 using the same CVD method. For $–NH_2$ or $–CH_3$ end groups interacting with MoS_2, there are different changes in the properties, such as different Raman shifts or different doping. These different end groups induce different electronic changes to the surface of the MoS_2. But, if the silane molecule bonds to the oxygen impurities on the surface and creates a cross-linked silane network, the different end groups of the silane would have minimal effects on the properties of the MoS_2 because the siloxane network would prevent any direct interaction.

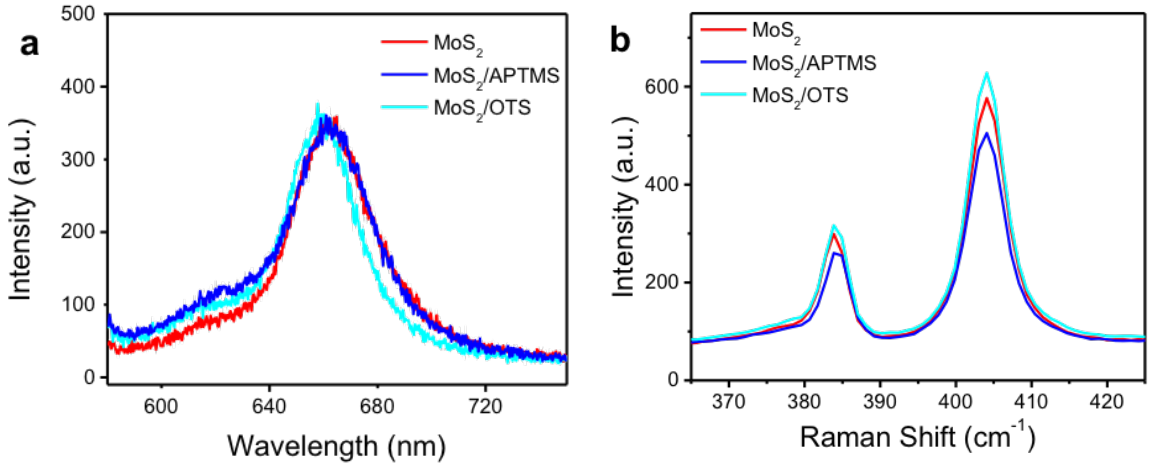

Figure 3.4: Raman and PL of MoS_2 before and after OTS functionalization

a) Photoluminescence spectra of MoS_2 before and after functionalization with APTMS and OTS. b) Raman spectra of MoS_2 before and after functionalization with APTMS and OTS shows the absence of a statistically significant change in peak position.

After performing the OTS surface functionalization on MoS_2, the same effects are seen compared to APTMS surface functionalization of MoS_2. The OTS functionalization does not cause any changes in the Raman or the photoluminescence spectra (**Figure 3.4**). Further, the same downshift in binding energy of the Mo 3d and S 2p XPS peaks was observed (**Figure 3.5**). This indicates that the most important component in the functionalization process is the silane, and opens the door for many different end groups to be used. Since the end groups of the silanes do not dope the MoS_2 when there is a siloxane cross-linked network. This further supports the conclusion that the APTMS molecule bonds to the MoS_2 through a silane linkage and give more evidence of the validity of the proposed model.

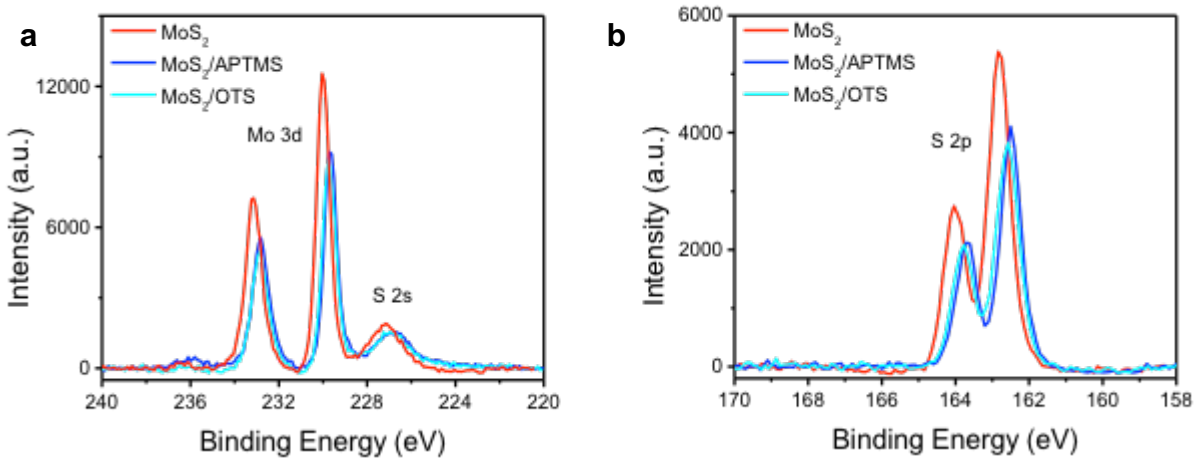

Figure 3.5: XPS spectra of MoS_2 before and after OTS functionalization

a) Mo 3d XPS peaks of MoS_2 functionalized with APTMS and OTS, compared to as grown MoS_2.
b) S 2p XPS peaks of MoS_2 functionalized with APTMS and OTS, compared to as grown MoS_2.

However, creating this interface between the APTMS and MoS_2 has an effect on the electronic environment of the Mo and S atoms, seen by the XPS spectra (**Figure 3.5**). The functionalization of MoS_2 by both APTMS and OTS causes charge transfer between the MoS_2 surface and the silane molecules. The heteropolar Mo-S bond allows for charge density modulation of the MoS_2, which is facilitated by the silane molecules.[28] The Mo 3d and S 2p XPS

doublets shift downwards in binding energy after the addition of the APTMS and OTS thin layer. A shift in the binding energy indicates a change in the charge density of the Mo, which can be caused by charge transfer between the Mo and the O-Si bond. When the oxygen atom of the silane molecules bonds in a sulfur vacancy, it creates another heteropolar bond between the Mo and O, which subsequently modifies the electron density of the Mo and S, causing the charge transfer to occur. When charge transfer occurs, it changes the valance band maximum (VBM) of the MoS_2, which is the measure of the difference between the Valance band and the Fermi level of the MoS_2. Using XPS, we were able to probe the VBM of the MoS_2 surface before and after the addition of APTMS and OTS. The APTMS and OTS caused the VBM to increase to 1.22 eV and 1.33 eV, respectively, compared to a VBM of 1.02 eV for non-functionalized MoS_2 (**Figure 3.6**). However, the photoluminescence spectra of the functionalized MoS_2 does not show any signs of doping or any change in the bandgap of MoS_2 (**Figure 3.4a**). Therefore, the Fermi level of the MoS_2 does not change with functionalization, pointing to only a change in the VBM at the surface.

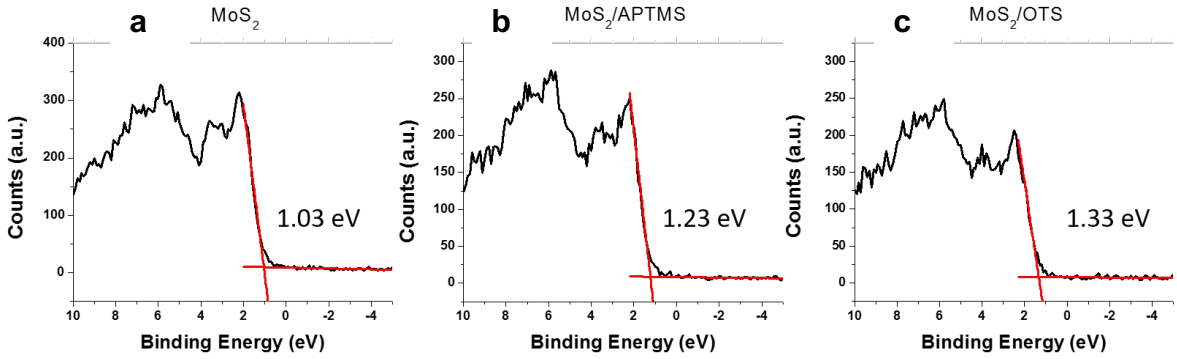

Figure 3.6: VBM of MoS_2

Valance band maximum spectra of a) MoS_2 as grown b) MoS_2 functionalized with APTMS and c) MoS_2 functionalized with OTS. The VBM increases after functionalization.

The oxygen atom of the silane molecule is more electronegative than the sulfur atom of the MoS_2; the charge transfer takes place when the oxygen atom pulls charge density around from the Mo-S bond. The silane molecule works as an electron density acceptor, which decreases the surface charge density of the MoS_2 and lowers the surface Valance band energy.

With this in mind, the oxygen linkage to the silane molecule must allow for charge density to be pulled from the Mo and S atoms, leading to a downshift in binding energy and an increase in VBM. Even though the same oxygen substitutional impurities are present before the addition of the APTMS molecule, the charge density cannot be easily transferred from the Mo and S until the covalent linkage to the APTMS is made. Overall, covalent functionalization facilitates a surface charge transfer that is not seen with only oxygen substitutional impurities.

Model of APTMS functionalization of MoS_2

Based on all these results, we propose the following model to schematically and mechanistically explain the surface functionalization of MoS_2 by APTMS (**Figure 7**). This model is based on two aspects of the MoS_2/APTMS interaction. First, we considered the evidence pertaining to the directionality of the APTMS in reference to the MoS_2 surface. The absence of any change in the Raman or PL spectra indicates the $–NH_2$ group does not directly interact with the MoS_2 surface. If the $–NH_2$ group does not interact directly, this rules out both the APTMS lying flat and the configuration of the $–NH_2$ group close to the MoS_2 with the silane opposite. This leads to the conclusion that the oxygen attached to the silane moiety is directly interacting with the surface of MoS_2, leaving the $–NH_2$ group free to be used in further surface modification. The second aspect of the proposed model looks at the new bonds present in the final species, both between adjacent APTMS molecules and between the APTMS and the MoS_2.

The Si 2p XPS confirms the presence of cross-linking between adjacent APTMS molecules through a Si-O-Si bond, which is reflected in the proposed model by the siloxane bonding between adjacent Si atoms. Further, since there is no S-O bond present, the APTMS bonds to the MoS_2 through a Mo-O linkage, with the oxygen filling in sulfur vacancies on the surface. These vacancies only exist in scattered spots on the MoS_2 surface, so not every APTMS is covalently bonded to the MoS_2, but all APTMS are covalently bonded to one another. This helps to anchor the whole APTMS thin layer to the surface of the MoS_2 surface.

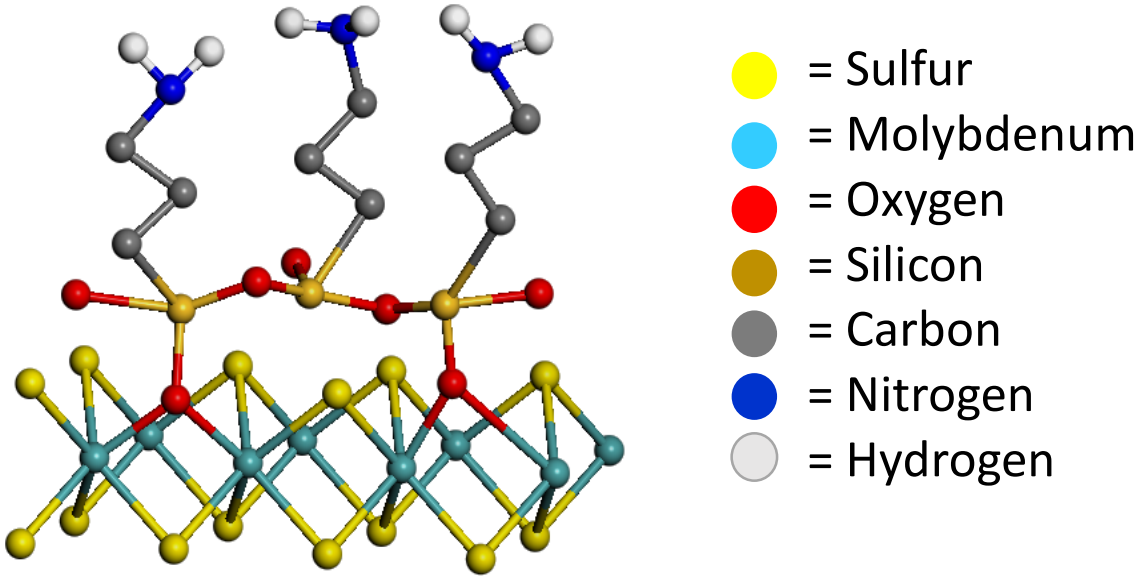

Figure 3.7: Schematic representation of MoS_2 functionalized with APTMS
The representation shows the proposed bonding of the APTMS to the MoS_2 surface. The APTMS bonds in sulfur vacancies on the surface and also cross-links with other APTMS molecules to create a covalently bonded monolayer.

Conclusion

Overall, this study has proposed a facile route to create a covalently bonded organic adlayer on the surface of MoS_2. The covalent Si-O-Mo bond makes use of the oxygen substitutional impurities present on the surface of native MoS_2. The CVD method is quick, easy,

and does not harm the underlying MoS_2 structure. By utilizing the silane to MoS_2 linkage, this method has the possibility of incorporating many different organic end groups on the surface of MoS_2.

REFERENCES

(1) KC, S.; Longo, R. C.; Wallace, R. M.; Cho, K. Surface Oxidation Energetics and Kinetics on MoS 2 Monolayer. *J. Appl. Phys.* **2015**, *117* (13), 135301.

(2) Chou, S. S.; De, M.; Kim, J.; Byun, S.; Dykstra, C.; Yu, J.; Huang, J.; Dravid, V. P. Ligand Conjugation of Chemically Exfoliated MoS 2. *J. Am. Chem. Soc.* **2013**, *135* (12), 4584–4587.

(3) Makarova, M.; Okawa, Y.; Aono, M. Selective Adsorption of Thiol Molecules at Sulfur Vacancies on MoS 2 (0001), Followed by Vacancy Repair via S–C Dissociation. *J. Phys. Chem. C* **2012**, *116* (42), 22411–22416.

(4) Cho, K.; Min, M.; Kim, T.-Y.; Jeong, H.; Pak, J.; Kim, J.; Jang, J.; Yun, S. J.; Lee, Y. H.; Hong, W.; Lee, T. Electrical and Optical Characterization of MoS 2 with Sulfur Vacancy Passivation by Treatment with Alkanethiol Molecules. *ACS Nano* **2015**, *9* (8), 8044–8053.

(5) Nguyen, E. P.; Carey, B. J.; Ou, J. Z.; van Embden, J.; Gaspera, E. Della; Chrimes, A. F.; Spencer, M. J. S.; Zhuiykov, S.; Kalantar-zadeh, K.; Daeneke, T. Electronic Tuning of 2D MoS 2 through Surface Functionalization. *Adv. Mater.* **2015**, *27* (40), 6225–6229.

(6) Ding, Q.; Czech, K. J.; Zhao, Y.; Zhai, J.; Hamers, R. J.; Wright, J. C.; Jin, S. Basal-Plane Ligand Functionalization on Semiconducting 2H-MoS2Monolayers. *ACS Appl. Mater. Interfaces* **2017**, *9* (14), 12734–12742.

(7) Zhang, Z.; Huang, W.-Q.; Xie, Z.; Hu, W.; Peng, P.; Huang, G.-F. Noncovalent Functionalization of Monolayer MoS 2 with Carbon Nanotubes: Tuning Electronic Structure and Photocatalytic Activity. *J. Phys. Chem. C* **2017**, *121* (40), 21921–21929.

(8) Hong, J.; Hu, Z.; Probert, M.; Li, K.; Lv, D.; Yang, X.; Gu, L.; Mao, N.; Feng, Q.; Xie, L.; Zhang, J.; Wu, D.; Zhang, Z.; Jin, C.; Ji, W.; Zhang, X.; Yuan, J.; Zhang, Z. Exploring Atomic Defects in Molybdenum Disulphide Monolayers. *Nat. Commun.* **2015**, *6*, 6293.

(9) Voiry, D.; Goswami, A.; Kappera, R.; Silva, C. de C. C. e; Kaplan, D.; Fujita, T.; Chen, M.; Asefa, T.; Chhowalla, M. Covalent Functionalization of Monolayered Transition Metal Dichalcogenides by Phase Engineering. *Nat. Chem.* **2014**, *7* (1), 45–49.

(10) Azcatl, A.; McDonnell, S.; K. C., S.; Peng, X.; Dong, H.; Qin, X.; Addou, R.; Mordi, G. I.; Lu, N.; Kim, J.; Kim, M. J.; Cho, K.; Wallace, R. M. MoS 2 Functionalization for Ultra-Thin

Atomic Layer Deposited Dielectrics. *Appl. Phys. Lett.* **2014**, *104* (11), 111601.

(11) Lee, B.; Chen, Y.; Duerr, F.; Mastrogiovanni, D.; Garfunkel, E.; Andrei, E. Y.; Podzorov, V. Modification of Electronic Properties of Graphene with Self-Assembled Monolayers. *Nano Lett.* **2010**, *10* (7), 2427–2432.

(12) Adhikari, P. D.; Jeon, S.; Cha, M.-J.; Jung, D. S.; Kim, Y.; Park, C.-Y. Immobilization of Carbon Nanotubes on Functionalized Graphene Film Grown by Chemical Vapor Deposition and Characterization of the Hybrid Material. *Sci. Technol. Adv. Mater.* **2014**, *15* (1), 15007.

(13) Mouri, S.; Miyauchi, Y.; Matsuda, K. Tunable Photoluminescence of Monolayer MoS_2 via Chemical Doping. *Nano Lett.* **2013**, *13* (12), 5944–5948.

(14) Chhowalla, M.; Shin, H. S.; Eda, G.; Li, L.-J.; Loh, K. P.; Zhang, H. The Chemistry of Two-Dimensional Layered Transition Metal Dichalcogenide Nanosheets. *Nat. Chem.* **2013**, *5* (4), 263–275.

(15) Wang, Q. H.; Kalantar-Zadeh, K.; Kis, A.; Coleman, J. N.; Strano, M. S. Electronics and Optoelectronics of Two-Dimensional Transition Metal Dichalcogenides. *Nat. Publ. Gr.* **2012**, *7* (11), 699–712.

(16) Zhao, W.; Ribeiro, R. M.; Eda, G. Electronic Structure and Optical Signatures of Semiconducting Transition Metal Dichalcogenide Nanosheets. *Acc. Chem. Res.* **2015**, *48* (1), 91–99.

(17) Jariwala, D.; Sangwan, V. K.; Lauhon, L. J.; Marks, T. J.; Hersam, M. C. Emerging Device Applications for Semiconducting Two-Dimensional Transition Metal Dichalcogenides. *ACS Nano* **2014**, *8* (2), 1102–1120.

(18) Kim, J. S.; Yoo, H. W.; Choi, H. O.; Jung, H. T. Tunable Volatile Organic Compounds Sensor by Using Thiolated Ligand Conjugation on MoS2. *Nano Lett.* **2014**, *14* (10), 5941–5947.

(19) Jiang, S.; Tang, G.; Bai, Z.; Wang, Y. Surface Functionalization of MoS2 with POSS for Enhancing Thermal, Flame-Retardant and Mechanical Properties in PVA Composites. *RSC Adv.* **2014**, 3253–3262.

(20) Pimenta, M. A.; del Corro, E.; Carvalho, B. R.; Fantini, C.; Malard, L. M. Comparative Study of Raman Spectroscopy in Graphene and MoS 2 -Type Transition Metal Dichalcogenides. *Acc. Chem. Res.* **2015**, *48* (1), 41–47.

(21) Kiriya, D.; Tosun, M.; Zhao, P.; Kang, J. S.; Javey, A. Air-Stable Surface Charge Transfer Doping of MoS_2 by Benzyl Viologen. *J. Am. Chem. Soc.* **2014**, *136* (22), 7853–7856.

(22) Voiry, D.; Goswami, A.; Kappera, R.; Silva, C. de C. C. e; Kaplan, D.; Fujita, T.; Chen, M.; Asefa, T.; Chhowalla, M. Covalent Functionalization of Monolayered Transition Metal

Dichalcogenides by Phase Engineering. *Nat. Chem.* **2014**, *7* (1), 45–49.

(23) Kiriya, D.; Tosun, M.; Zhao, P.; Kang, J. S.; Javey, A. Air-Stable Surface Charge Transfer Doping of MoS2 by Benzyl Viologen. *J. Am. Chem. Soc.* **2014**, 8–11.

(24) Li, Y.; Xu, C.-Y.; Hu, P.; Zhen, L. Carrier Control of MoS 2 Nanoflakes by Functional Self-Assembled Monolayers. *ACS Nano* **2013**, *7* (9), 7795–7804.

(25) Najmaei, S.; Zou, X.; Er, D.; Li, J.; Jin, Z.; Gao, W.; Zhang, Q.; Park, S.; Ge, L.; Lei, S.; Kono, J.; Shenoy, V. B.; Yakobson, B. I.; George, A.; Ajayan, P. M.; Lou, J. Tailoring the Physical Properties of Molybdenum Disulfide Monolayers by Control of Interfacial Chemistry. *Nano Lett.* **2014**, *14* (3), 1354–1361.

(26) Simonsen, M. E.; Sønderby, C.; Li, Z.; Søgaard, E. G. XPS and FT-IR Investigation of Silicate Polymers. *J. Mater. Sci.* **2009**, *44* (8), 2079.

(27) Li, H.; Ye, H.; Xu, Z.; Wang, C.; Yin, J.; Zhu, H. Freestanding MoO_2 /Mo_2C Imbedded Carbon Fibers for Li-Ion Batteries. *Phys. Chem. Chem. Phys.* **2017**, *19* (4), 2908–2914.

(28) Cai, Y.; Zhou, H.; Zhang, G.; Zhang, Y. Modulating Carrier Density and Transport Properties of MoS 2 by Organic Molecular Doping and Defect Engineering. *Chem. Mater.* **2016**, *28* (23), 8611–8621.

Chapter 4: Electronic Properties of derivatives of bis(triethylsilylethynyl) anthradithiophene (TES-ADT)

Like most scientifically relevant materials, there are both advantages and disadvantages to the use of organic semiconductors in modern electronics. The advantages are that organic materials are generally lightweight, flexible, and inexpensive and easy to process. Further, the optical and electronic properties of organic materials can be more easily manipulated and synthetically tailored to specific applications. On the downside, organic semiconductors have lower mobility, poor stability, and more film-to-film inconsistency compared to typical inorganic semiconductors.[1] Organic electronics will not totally replace silicon based devices in the foreseeable future, but they are already carving out a niche in modern electronic with uses in organic light-emitting diodes (OLEDs), organic photovoltaics (OPVs), and organic field-effect transistors (OFETs). Organic electronics are favorable to these three applications because organic materials can be designed to have specific properties, such as band gap. Studying the design of organic molecules and how small changes in structure, such as changes in side chains, change the optical and electronic properties, helps to expand the versatility of organic electronics in all these applications. In this chapter, I will focus on how organic molecules can be used in OFETs.

Organic Field Effect Transistors

One well known semiconducting polymer is poly(3-hexylthiophene) (P3HT). P3HT has excellent solubility and therefore is easy to solution process into thin films, a feat that is not

always easy for many organic small molecules and polymers (just ask the grad students in the Wei You group). Because of this, a large amount of research has gone into the development and improvement of P3HT transistors over the last 25 years. Early studies on P3HT show the importance of the microcrystalline domains of P3HT films on the mobility.[2] Sirringhaus *et al.* reported that the microstructure of P3HT on a surface was dependent upon the molecular weight, regioregularity and deposition conditions of the P3HT. By using this, they were able to induce an edge on structure of the P3HT core in relation to the substrate, which improved the mobility by 3 orders of magnitude. This illustrates the importance of the crystal structure and the deposition technique used when making films of organic semiconductors.

In the realm of small molecule organic semiconductors, pentacene is one of the most studied. The crystal structure of pentacene provides favorable overlap between adjacent units, which leads to a large carrier mobility. But, pentacene also easily oxidizes in air which causes a disruption of the favorable crystal structure and a reduction in the π conjugation of the system. These changes gradually reduce the mobility over time.[3] Because pentacene showed such a promising mobility, routes to make the molecule more solution processable and more stable while still having the favorable π stacking interactions were explored. John Anthony and co-workers looked into ways to functionalize pentacene and study how this effected the electronic properties. They synthesized triisopropylsilyl pentacene (TIPS-pentacene), which adds to long organic chains to either side of the pentacene backbone. When using this in a solution processed thin film transistor, they were able to get mobilities as high as 1.5 cm^2/Vs. Adding these bulking side chains to the pentacene backbone helped to encourage a favorable π-

stacked structure in the films.[4] This shows the positive effect adding side chains can have on small molecule organic semiconductors.

TES-ADT

One small organic molecule that has been frequently studied for use in OFETs is bis(triethylsilylethynyl) anthradithiophene (TES-ADT). TES-ADT is solution processable and has shown favorable mobilities for an organic compound on the order of 0.1 cm^2/Vs.[5] Further, it has been shown that fluorination of TES-ADT can lead to even higher OFET mobility on the order of 1 cm^2/Vs.[6] TES-ADT also has the potential to be used to flexible electronics.[7] Since TES-ADT has been so widely research for OFETs, it is a good starting point to finding other small molecules that have favorable electronic properties.

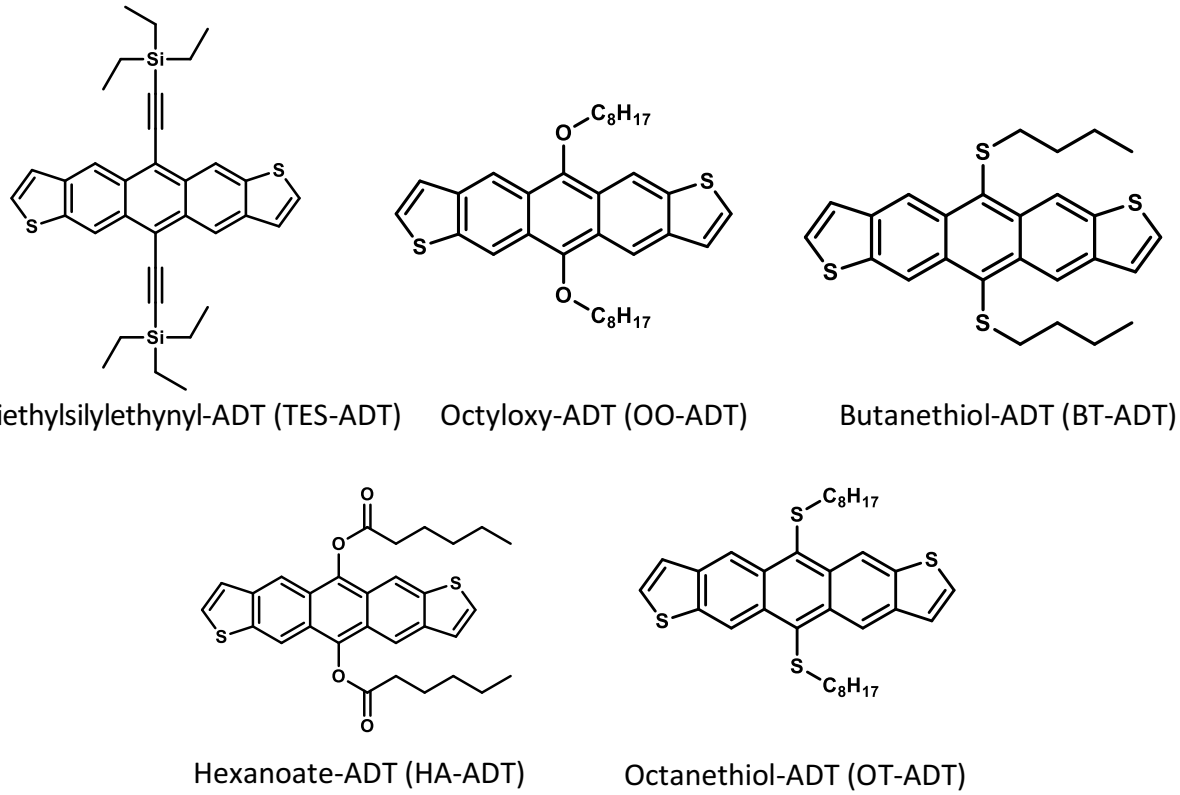

Triethylsilylethynyl-ADT (TES-ADT) Octyloxy-ADT (OO-ADT) Butanethiol-ADT (BT-ADT)

Hexanoate-ADT (HA-ADT) Octanethiol-ADT (OT-ADT)

Figure 4.1: Structures of TES-ADT and derivatives

Structures of the small molecules used in this study.

Results and Discussion

This chapter will focus on looking at the electronic properties of derivatives of the small molecules TES-ADT. These derivatives were all synthesized by David Dirkes of the You group and are shown in **Figure 4.1**. While these molecules were originally synthesized to look at the singlet fission properties, the favorable electronic properties of TES-ADT led us to believe that these other derivatives may also be able to be used in OFETS. In this chapter, I will describe the film formation and electronic properties of these small molecules.

OFET Fabrication

The first challenge to making transistors out of these small organic molecules was finding a way to fabricate films of these molecules. For the transistors, all films were fabricated on Si/SiO_2 substrates with 300 nm of SiO_2. Depending on the sample, Ti/Au drain and source contacts were thermally evaporated before or after thin film deposition. Different methods were tried to fabricate thin films including spin coating, drop casting, and blade-coating. The morphology of the organic film can have a large effect on the electronic properties which is why different methods were used to try and produce the best overall morphology.[8] Overall, spin coating and blade coating created the best films. The OFETs were testing using a probe station with a Keithley 2636b. Measurements were done in the dark because some of the molecules used have been shown to degrade in light.

TES-ADT OFETs

First, we fabricated transistors using TES-ADT. TES-ADT transistors have previously been made using spin-coating, so that is the method I used. First, a 20 mg/mL solution of TES-ADT in toluene was made and heated at 80 °C. The solution was filtered with a 0.45 μm filter and was spun cast at 3000 rpm for 1 minute onto a Si/SiO_2 with gold source-drain contacts already deposited. **Figure 4.2** shows microscope images of the TES-ADT spin coated film. The material fully covered the surface of the substrate, which was favorable for transistor fabrication.

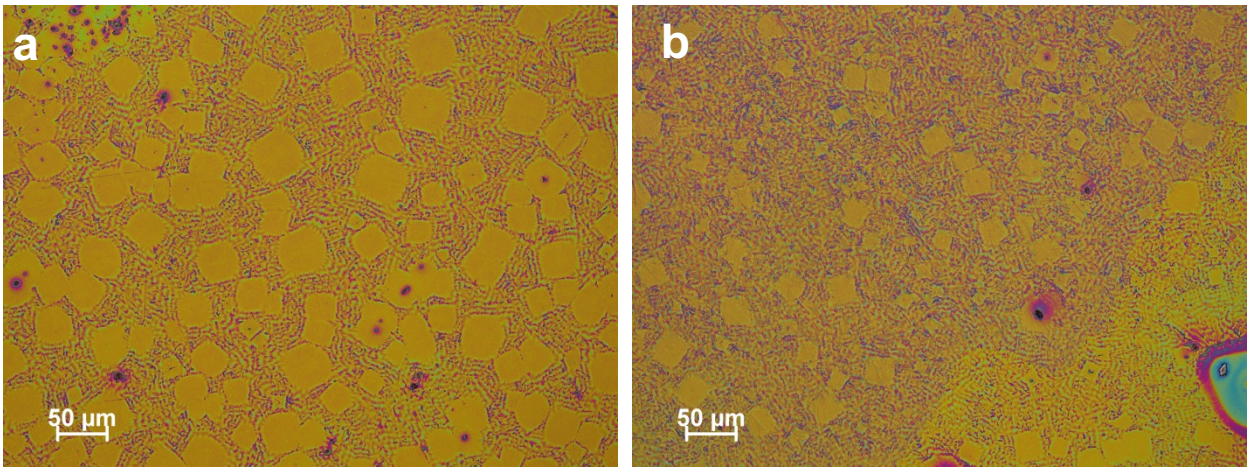

Figure 4.2: Microscope images of TES-ADT films

a) Microscope picture of a TES-ADT film made by spin coating. b) Microscope picture of a different area of a TES-ADT film made by spin coating.

The OFETs made from TES-ADT were then tested to find the field-effect mobility and on/off ratio. The transfer curves in **Figure 4.3** show that the molecule is indeed p-type, which was expected. By using these results, the mobility was found to be 0.02 cm^2/Vs and on/off ratio was 10^4. These results are somewhat lower than the previously reported TES-ADT results reported earlier, but the fabrication here did not use any surface treatment or solvent annealing that is normally used for TES-ADT transistors. Here, I wanted to see how the TES-ADT

performs when using the fabrication setup of the You group and I wanted to create a basic baseline to compare to the other molecules that were tested.

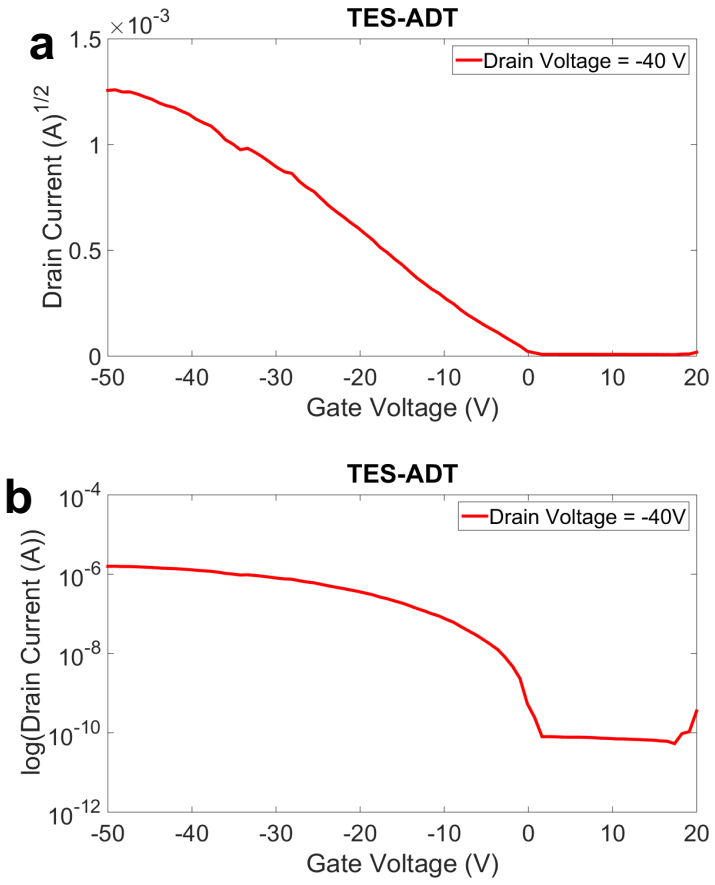

Figure 4.3: Electronic measurements of TES-ADT transistors

a) Transfer curve of TES-ADT OFET. b) Log plot of TES-ADT OFET.

BT-ADT OFETs

The next molecule used was butanethiol-ADT (BT-ADT). For this molecule, the same spin-coating conditions as TES-ADT were used. For most molecules tested in this chapter, the spin-coating conditions used for TES-ADT were tried first. For some, like the BT-ADT, consistent films were able to be fabricated. For others, more conditions needed to be tried. **Figure 4.4** shows microscope images of the films made using BT-ADT. Similarly to TES-ADT, the films fully

coat the substrate. But, the BT-ADT films have a swirling look to them under the microscope. This suggests that the packing of the molecules is different compared to the TES-ADT films.

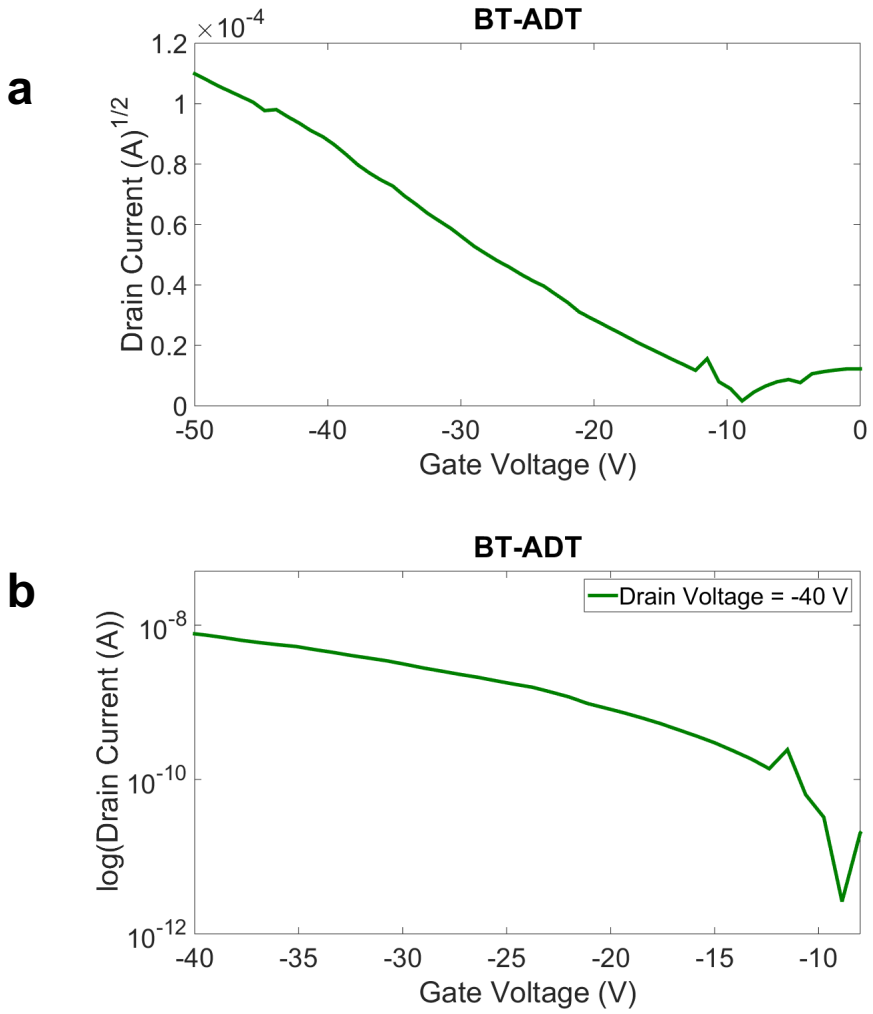

Figure 4.4: Electronic measurements of BT-ADT transistors

a) Transfer curve of BT-ADT OFET. b) Log plot of BT-ADT OFET.

Even though the BT-ADT films were consistent and fully covered the active area of the transistor, the electronic properties were not as good as the TES-ADT transistors. **Figure 4.5** shows the transfer curves for the OFETs made using BT-ADT. For these curves, the current was much lower than the TES-ADT curves. Further, the mobility calculated for BT-ADT was 2.9 x 10^{-4} cm^2/Vs and the on/off ratio was 10^3. The low mobility was initially discouraging but the fact

that the molecules are conductive and do indeed produce transistor-like behavior is promising. Changing the fabrication techniques for transistors such as adding solvent vapor annealing has been shown to raise the mobility.[5] This initial result of conductivity in BT-ADT is a good starting point for improving the electronic properties in the future.

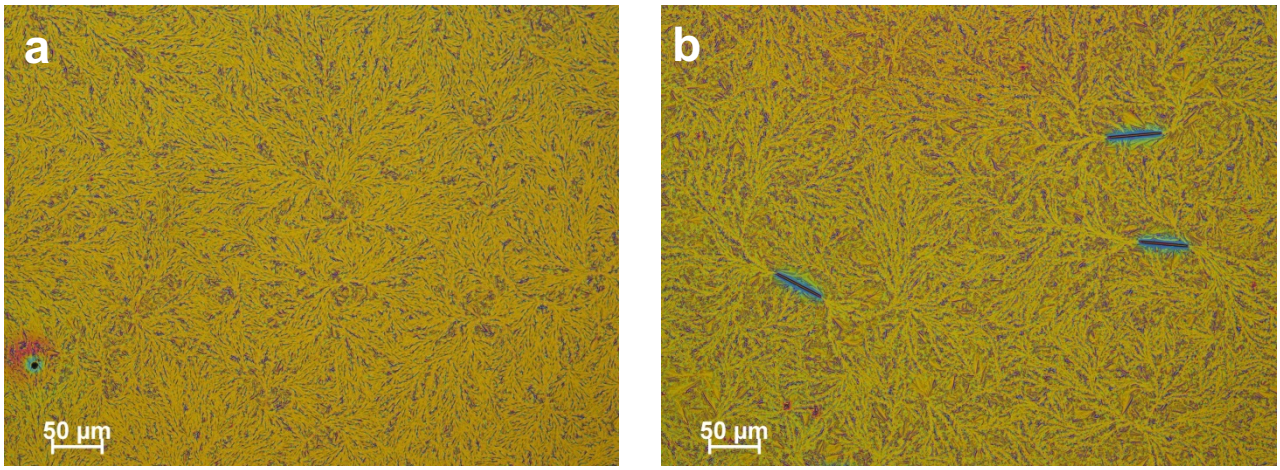

Figure 4.5: Microscope images of BT-ADT films

a) Microscope picture of a BT-ADT film made by spin coating. b) Microscope picture of a different area of a BT-ADT film made by spin coating.

OO-ADT OFETs

Next, films of octyloxy-ADT (OO-ADT) were fabricated. The same conditions as for TES-ADT were again used. This time, the films did not look as smooth of as consistent as the previous two experiments. **Figure 4.6** shows microscope images of the spin-coated films. The microscope images show that the films do not completely cover the surface. The smaller blue areas seen are the underlying SiO_2. Further, the morophology of the films is much different than the TES-ADT and the BT-ADT films. The OO-ADT films are made up of many needle-like crystals in very close proximity to each other.

The OO-ADT transistors were fabricated in two different ways. For one transistor, a top contact configuration was used where the gold contacts were evaporated after the film was

deposited. The other transistor used the bottom contact configuration, where the gold contacts were first evaporated onto the Si/SiO_2 substrate and then the film was deposited. Using two different configurations helps to see if one configuration greatly improves the electronic properties.[9–12]

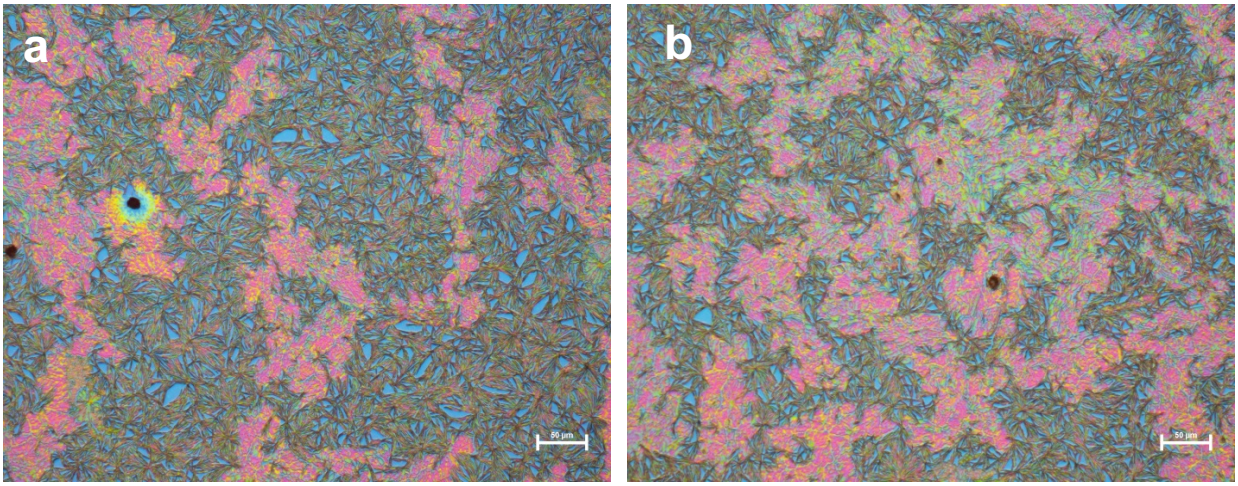

Figure 4.6: Microscope images of OO-ADT films
a) Microscope picture of a OO-ADT film made by spin coating. b) Microscope picture of a different area of a OO-ADT film made by spin coating.

Figure 4.7 shows the transfer curves for both top contact and bottom contact transistors made with OO-ADT. The current is slightly different for each, but that is due to the different channel length and width used for each. This was done to see how much of an effect different channel length and width have on the final transistor measurements. When calculating the mobility, the channel length and width is used and therefore using different channel lengths and width for each should not have a large effect on the final mobility. The top contact OO-ADT transistors had a mobility of 2.8×10^{-4} cm^2/Vs and an on/off ratio of $\sim 10^{2.5}$. The bottom contact OO-ADT transistors had a mobility of 1.2×10^{-4} cm^2/Vs and an on/off ratio of $\sim 10^3$. Even though the transfer curves for the OO-ADT transistors have normal transistor characteristics, the mobility is still low. Further, doing top contact or bottom contact makes not

noticeable difference in the electronic properties. Even though the mobility is low, there are already obvious places for improvement. One opportunity for improvement is improving the film quality to coat the whole channel evenly. This could be done by changing the solvent or deposition method.

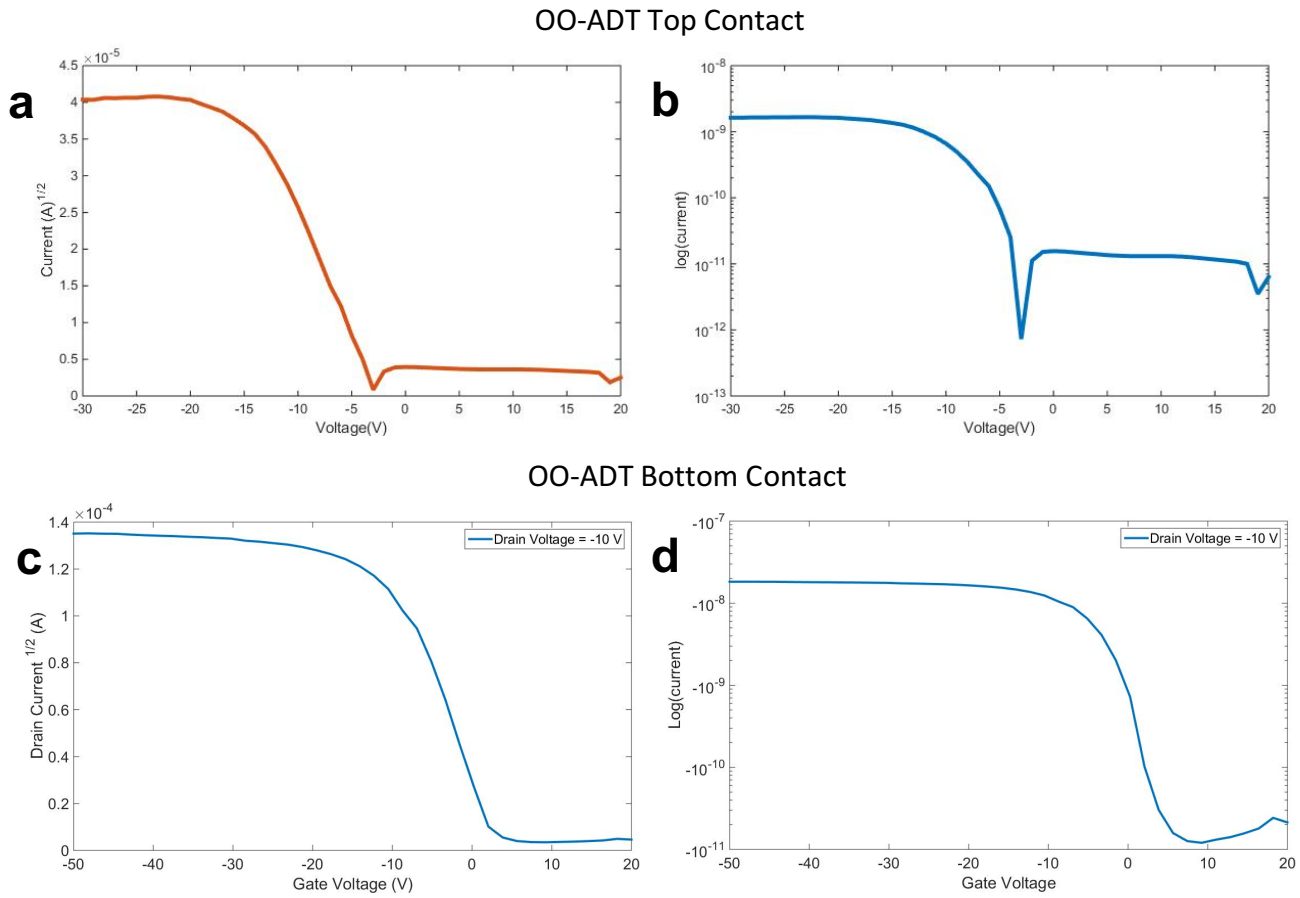

Figure 4.7: Electronic measurements of OO-ADT transistors

a) Transfer curve of top contact OO-ADT OFET. b) Log plot of top contact OO-ADT OFET. c) Transfer curve of bottom contact OO-ADT OFET. d) Log plot of bottom contact OO-ADT OFET.

OT-ADT OFETs

With the large number of ADT derivatives tested in this study, it was not surprising that some of the derivatives just did not work. One such material was the octylthiol-ADT (OT-ADT).

This molecule is very similar to the BT-ADT discussed earlier, with the only different being that the OT-ADT has an 8 carbon sidechain while the BT-ADT has a 4 carbon sidechain. Since the electronic properties of the BT-ADT were able to be measured, it was expected that the OT-ADT would also be able to be measured. Films were made using the same conditions as the TES-ADT transistors. Initially, the films looked like they coated the whole surface of the substrate. Therefore, the transistors were tested but the tests yielded no viable results. No mobility or on/off ratio could be found for the OT-ADT transistors.

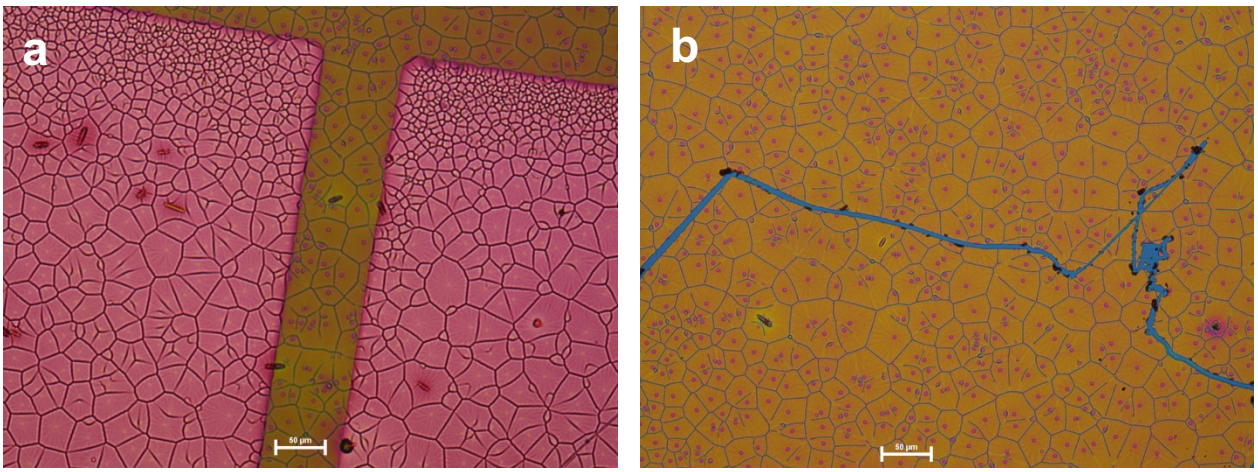

Figure 4.8: Microscope images of OT-ADT films

a) Microscope picture of a OT-ADT film made by spin coating. The pink rectangle is where the film coats the gold contact. b) Microscope picture of a different area of a OT-ADT film made by spin coating. Scale bara is 50 μm.

Upon closer examination of the OT-ADT films, it was seen that the film was not actually uniform. The film formation was made up of many small islands that were separated by what was assumed to be large grain boundaries. **Figure 4.8** shows microscope images of the OT-ADT films. The small islands can be seen in between the gold contacts. Since no electrical current was able to be detected from these devices, it is assumed that the boundaries between these islands inhibit any electrical transport between the contacts.

HA-ADT OFETs

The hexanoate-ADT (HA-ADT) films also presented a challenge in creating a uniform film. When using the same spin coating conditions as the TES-ADT transistors, the HA-ADT film created was very sparse and made up of individual crystals and not a uniform film. **Figure 4.9a** shows how the spin-coated films looked. Even with trying different spin speeds, the films still were not uniform. Next, drop coasting was attempted with HA-ADT. Drop coasting has been previously used to create TES-ADT and TIPS-pentacene transistors. [7,13] **Figure 4.9b** shows the drop-casted films on a bottom-contact transistor substrate. Drop casting created large square-needle like crystals on the substrate. Some of these crystals did span the whole channel so electrical measurements were attempted. These transistors produced a very low mobility of 3.3 x 10^{-5} cm^2/Vs. Even though the electrical measurements were poor, the fact that some mobility could be measurement from a visibly poor film suggested that the HA-ADT could make a good transistor if only good, consistent films were able to be made.

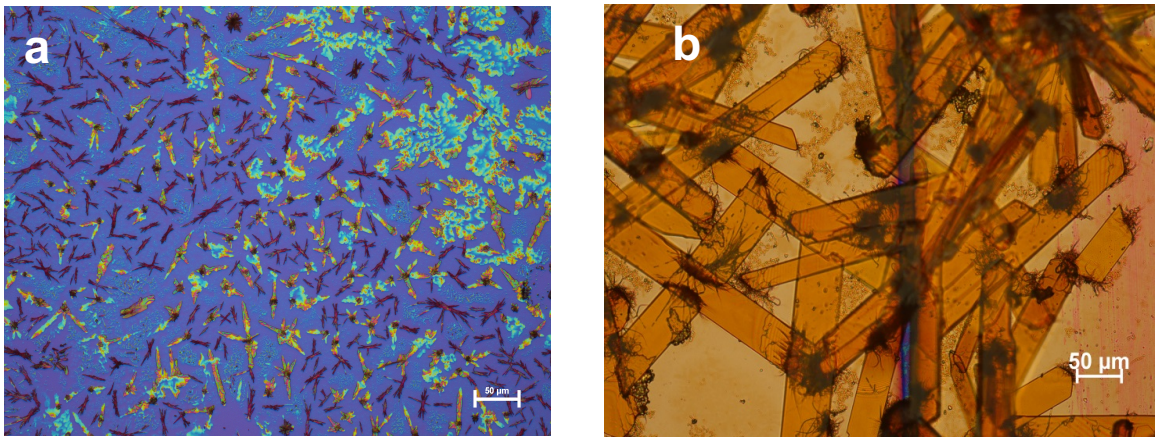

Figure 4.9: Microscope images of HA-ADT films

a) Microscope picture of a HA-ADT film made by spin coating. b) Microscope picture of a HA-ADT film made by drop casting. Scale bar is 50 µm.

To attempt to get better films, blade coating was tried next. A custom build blade coater made by Dr. Mary Allison Kelly, a recent graduate of the You group, was used.[14] Figure 4.10 shows images of the whole substrate and a close-up microscope view of films of HA-ADT made with blade-coating. These films look vastly different than both the spin-coating and drop coast films discussed earlier. The blade coated films do not show any large crystals, but instead coated the whole surface of the substrate.

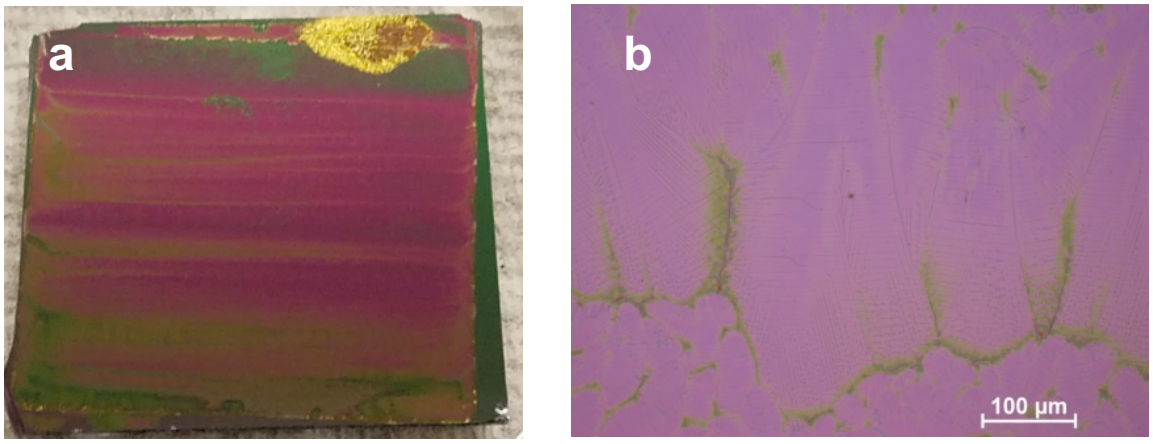

Figure 4.11: Images of HA-ADT films made with blade-coating

a) Picture of a HA-ADT film made by spin coating. b) Microscope picture of a HA-ADT film made by spin coating.

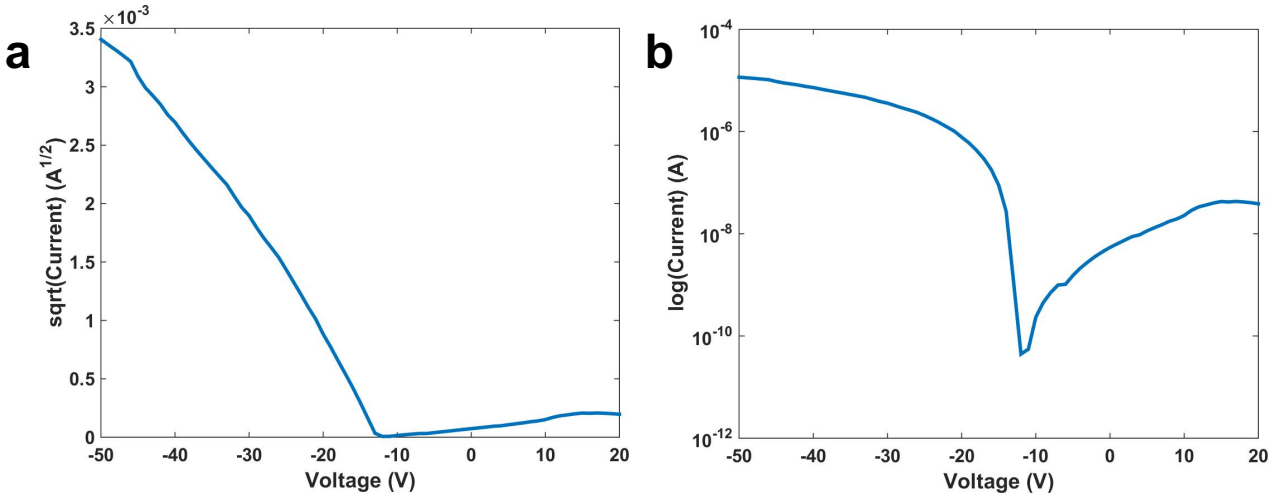

Figure 4.10: Electronic measurements of HA-ADT transistors

a) Transfer curve of HA-ADT OFET. b) Log plot of HA-ADT OFET

Blade-coating was then used to deposit HA-ADT films on bottom contact substrates. The electronic properties of these films were the best of any of the previous films tested. The mobility was 0.69 cm^2/Vs and the on/off ratio was 10^4. This mobility was even higher than the initial TES-ADT films tested. This was a very promising result towards using ADT derivatives in future organic electronics applications. Further, it shows the importance of film formation and morphology on the electronic properties of organic materials. By improving the film consistency, the mobility was greatly improved.

Conclusion

The fabrication of OFETs of small molecule ADT derivatives shows promising results for future applications using these molecules. Future work could include using blade coating to deposit films of all the derivatives discussed to see how this changes the film formation and the electronic properties.

REFERENCES

(1) Cui, Z.; Zhou, C.; Qiu, S.; Chen, Z.; Lin, J.; Zhao, J.; Ma, C.; Su, W. *Printed Electronics: Materials, Technologies and Applications*; Wiley, 2016.

(2) Sirringhaus, H.; Brown, P. J.; Friend, R. H.; Nielsen, M. M.; Bechgaard, K.; Langeveld-Voss, B. M. W.; Spiering, A. J. H.; Janssen, R. A. J.; Meijer, E. W.; Herwig, P.; de Leeuw, D. M. Two-Dimensional Charge Transport in Self-Organized, High-Mobility Conjugated Polymers. *Nature* **1999**, *401* (6754), 685–688.

(3) Klauk, H. Organic Thin-Film Transistors. *Chem. Soc. Rev.* **2010**, *39* (7), 2643.

(4) Anthony, J. E.; Brooks, J. S.; Eaton, D. L.; Parkin, S. R. Functionalized Pentacene: Improved Electronic Properties from Control of Solid-State Order [20]. *J. Am. Chem. Soc.* **2001**, *123* (38), 9482–9483.

(5) Dickey, K. C.; Anthony, J. E.; Loo, Y.-L. Improving Organic Thin-Film Transistor Performance through Solvent-Vapor Annealing of Solution-Processable Triethylsilylethynyl Anthradithiophene. *Adv. Mater.* **2006**, *18* (13), 1721–1726.

(6) Subramanian, S.; Sung, K. P.; Parkin, S. R.; Podzorov, V.; Jackson, T. N.; Anthony, J. E. Chromophore Fluorination Enhances Crystallization and Stability of Soluble Anthradithiophene Semiconductors. *J. Am. Chem. Soc.* **2008**, *130* (9), 2706–2707.

(7) Yi, H. T.; Payne, M. M.; Anthony, J. E.; Podzorov, V. Ultra-Flexible Solution-Processed Organic Field-Effect Transistors. *Nat. Commun.* **2012**, *3* (May), 1259.

(8) Locklin, J.; Bao, Z. Effect of Morphology on Organic Thin Film Transistor Sensors. *Anal. Bioanal. Chem.* **2005**, *384* (2), 336–342.

(9) Ishikawa, Y.; Wada, Y.; Toyabe, T. *Origin of Characteristics Differences between Top and Bottom Contact Organic Thin Film Transistors*; 2010; Vol. 107.

(10) Cosseddu, P.; Bonfiglio, A. A Comparison between Bottom Contact and Top Contact All Organic Field Effect Transistors Assembled by Soft Lithography. *Thin Solid Films* **2007**, *515* (19), 7551–7555.

(11) Oh, S.; Baeck, J. H.; Shin, H. S.; Bae, J. U.; Park, K. S.; Kang, I. B. Comparison of Top-Gate and Bottom-Gate Amorphous InGaZnO Thin-Film Transistors With the Same SiO_2/a-

InGaZnO/SiO_2 Stack. *IEEE Electron Device Lett.* **2014**, *35* (10), 1037–1039.

(12) Mittal, P.; Kumar, B.; Negi, Y. S.; Kaushik, B. K.; Singh, R. K. Channel Length Variation Effect on Performance Parameters of Organic Field Effect Transistors. *Microelectronics J.* **2012**, *43* (12), 985–994.

(13) Kim, C. S.; Lee, S.; Gomez, E. D.; Anthony, J. E.; Loo, Y. Solvent-Dependent Electrical Characteristics and Stability of Organic Thin-Film Transistors with Drop Cast Bis(triisopropylsilylethynyl) Pentacene. *Appl. Phys. Lett.* **2008**, *93* (10), 103302.

(14) Kelly, M. Fundamental Studies of Ternary Blends for Bulk Heterojunction Solar Cells, University of North Carolina at Chapel Hill, 2017.

Chapter 5: Melt Infiltration Approach to the Fabrication of Mixed Cation 2D Perovskites

Perovskite solar cells (PSCs) have seen a rapid rise to fame in a very short period of time. Reported efficiencies have gone from around 12% in 2010 to over 22% in 2017 (Figure 1.1). Researchers from around the world have jumped on the chance to study this promising material and new discoveries and advances in perovskite solar cell researching are happening all the time.

The typical optimistic first year graduate student may look at these facts and say, "Wow! Over 20% efficiency in only 5 years. That's amazing!". And frankly, it is pretty amazing. But, the typical cynical fifth year graduate student may look at this and ask, "What's the catch?". The answer to this question leads to a major problem in current perovskite solar cell research: stability. PSCs suffer from degradation when exposed to environment factors such as light, air, heat, and humidity.[1] This presents an obvious problem since a solar cell is meant to be outside, under a shining sun. Solutions to this problem are already in motion but more can still be done. Some things can help to improve PSC stability are studies in the formation and degradation mechanism of perovskite films, new materials that can be substituted into the champion methylammonium lead iodide perovskite, and ways to encapsulate solar cells. In this chapter, I will report on a mixed cation layered perovskite material and present a melt infiltration method to fabricating films of mixed cation perovskites.

Inorganic-Organic Hybrid Perovskites

The name perovskite comes from the name of the crystal structure. A material is called a perovskite if it has a crystal structure like the mineral $CaTiO_3$. Perovskites were given their name by Gustav Rose in 1839 to honor Count Lev Alekseevich Perovski, who was a key player in the development of the mining industry in Russia and also a mineral collector.[2] Nowadays, the term perovskite is used to refer to materials that have the ABX_3 structure. For the inorganic-organic hybrid perovskites talked about there, the "A" is typically an organic cation, such as methylammonium (CH_3NH_3). The "B" is a metal, such as Pb or Sn and the "C" is a halogen, most commonly Cl, I, or Br.

The most common perovskite used is PSCs today is the methylammonium lead iodide ($MAPbI_3$) perovskite. This material mirrors the ABX_3 structure (figure) and is often referred to as a 3D perovskite. Over the past 5 years, perovskites with 3D structures have seen a huge increase in PCE when used in solar cells from 9% to over 20%.[3] Many of these solar cells suffer from the stability problems mentioned earlier. A large portion of current research in perovskite solar cells looks at understanding the fundamentals of perovskites and looking into ways to improve the stability. Other research in perovskite solar cells looks at using different anions and cations to make the perovskites and how to change the perovskite structure.[4]

2D Perovskites

One subset of perovskites are known as 2D perovskites. These perovskites are not 2D in the sense of the 2D materials discussed in Chapter 2 and 3. While the 2D materials are called 2D because of their thinness, 2D perovskites are known as 2D because their structure is composed of 2D-like sheets. One initial 2D perovskite is the butylammonium lead iodide ($BAPbI_4$)

perovskite that has been intensely studied by Mitzi *et. al.*[5] Other kinds of 2D perovskites are mixed cation 2D perovskites. These perovskites commonly incorporate two different cations, such as butylammnoium (BA) and methylammonium (BA), in different ratios to create the final structure. In this structure, the MA cation and the PbI_2 form layers of the 3D octahedral perovskite structure and the BA cation acts as a space between these layers. The thickness the 3D layers determine the final structure and properties of the perovskites. For examples, if the MA and PbI_2 form a layer than is equivalent to two until cells thickness, the peroskite is informally called n=2, and so on for n=3 and n=4 layer numbers. 2D mixed perovskites using BA and MA have been shown to be more stable than the 3D $MAPbI_3$ perovskite and solar cell efficiency around 12.5% has been reported.[6,7] While there is still much to be studied about 2D mixed cation perovskites, one potential area of study is how can the structure and composition of the perovskites be controlled?[8] In this Chapter, I present a melt infiltration method to make films of different layer numbers of these mixed cation perovskites. Further, I will more deeply look into the formation of these perovskites over time.

Deposition Techniques to Fabrication Perovskite Films

There are many different ways to make perovskites. In generally, inorganic-organic hybrid perovskites can either first be fabricated as crystals and then into films, or be directly fabricated as films. The most simple way to make perovskite crystals just involves the mixing of the two main components. For example, to make $MAPbI_3$, one can mix methylammonium iodide with lead iodide and dissolve in a solvent such as DMF. The solvent can be evaporated to give a perovskite powder or it can be spin-coated to give a perovskite film. But, not all perovskites can be made in the same fashion because of things like differences in solubility of

components, different wetting characteristics of substrates, and the susceptibility to degradation by heat of some perovskite precursor materials. Therefore, a variety of different deposition techniques have emerged to fabrication the best perovskite films possible.

Spin-Coating Techniques for Perovskite Film Formation

One of the most widely used techniques to prepare perovskite films is spin-coating. There are two main spin-coating methods used, a one step deposition technique (**Figure 5.**1) and a two step deposition technique (**Figure 5.2**).

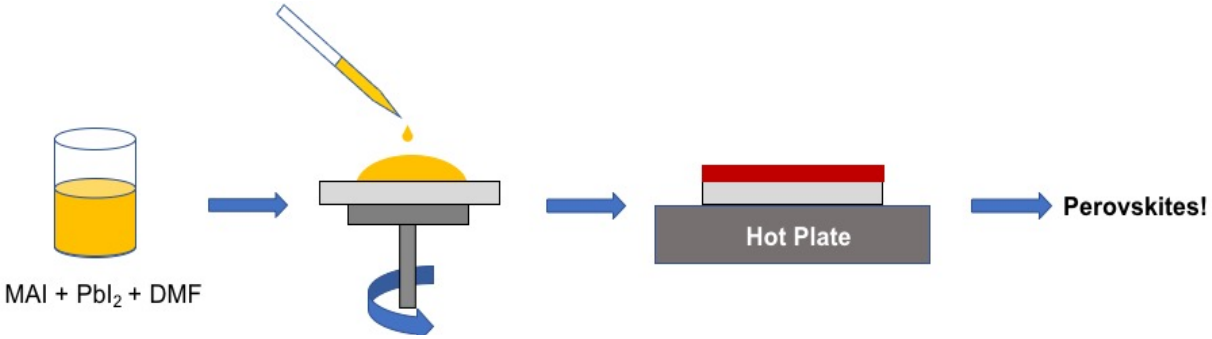

Figure 5.1: One-step spin coating approach to perovskite film fabrication
A solution of all starting components is spin-coating on the desired substrate in one step.

In a one-step deposition technique, a perovskite precursor solution Is first made. This solution should contain all necessary components to make the perovskite and should be in a solvent where all components are soluble. For example, to make $MAPbI_3$ you could mix methylammonium iodide and lead iodide in DMF or to make $BAPbI_4$ you could mix butylammonium iodide and lead iodide in DMF. After preparation of the solution and confirmation that all components have dissolved, the solution is spin-coated at a high speed and subsequently annealed to evaporate excess solvent. This procedure will then produce a perovskite film. Many small things can be changed during this process to produce differences in

film morphology or thickness such as concentration and ratio of the precursor solution, spin speed, and annealing temperature.[9]

The two-step deposition technique typically begins with first making a PbI_2 film. This film is made by making a solution of PbI_2 in DMF, followed by spin coating this solution on a substrate and then annealing the PbI_2 film. Then, a solution of the organic salt (i.e. MAI, BAI, PEAI) is made in a different solvent, such as IPA. This solution is then spin-coated on top of the PbI_2 film and annealed to create the final perovskite film.[10] An advantage of the two-step deposition technique is there is no need for a solvent that can dissolve all components, which is sometimes hard to find.

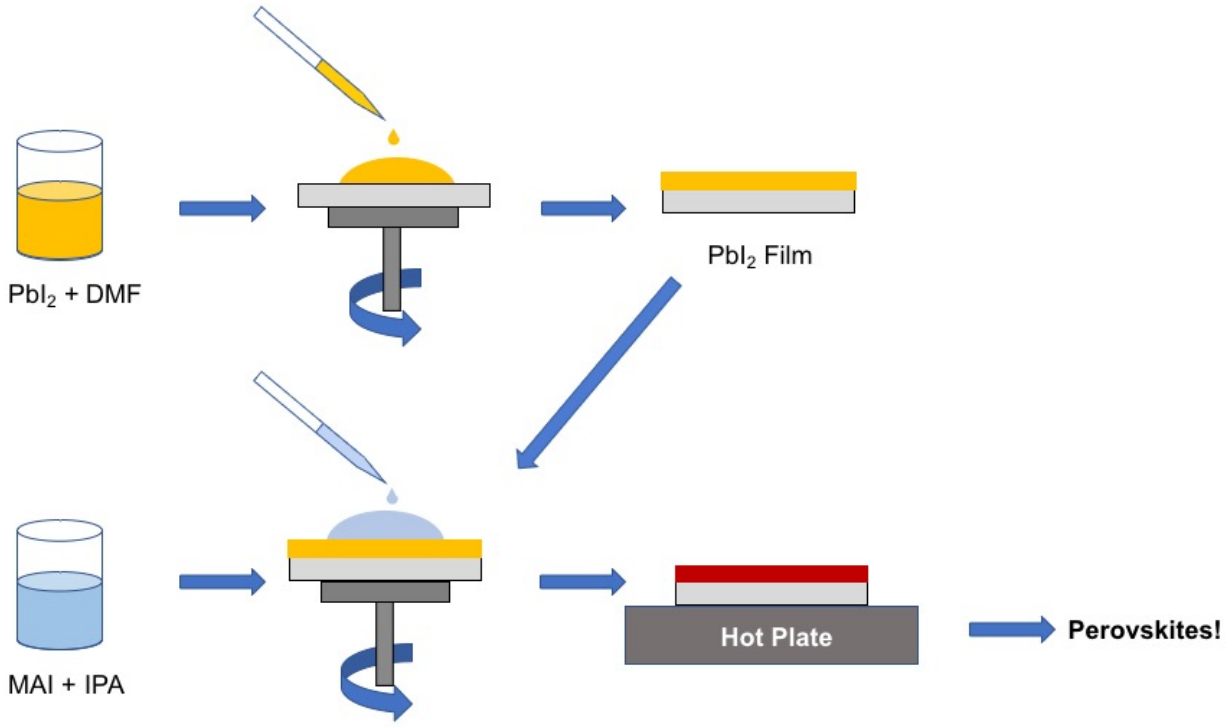

Figure 5.2: Two-step spin coating approach to perovskite film fabrication
In the two step approach, the PbI_2 film is fabricated first. Then, the desired cation is spin coated on top of the pre-made PbI_2 film.

Thermal Evaporation Techniques for Perovskite Film Formation

Perovskite films can also be made using thermal evaporation techniques. For example, a dual-source vacuum deposition technique can be used to fabricate thin films of $MAPbI_3$ perovskites. In this process, MAI and PbI_2 are simultaneously thermally evaporated from different sources onto a substrate.[11] Advantages of this process is it can produce uniform films where the thickness can easily be controlled. Also, the solubility of the components does not matter. On the downside, not all perovskites can survive the conditions needed to do this evaporation and a specialized (sometimes expensive) set up is needed.

Mitzi *et al.* development a different evaporation method that uses a single source thermal ablation (SSTA) technique.[12] The first step of this process is to first make a solution of perovskites, such as phenylethylammonium lead iodide ($PEAPbI_4$). These crystals are then dried on a foil, which is placed into the thermal ablation chamber. Heating up the foil causes the perovskite crystals to ablate and then reassemble on a substrate placed above the foil. Mitzi *et al.* showed that films made in this fashion are single phase and highly orientated. This process can also be used to make mixed-organic perovskites because the thermal ablation of all the components placed into the chamber happens relatively simultaneously.

Melt Infiltration Approach to Fabrication 2D layered perovskites

In order to study the formation and ion diffusion of the 2D layered perovskites, I developed a melt infiltration method to fabricate the perovskites. This method takes inspiration from both the two-step spin coating technique mentioned earlier and from a melt processing approach developed by Mitzi *et. al.*[13]

Butylammnoium Iodide Synthesis

Butylammonium iodide (BAI) was synthesized by the reaction of hydroiodic acid (HI) and *n*-butylamine. First, hydroiodic acid was purified using a 0.36 M tributylphosphate solution in chloroform. After 5 extractions, a clear HI solution was produced. Then, the HI was slowly added to a cold solution of 5 mL *n*-butylamine and 5 mL ethanol. Evaporating the solvent leads to the product, a white powder. The product was then recrystallized in a solution of diethylether and dried overnight.

One-step spin-coating method to 2D perovskite fabrication

First, a solution was prepared of BAI, MAI and PbI_2 in DMF. A 1M concentration of PbI_2 was used for all solutions. To prepare different layer numbers, a 1M concentration of the desired ratio of MAI:BAI shown in **Table 5.1** was used. The solution was stirred and heated at 70 °C. The films were spin-coated at 5000 rpm for 25 seconds and then post-annealed at 80 °C for 1 min. The whole fabricated was done in an ambient environment.

Table 5.1: Chemical formula of different mixed perovskites

Layer Number	Chemical Formula	MA:BA ratio
n=2	$BA_2MAPb_2I_7$	1:2
n=3	$BA_2MA_2Pb_3I_{10}$	1:1
n=4	$BA_2MA_3Pb_4I_{13}$	3:2
n=∞	$MAPbI_3$	1:0

Melt Infiltration approach to 2D perovskite fabrication

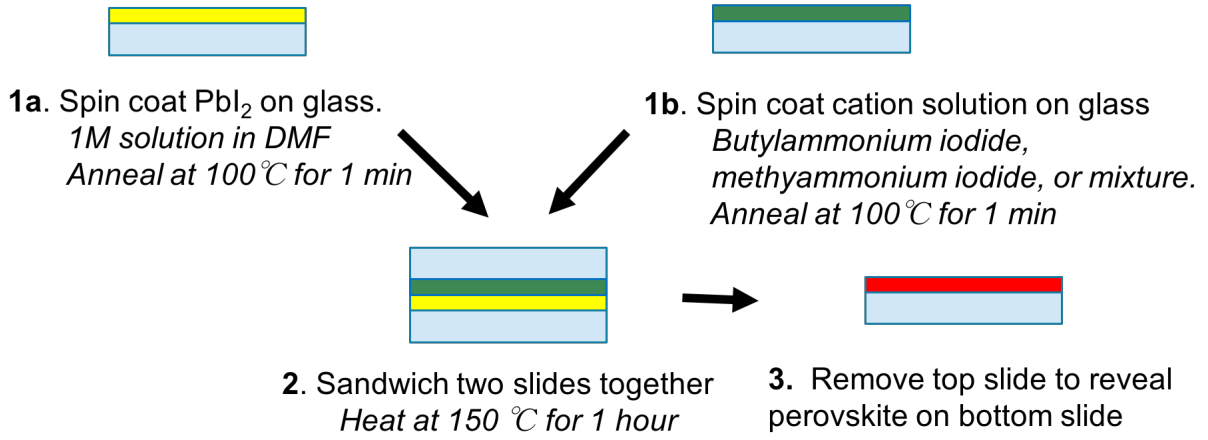

Figure 5.3: Melt Infiltration approach to fabricating perovskites

The melt infiltration approach involves first creating two separate films of PbI_2 and MAI/BAI through spin coating. Then, these films are sandwhiched together and heated to create the final perovskite film.

The melt infiltration procedure most closely resembles the common two step deposition technique used to fabricate perovskites. A schematic representation of the process is shown in **Figure 5.3**. First, a film of PbI_2 is made using a 1M solution in DMF. The solution is heated at 80 °C for 1 hour and then is spun coat onto a hot glass substrate that is heated at 100 °C for 1 min. The film is spun coat for 1 min. at 3000 rpm with a 3000 rpm acceleration. Then, the film is annealed at 100 °C for 1 min. to evaporate any residual solvent. Next, the cation film is made using a 1M solution in IPA of BA, MA or a mixture of BA and MA. This film is made in a glovebox to avoid the films absorbing too much water from the ambient environment. The same spin coating conditions of 3000 rpm with a 3000 rpm acceleration for 1 min are used and the film is annealed at 100 °C for 1 min. After all films are made, the two films are sandwiched together with the PbI_2 film on the bottom. Then, the sandwiched films are heated at 150 °C for 1 hour. The final perovskite film forms on the bottom slide and the top slide is discarded. Slight

modifications in BA:MA ratio, concentration, and final heating time were made produce different perovskite films and those results will be discussed later in this chapter.

Results and Discussion

One step spin coating method

When investigating the properties of formation of 2D mixed perovskites, it's first important to fabricate films of known layer number using a conventional one-step spin coating method. There were a few different reasons that I decided to do this. First, I wanted to test the MAI and BAI available to me to make sure that it could form perovskites and had not degraded due to moisture. Second, by making films in a conventional way, I could compare how the melt infiltration approach is different. Before beginning the melt infiltration project, I first looked into how the methyl ammonium butyl ammonium 2D mixed perovskites are usually made into films. One of the most common ways is the one-step spin coating approach mentioned earlier in this chapter (**Figure 5.1**)) I followed a procedure previously used in the You group to make MAI/BAI mixed perovskites with layer numbers equal to n=2, n=3, and n=4. Additionally, I made films of $MAPbI_3$ and $BAPbI_4$ perovskites. This helped to see how films of the different perovskites behave and get UV/Vis and XRD data to use as a comparison later in this chapter.

When spin coating layer perovskites, it is typical to use a solution containing the molar ratio of MAI:BAI that corresponds to the molar ratio of the final layer number wanted (**Table 5.1**). For example, for an n=2 perovskite the chemical formula is $BA_2MAPb_2I_7$, which gives a MA:BA ratio of 1:2. Therefore, when preparing the perovskite films with an n=2 layer number, I used a 1:2 MA:BA ratio. Similarly, I used a 1:1 ratio for n=3 and a 3:2 ratio for n=4.

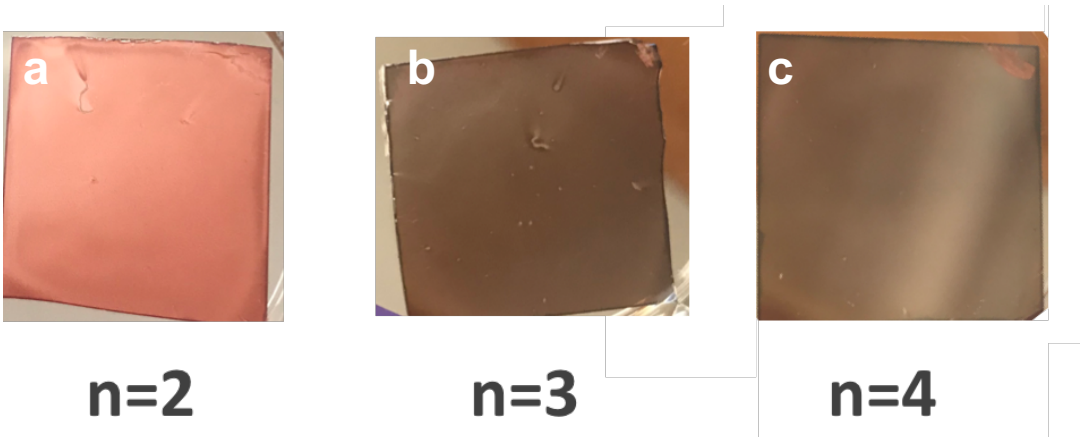

Figure 5.4: Images of spin coated mixed perovskite films

a) Film of n=2 mixed perovskite b) film of n=3 mixed perovskite c) film of n=4 mixed perovskite. All films were made using the one step spin coating method and the molecular ratios of MAI:BAI for each layer number.

After preparing the films, the first noticeable different about the different layer numbers is the color (**Figure 5.4**). An n=2 film is a pinkish color while both n=3 and n=4 are black. The 3D $MAPbI_3$ perovskite is also black while the BA_2PbI_4 perovskite is yellow. This presents an easy way to differentiate between n=2 films and other layer numbers. This difference in color manifests itself in a difference in the UV/Vis spectra for the different films. In looking at the UV/Vis spectra for the different layer numbers, different peaks can be seen (**Figure 5.5**). First, the n=2 film has a prominent peak at 569 nm. This peak corresponds to the n=2 layer number and therefore this film is predominantly the n=2 phase.[14] Now, films of 2D mixed perovskites are not typically single phase films even if the precursors ratio are intended for a single phase. Being able to produce a single phase film is not easy but single phase crystals of different layer numbers can be grown which helps gain insight into the structure and properties of perovskites with different layer numbers. This is obvious when looking at UV/Vis spectrum for both the n=3 and n=4 films. First, the film made using the molar ratio of an n=3 layer perovskite (1:1) has UV/Vis peaks at 569 and 605 nm. These peaks are known to

corresponds to n=2 and n=3 components in solution processed 2D perovskite films.[14] The n=4 film also has peaks at 569 and 605 nm and additionally has small peaks at 640 and 740 nm. The peak at 640 corresponds to the n=4 perovskite phase while the peak at 740 is the characteristic shoulder peak of the 3D perovskites $MAPbI_3$. This shows that the film made using the ratio for n=3 has characteristics from both n=2 and n=3 and the final film contains a mixture of the two different layer numbers. The n=4 perovskite produces the most peaks and is a mixture of n=2, n=3, n=4 layered perovskites along with 3D $MAPbI_3$ perovskite components. Even though the starting ratio was intended for one phase, the final films for both the n=3 and n=4 ratios produced mixed phase films.

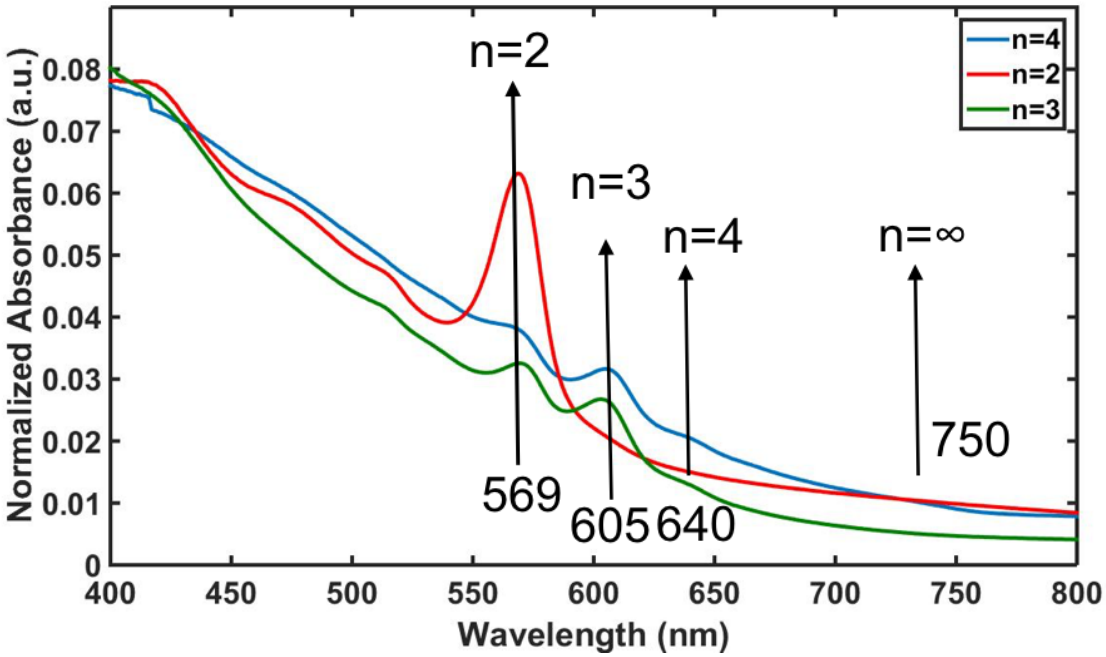

Figure 5.5: UV/Vis of spin coated mixed perovskites

The UV/Vis spectra of the spin coated perovskites show different peaks depending on the ratio used. When using the n=2 ratio (red line) there is a large peak at 569 nm. The n=3 (green line) and n=4 (blue line) ratios both shows peaks at 569 nm and 605 nm. The n=4 ratio also shows a broad shoulder at 750 nm which corresponds to the 3D perovskite.

Powder XRD of the films also gives more insight into the makeup of the solution processed spin coated films. Comparing the films to the calculated spectrum of the crystal structure of each individual layer number allows the film to be more thoroughly characterized. First, the n=2 film produces the most prominent peaks in the range between 2-12° (**Figure 5.6a**). This region can be used to easily differentiate between the n=2, n=3, and n=4 2D perovskites.[15] The two peaks seen in **Figure 5.6a** match up to the calculated peaks for a n=2 phase solution processed film. The peaks do show a slight shift which can be attributed to error in the instrument. XRD presents another useful tool for characterizing films of 2D perovskites. For the n=2 ratio film, the color, UV/Vis and the XRD all support the conclusion that the film contains the n=2 perovskite phase.

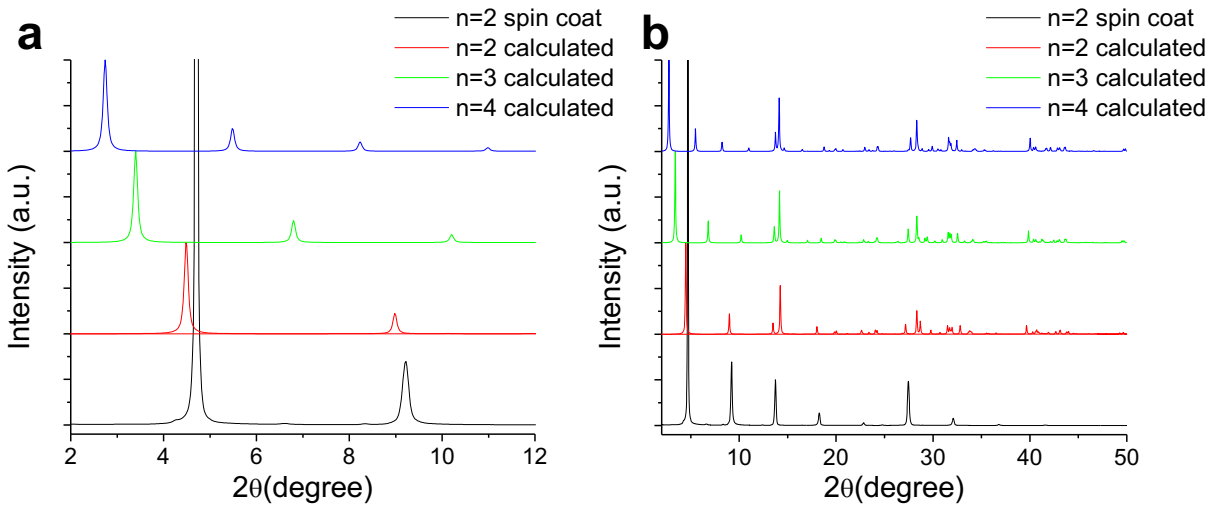

Figure 5.6: XRD spectra of n=2 spin coated perovskite films

a) The low angle region of the XRD spectrum for the n=2 spin coated films. The peaks most closely match with the calculated peaks for n=2 films. b) Full XRD spectrum for the n=2 spin coated films. Many of the higher angle peaks match with multiple of the calculated spectrum and are not useful in differentiating between different mixed perovskites.

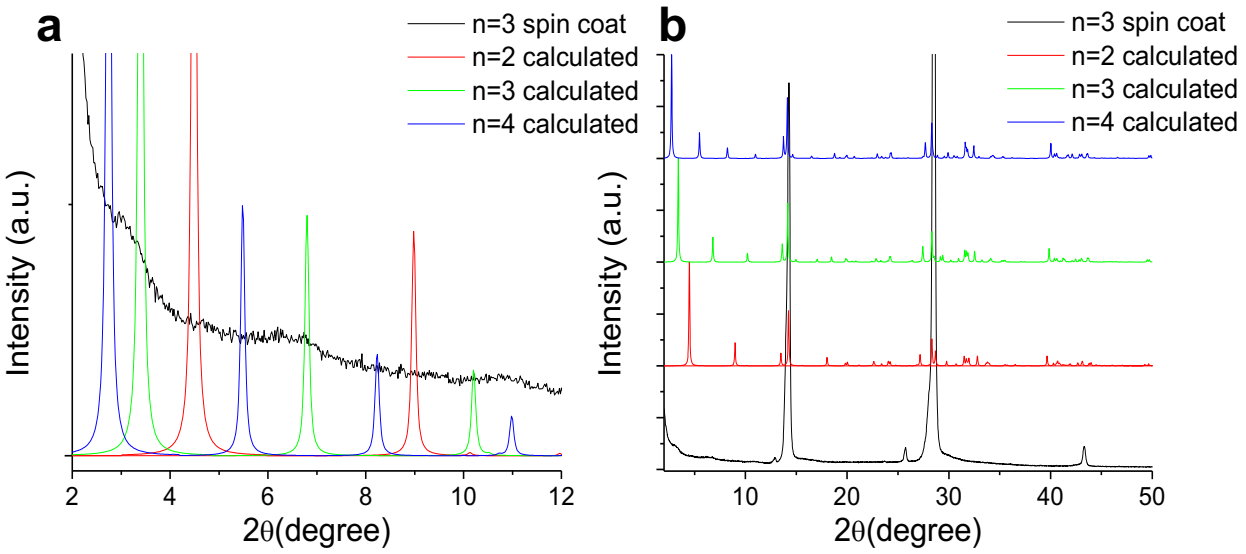

Figure 5.7: XRD spectra of n=3 spin coated perovskite films

a) The low angle region of the XRD spectrum for the n=3 spin coated films. Two broach peaks in the n=3 spectra match the n=3 calculated spectra. b) Full XRD spectrum for the n=3 spin coated films.

The XRD peaks for the n=3 and n=4 ratios are not as easy to interpret as the n=2 film. The n=3 film has a few very broad peaks in the 2-12° region (**Figure 5.7a**). The broad peak between 6-7° roughly matches up with the n=3 calculated spectrum, but it is hard to pinpoint the exact layer number present from this spectrum. Looking at the n=4 spectrum, the peaks are slightly more prominent compared to the n=3 but still are broad (**Figure 5.8a**). The peaks seen roughly match up to the n=2 and n=3 calculated spectrum. From the UV/Vis, there are both the n=2 and n=3 phases present (**Figure 5.6**). Interpretation of the XRD spectrum for the n=3 and n=4 films does not give as useful results as the n=2 film. This may be because the n=3 and n=4 films are made up of a mixture of different layer numbers with even some 3D component in the n=4, which does not lead to as crystalline a film and therefore does not give prominent XRD peaks. Overall, using the molecular ratios of the n=2, n=3, and n=4 does not lead to single phase films but does give a starting point to producing films of mixed cation layered 2D perovskites.

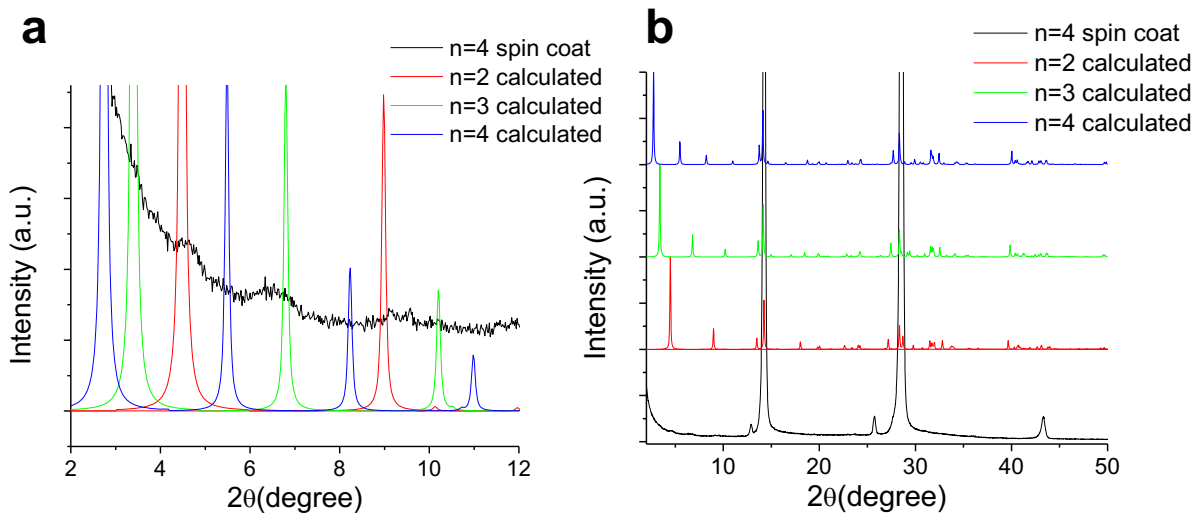

Figure 5.8: XRD spectra of n=4 spin coated perovskite films

a) The low angle region of the XRD spectrum for the n=4 spin coated films. b) Full XRD spectrum for the n=4 spin coated films.

Films of MAI and BAI

The melt infiltration process depends on having two different films of the necessary perovskite components to produce a final perovskite film. For the melt infiltration process to work properly, I first needed to fabricate films of a MAI/BAI mixture. To figure out the best conditions to make spin coated films of a MAI/BAI mixture, I first experimented with different solvent conditions. To begin, three different solvents that both MAI and BAI are soluble in were chosen; diemethylformamide (DMF), isopropyl alcohol (IPA), and n-butanol. For this experiment, a 2:1 molar ratio of MAI:BAI was dissolved in 1 mL of each solvent. The films were fabricated by spin coating at 3000 rpm for 1 min. and then drying on a 100 C hot plate for 1 min. **Figure 5.9** shows pictures of the 3 different films. The film made using n-butanol (**Figure 5.9c**) is clearly the least uniform of the 3 films and therefore n-butanol was eliminated as a

possible solvent. By closely examining the films made using DMF and IPA, the films using IPA had less aggregation and produced a more uniform film (**Figure 5.9b**). Therefore, IPA was the solvent chosen to use to make films of MAI/BAI in any further experiments.

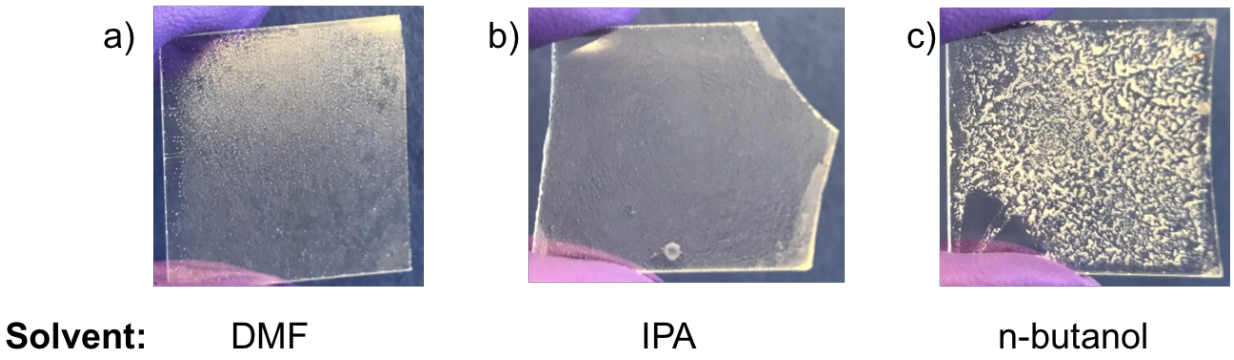

Figure 5.9: Pictures of MAI/BAI films

Spin-coated films of a 2:1 molar ratio mixture of MAI:BAI made with a) DMF, b) IPA, and c) *n*-butanol.

One interesting thig about the film formation of MAI/BAI films is that the films of the mixture are vastly more uniform than films made using just MAI or just BAI dissolved in IPA. One their own, MAI and BAI do not produce uniform films from spin coating. **Figure 5.10** shows

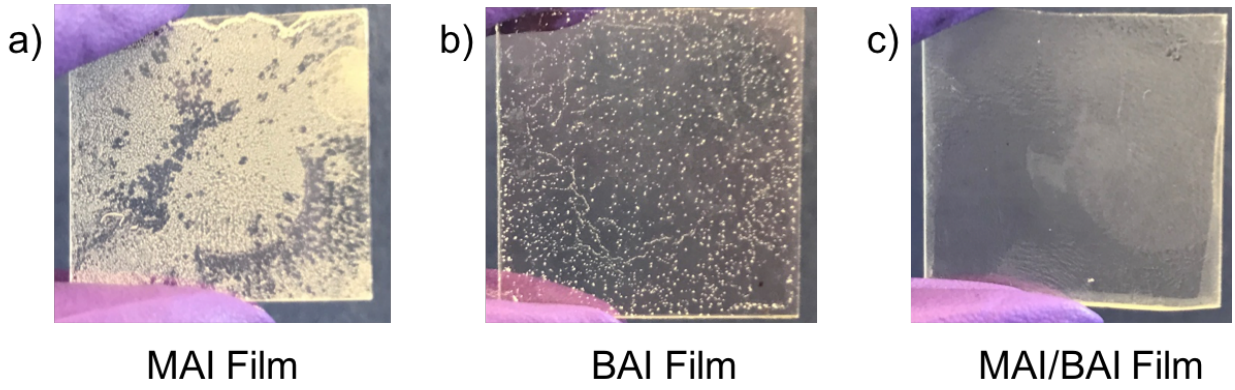

Figure 5.10: Pictures of MAI and BAI individual films

Spin-coated films of a) MAI, b) BAI, and c) a mixture of MAI/BAI. The mixture film is the most uniform of the three pictured.

that films of just MAI (**Figure 5.10a**) and BAI (**Figure 5.10b**) are not uniform but films of a mixture of MAI/BAI are uniform (**Figure 5.10c**).

Ratios of MA:BA films

When developing the melt infiltration method, I needed to spend time considering how to best make the two precursor films: the MAI/BAI film and the PbI_2 film. The first part of this is

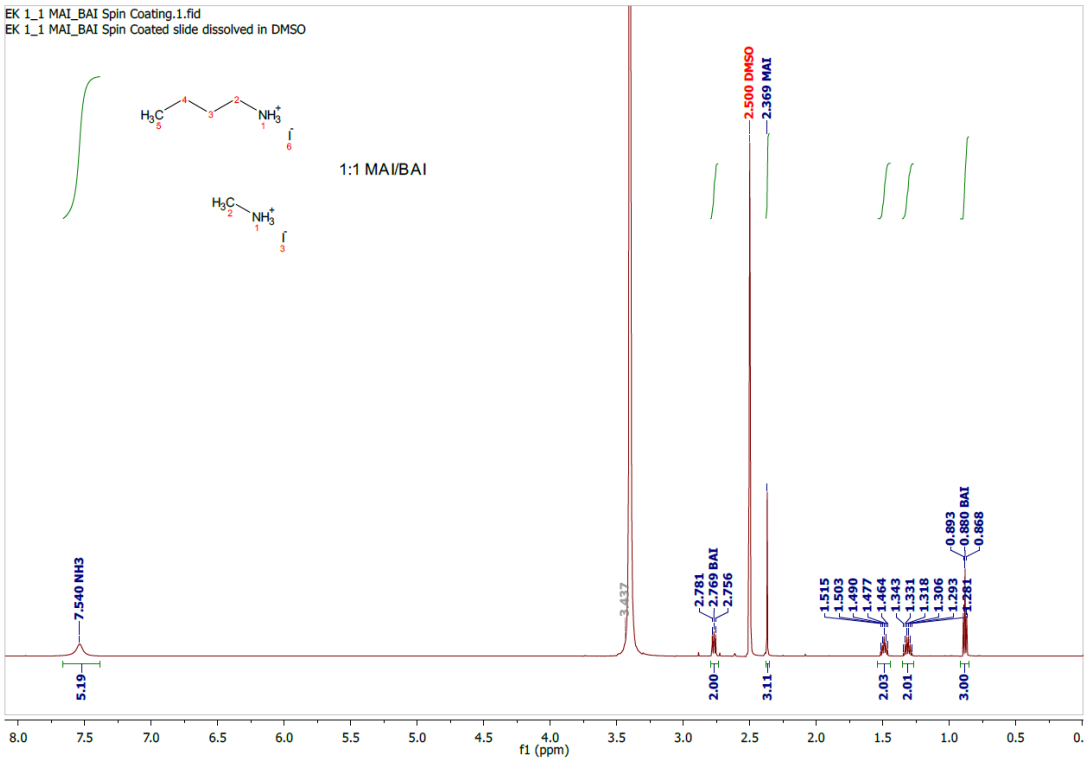

Figure 5.11: ^{1}H NMR of MAI:BAI film

The ^{1}H NMR shows that the ratio of MAI:BAI on the film after spin coating is 1:1, which is the same as the measured ratio.

mentioned above with finding the best solvent to use to make a MAI:BAI film. Next, I wanted to make sure that the ratio I measured was the same as the ratio on the spin coated film.

Since the melt infiltration method uses different ratios of MAI:BAI to produce different layer numbers of perovskites, I needed to make sure that the ratio measured matched the ratio on the MAI/BAI film. To do this, I used H^{1}NMR to calculate the ratio of MAI to BAI after film

preparation by dissolving the spin coated film in deuterated DMSO. Doing this with a 1:1 MAI:BAI film confirmed that the ratio after spin coating was still 1:1. (**Figure 5.11**) The $-CH_3$ group of the BAI has a triplet at 0.88 ppm. The $-CH_3$ of the MAI has a singlet at 2.369 ppm. By integrating these two areas, the ratio of MAI:BAI is 3.11:3.00 or 1.03:1.00. This is very close to the wanted 1:1 ratio.

I also used XRD to characterize the MAI:BAI films. Comparing XRD spectra of the films of just BAI and just MAI to the film of the mixture shows that the mixture film possesses attributes of both films (**Figure 5.12a**). The XRD spectrum was also used to compare to the XRD of the final perovskite films to see if any bulk MAI or BAI was present in the films. Similarly, the PbI_2 films were characterized with XRD (**Figure 5.12b**). PbI_2 has a large XRD peak at 12.6 °.

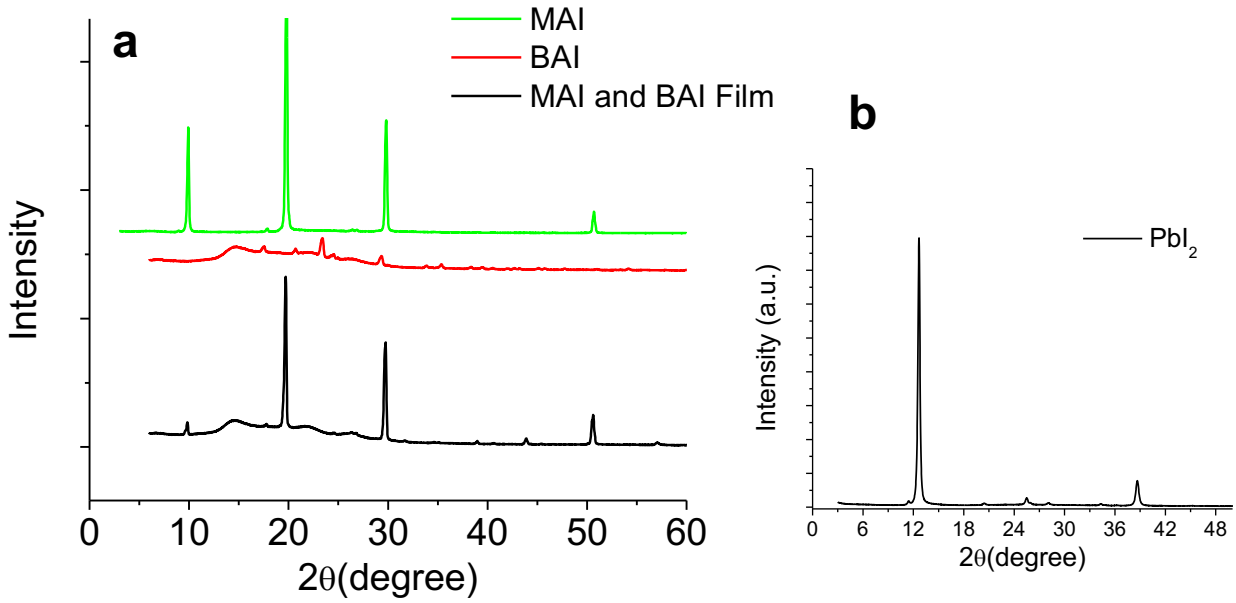

Figure 5.12: XRD Spectra of MAI:BAI and PbI_2 Films

a) XRD spectrum of individual MAI and BAI films compared to a mixture MAI:BAI film. The mixture film shows peaks that match both individual films. b) XRD spectra of a PbI_2 film. The major peak is at 12.6 °.

Melt Infiltration of $MAPbI_3$ and $BAPbI_4$

The mixed perovskites used in this study are composed of the cations MA and BA with PbI_2. Using each of these cations separately with PbI_2 will form the single cation perovskites $MAPbI_3$ and $BAPbI_4$. Both of these perovskites have been vastly studied and have applications in solar cells and transistors.[3,16,17,8] These perovskites can be made with many of the methods mentioned earlier in this chapter such as the 1 step and 2 step spin coating methods and the CVD ablation method. To begin my investigation into the melt infiltration method, I wanted to see if the $MAPbI_3$ and $BAPbI_4$ perovskites could be made using melt infiltration. To do this, I prepared films of only BAI and only MAI and used these with films of PbI_2 to do melt infiltration. As mentioned earlier, films of just BAI and just MAI are not as uniform as their mixture counterparts. Nonetheless, using these films with the melt infiltration method yields the respective perovskites (**Figure 5.13**).

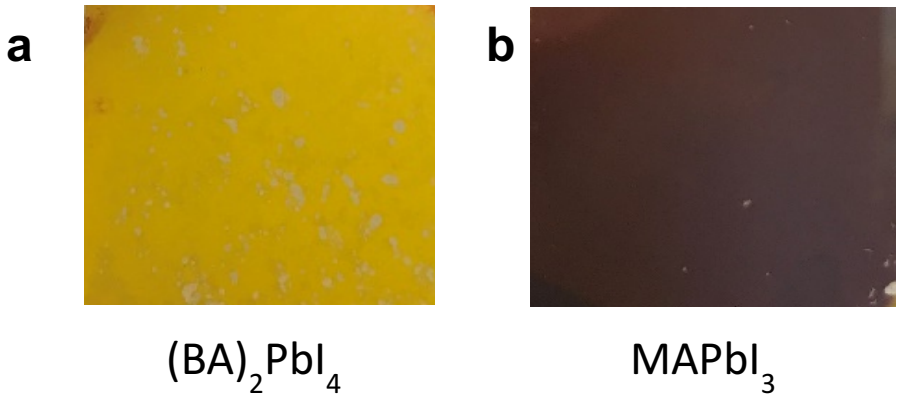

Figure 5.13: Pictures of $(BA)_2PbI_4$ and $MAPbI_3$ perovskite films

a) Picture of $(BA)_2PbI_4$ perovskite made with the melt infiltration method. b) Picture of $MAPbI_3$ perovskite made with the melt infiltration method.

First, the 2D perovskite $BAPbI_4$ made a yellow film, which is consistent with reported films.[18] The UV/Vis spectrum (**Figure 5.15a**) shows a single peak at 505 nm, which matches spectrum reported by Mitzi *et. al.*[18] But, when looking at the XRD spectrum (**Figure 5.14b**), more peaks than just what is reported for $BAPbI_4$.[5] The low angle peaks of the $BAPbI_4$ are present, but there are also peaks from PbI_2 in the film. This indicates that the film was not totally converted to $BAPbI_4$ during the melt infiltration process. This could be because the heating time was not long enough or the temperature was not high enough to fully convert the two precursor materials into the $BAPbI_4$ perovskite.

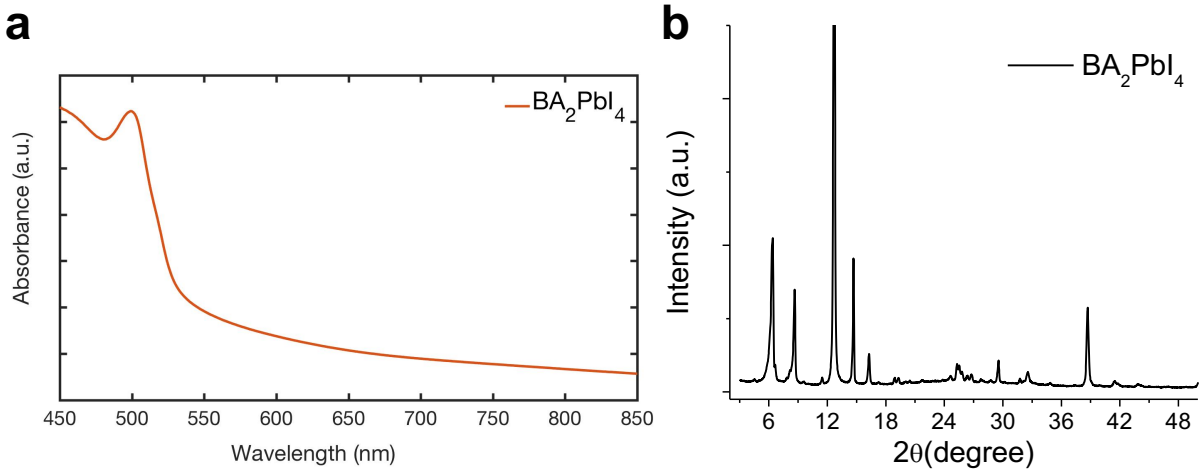

Figure 5.14: UV/Vis and XRD of $BAPbI_4$ perovskite

a) UV/Vis of $BAPbI_4$ perovskite made using melt infiltration. There is one peak at 505 nm. b) XRD spectrum of $BAPbI_4$ perovskite.

For the $MAPbI_3$ film produced using melt infiltration, the film turns the black color that is normal for $MAPbI_3$ films processed using a spin coating method. The UV/Vis shows the broad shoulder peak at 750 nm that is also characteristic of solution processed $MAPbI_3$ films. The XRD for the films shows the (110) peak of $MAPbI_3$ at 14.1°. There are also some small peaks seen in the XRD and some of these peaks match the PbI_2 spectrum, specifically the peak at 12.6°.

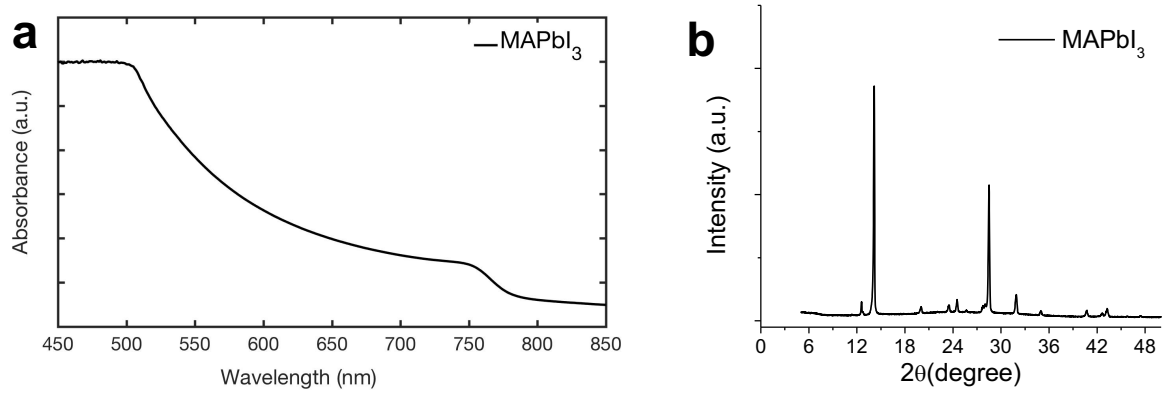

Figure 5.15: UV/Vis and XRD of $MAPbI_3$ perovskite

a) UV/Vis of $MAPbI_3$ perovskite made using melt infiltration. There is a broad shoulder at 750 nm that is characteristic to the 3D $MAPbI_3$ perovskites b) XRD spectrum of $MAPbI_3$ perovskite. There is a large peak at 14.1 °.

For both the $BAPbI_4$ and the $MAPbI_3$ films, lead iodide was still present in the films after melt infiltration. As I will discuss later, there was no lead iodide present when mixed MA:BA 2D perovskites were made using melt infiltration. The fact that PbI_2 is only seen when films are made using the individual components can be explained by looking at the quality of the films made with just BAI and just MAI. Films made with the individual components were not uniform and had areas not covered by the materials. This can be compared to films of the mixture, which were uniform and fully covered. When using these non-uniform films for melt infiltration, the areas not covered by materials could not be fully converted to perovskite and therefore still had lead iodide present. In the future, if melt infiltration films of $BAPbI_4$ and $MAPbI_3$ are wanted, a better film coverage of MAI and BAI films will have to be found.

Melt Infiltration of Mixed Perovskites

When I began using mixed cation films with the melt infiltration method, I started with a range of ratios to see how the films behaved. I started with the range 10:1, 2:1, 1:1, 1:2, and 1:10. The ratios of 1:2 and 1:1 correspond to the molecular ratios for the n=2 and n=3 layered perovskites, while the other ratios were chosen to see what happens when a large excess of one cation is used. I later added in a 5:1 ratio.

Figure 5.16: Pictures of a mixed perovskites made with melt infiltration

Pictures of the initial melt infiltration films. A range of ratios of MAI:BAI were used including a) 10:1 b) 2:1 c) 1:1 d) 1:2 e) 1:10.

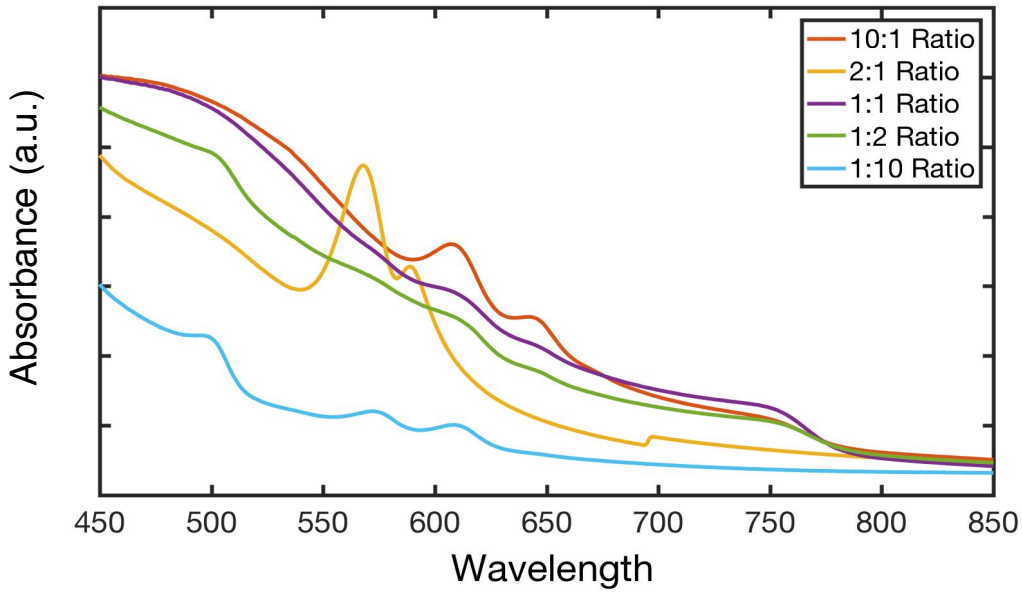

Figure 5.17: UV/Vis of mixed perovskites made with melt infiltration

The UV/Vis spectrum of the films shown in Figure 5.16.

I next focused on the ratios with the higher amount of MAI; 2:1, 5:1, and 10:1. These ratios produced the most uniform films of all the ratios initially tested and the colors matched most closely to the mixed perovskites made by spin coating. The first interesting thing about the films was the difference in color and the UV/Vis spectra. The 2:1 ratio film was the pink color of the n=2 film, while the 10:1 is the black color of n=3 and n=4 films (**Figure 5.18**). The 5:1 film was both black and pink and had attributes of both the 2:1 and 10:1 films. The UV/Vis spectrum give a similar result as the color analysis (**Figure 5.19**). The UV/Vis spectrum of the 2:1 film most closely resembles the n=2 spin coated film. It has a large peak at 569 nm that corresponds to an n=2 layer number and a smaller peak at 590 nm, which is a little lower than the typical n=3 peak. The large n=2 peak shows that the 2:1 ratio film consists of mainly n=2 perovskite. The smaller higher wavelength peak shows that there may be some n=3 layers or a mixture of n=2 and n=3, but the predominant phase is still n=2.

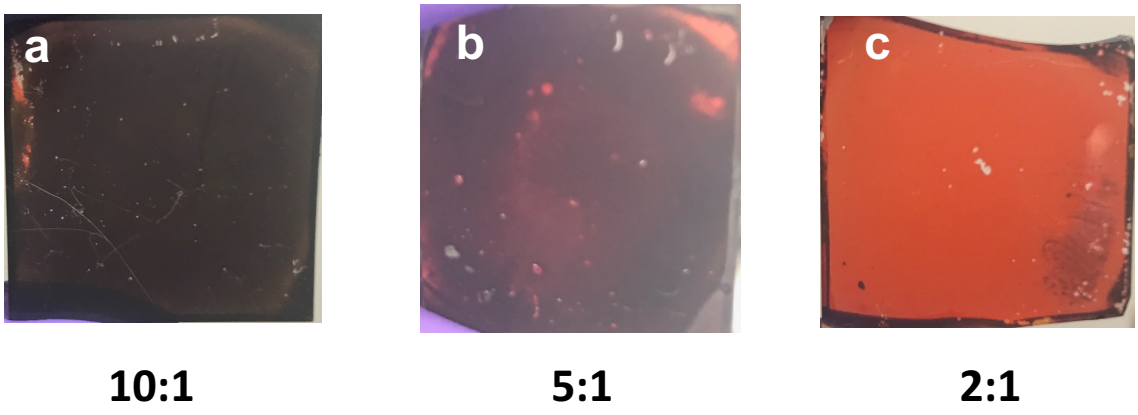

Figure 5.18: Pictures of the 10:1, 5:1, and 2:1 ratio melt infiltration films

Pictures of melt infiltration films made using a) 10:1 b) 5:1 and c) 2:1 ratio of MAI:BAI. The 5:1 ratio film shares attributes from both the 10:1 and 2:1 ratio films.

The 10:1 ratio film has peaks at 605, 640 and 750 nm. This points towards the film having components of n=3 and n=4 layers along with the 3D $MAPbI_3$ phase. The UV/Vis closely resembles the n=3 and n=4 spectrum of the spin coated perovskites. But, the 10:1 ratio melt infiltration film does not have a n=2 peak, while the spin coated films do. This shows that the melt infiltration films made with a 10:1 ratio are composed of layers of n=3, n=4, and n=∞ with no n=2. These films are closer to a pure phase n=3 or n=4 film than films made using the molecular ratio with a spin coating method since the spin coated films still have n=2 present.

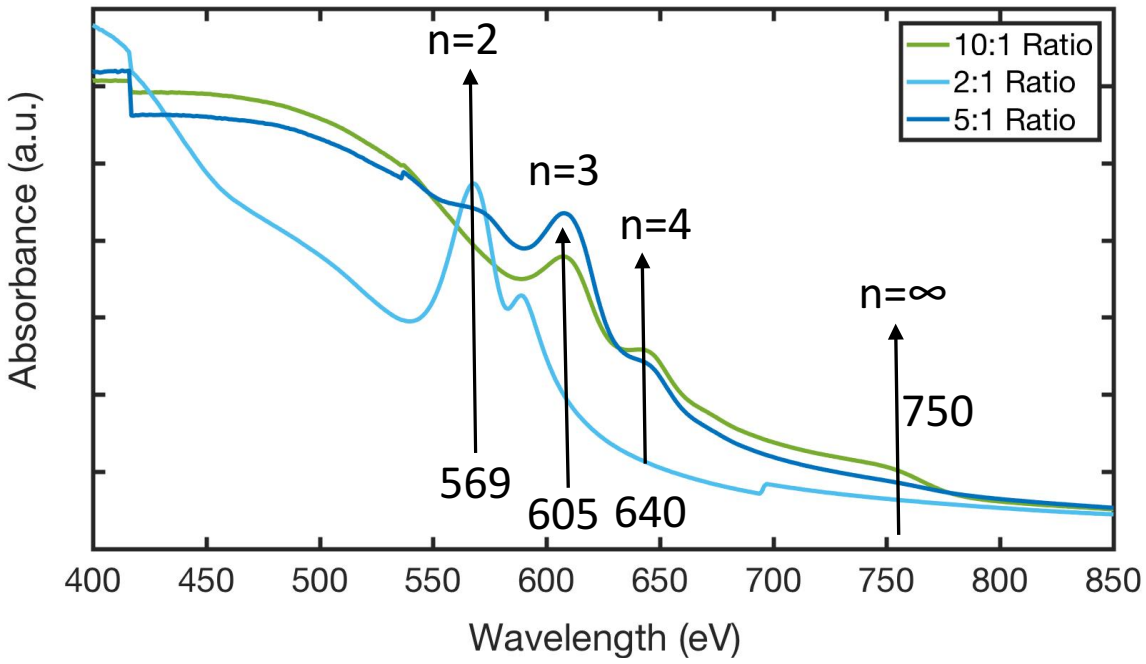

Figure 5.19: UV/Vis spectrum of 2:1, 5:1, and 10:1 MAI:BAI ratio films made with melt infiltration

The 2:1 ratio film (light blue) has peaks that correspond to both n=2 and n=3. The 10:1 ratio film (light green) has leaks that correspond to n=3, n=4, and n=∞. The 5:1 ratio film (dark blue) has a mixture of peaks that are seen in both the 2:1 and 10:1 films.

Looking at the UV/Vis of the 5:1 ratio film, the peaks seen are a mixture of the peaks seen in the 2:1 and 10:1 films. The 5:1 film has the n=2, n=3 and n=4 peak. The 5:1 film does not have the n=∞ peak that is present in the 10:1 film. This is interesting because the 5:1 is in between the 2:1 and 10:1 in terms of molecular ratio and it is also in between the 2 in terms of layer numbers present when analyzing the UV/Vis. This leads to the possibility that the layer number formed by the mixed cation perovskites is a gradual process that can be tuned by varying conditions such as ratio, temperature and heating time.

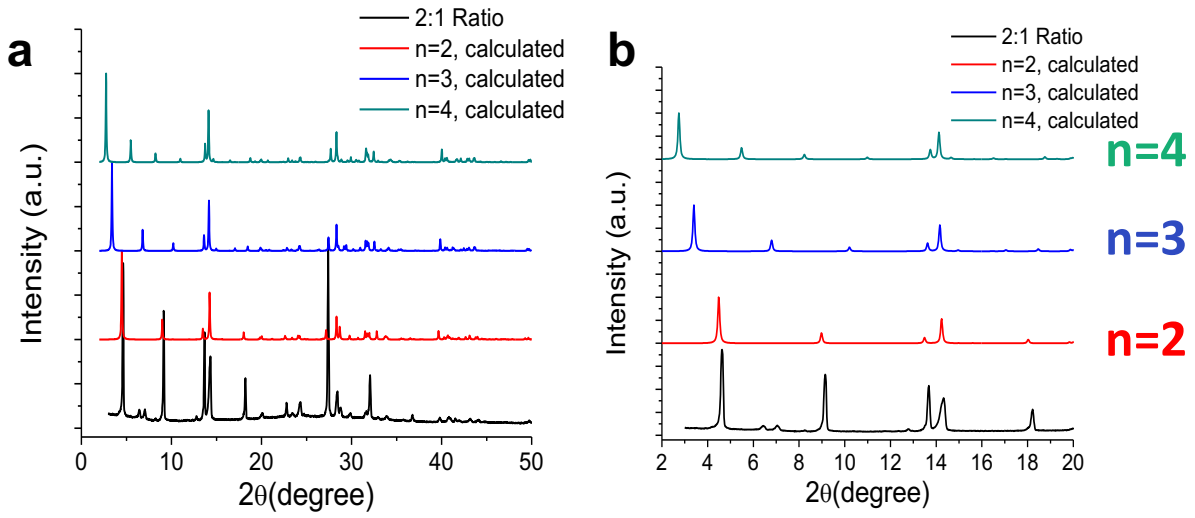

Figure 5.20: XRD of 2:1 ratio melt infiltration film

a) Full XRD spectrum for the 2:1 ratio melt infiltration films. b) The low angle region of the XRD spectrum for the 2:1 melt infiltration films.

The UV/Vis and color of the films gives a general idea of the layer number but XRD is able to give more insight into the layer number and orientation of the perovskites film (**Figure 5.20**). First, when comparing the XRD of the 2:1 film with the calculated spectrum of n=2, n=2, and n=4 films, the low angle peaks match up with the n=2 spectrum (**Figure 5.20b**). The lower angle spectrum has peaks at 4.61 (020), 9.17 (040) and 13.64 (060), which are all peaks that

correspond to an n=2 layer number. Second, the XRD does not have a peak at 12.63 that would correspond to PbI_2. Therefore, it can be inferred that the majority of the PbI_2 has been incorporated into the perovskite film.

Even though there is a smaller, higher wavelength peak present in the UV/Vis spectrum, the XRD suggests that the film is predominately composed of the n=2 layer number. Further, the melt infiltration 2:1 ratio film and the n=2 spin coating film have the same XRD peaks. From the color analysis, UV/Vis, and XRD of the 2:1 ratio melt infiltration films, it can be concluded that using a 2:1 ratio of MAI:BAI with the melt infiltration approach gives a film that is predominately n=2.

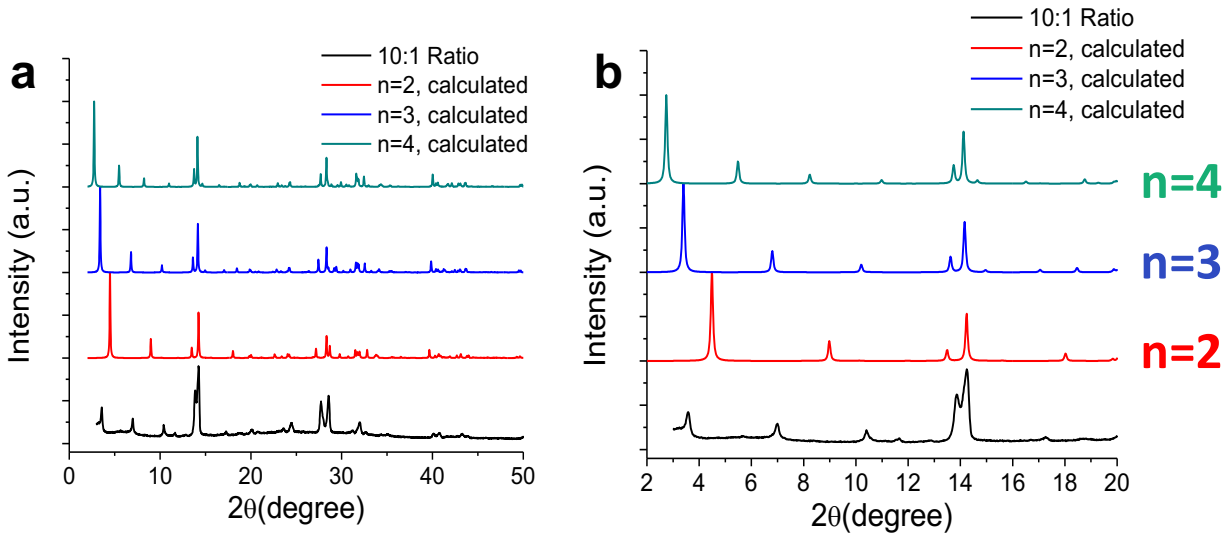

Figure 5.21: XRD of 10:1 ratio melt infiltration film

a) Full XRD spectrum for the 10:1 ratio melt infiltration films. b) The low angle region of the XRD spectrum for the 10:1 melt infiltration films.

Next, the XRD spectrum of the 10:1 ratio film was analyzed (**Figure 5.21**). The UV/Vis of this film suggest that it has both n=3, n=4, and n=∞ components. Looking at the XRD, the low angle XRD peaks of the 10:1 ratio film match the calculated peaks of an n=3 mixed perovskite (**Figure 5.21b**). Further, the 10:1 film XRD does not possess any peaks to indicate the present of

n=2 or n=4 layer numbers. The peaks present correspond to the 020 040 060 and 080 of the n=3 crystal structure. The low angle portion of the XRD spectrum for the 10:1 film is vastly different than the XRD spectrum of the n=3 and n=4 films made with the spin coating method. These films all have the n=3 peak in the UV/Vis but only the melt infiltration film has XRD peaks that correspond to an n=3 film. This could mean that the films are oriented differently on the substrate when made with spin coating versus melt infiltration because the XRD peaks seen in a given thin film XRD spectrum depend on if the perovskite film is oriented parallel or perpendicular to the surface. This is an interesting observation because it could lead to a way to more easily control the orientation of the perovskite film on a substrate.

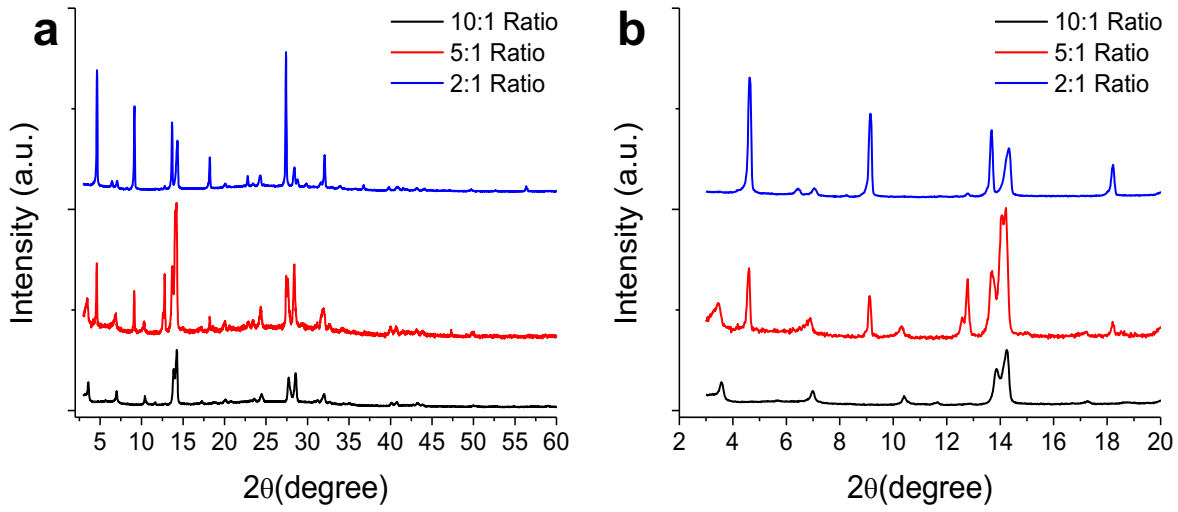

Figure 5.22: XRD of 5:1 ratio melt infiltration film

a) Full XRD spectrum for the 5:1 ratio melt infiltration films compared to the 10:1 and the 2:1 ratio films. b) The low angle region of the XRD spectrum for the 5:1 melt infiltration films compared to the 10:1 and 2:1 ratio films. The 5:1 XRD spectrum has peaks that match both the 10:1 and 2:1 ratio XRD spectra.

From the UV/Vis spectrum, the 5:1 ratio film had attributes of both the 2:1 and 10:1 ratio film. Therefore, it would be expected that the XRD of the 5:1 ratio film would have peaks that correspond to both n=2 and n=3 layers. Comparing the 2:1 and 10:1 XRD spectra to the 5:1

shows that in the low angle region, the 5:1 has peaks both the peaks of the 2:1 and 10:1 (**Figure 5.22**). This further suggests that the 5:1 film is a mixture of n=2 and n=3 mixed perovskites.

Table 5.2 gives a summary of the different starting ratios used.

Table 5.2: Summary of melt infiltration UV/Vis peaks and color

Starting Ratio of MAI:BAI	UV-Vis Peaks seen	Color	Majority of Film is…
2:1	n=2, n=3	Pink	n=2
5:1	n=3, n=4	Black	n=3
10:1	n=3, n=4	Black	n=3

Preparation Conditions

All the previous melt infiltration films were made inside the glovebox in a nitrogen environment. The glovebox also is free of moisture in the air which can harm perovskite films (cite). The spin coated films were made outside the glovebox in an ambient environment where the humidity can range from 20%-60% depending on the weather. In many cases, perovskites are very susceptible to oxygen and moisture in the air which causes degradation of the films. But, the MA/BA mixed perovskite have been reported to be more stable in an ambient environment compared to the 3D $MAPbI_3$ perovskite and therefore have successfully been made outside of a glovebox. When attempting to further develop the melt infiltration method, I did a trial run outside of the glovebox in order to more closely mirror the conditions used in the spin coating method. But, the experiment did not go as planned and the film formation behaved vastly different compared to the melt infiltration films made inside the glovebox.

First, when making the precursor films of MAI/BAI, the films visibly absorbed water from the air before they could even be used for melt infiltration. A range of ratios was attempted, including 1:1, 2:1, 5:1 and 10:1. All films visibly absorbed water prior to the melt infiltration. Next, when the films were used for melt infiltration, all films turned black very quickly and stayed black during the whole heating time of 60 min (**Figure 5.23**).

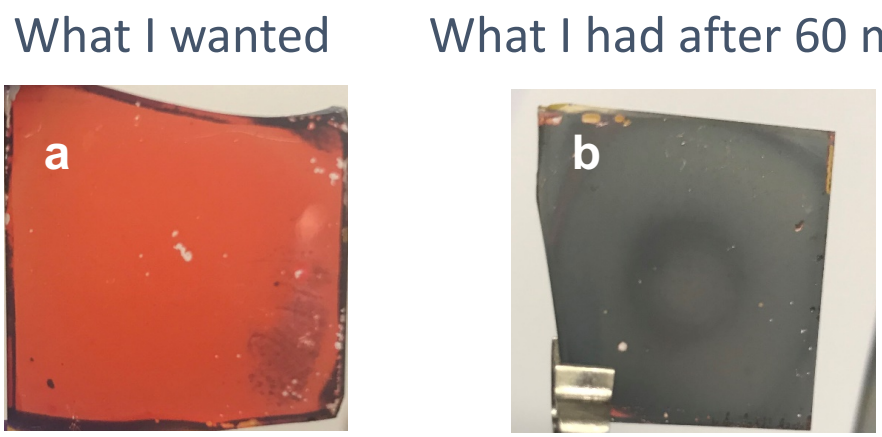

Figure 5.23: Pictures of melt infiltration perovskites made outside the glovebox
a) Picture of a 2:1 ratio melt infiltration film made inside the glovebox. b) Picture of 2:1 ratio melt infiltration film made in ambient conditions.

From previous results, it was expected that the 1:1 and the 2:1 films would be either partially or totally pink, but this was not the case. The UV/Vis of all the ratios produces the same result, with only a peak at 750 nm (**Figure 5.24**). This peak is from the $MAPbI_3$ perovskite. This suggests that the BAI is more unstable in an ambient environment compared to the MAI, and degrades more quickly. This leaves only the MAI to react with the PbI_2 film and subsequently produce a film of $MAPbI_3$. The large variation in the humidity in North Carolina produces unfavorable conditions for making melt infiltration perovskites. Therefore, the glovebox is the best option to produce consistent results when using the melt infiltration method.

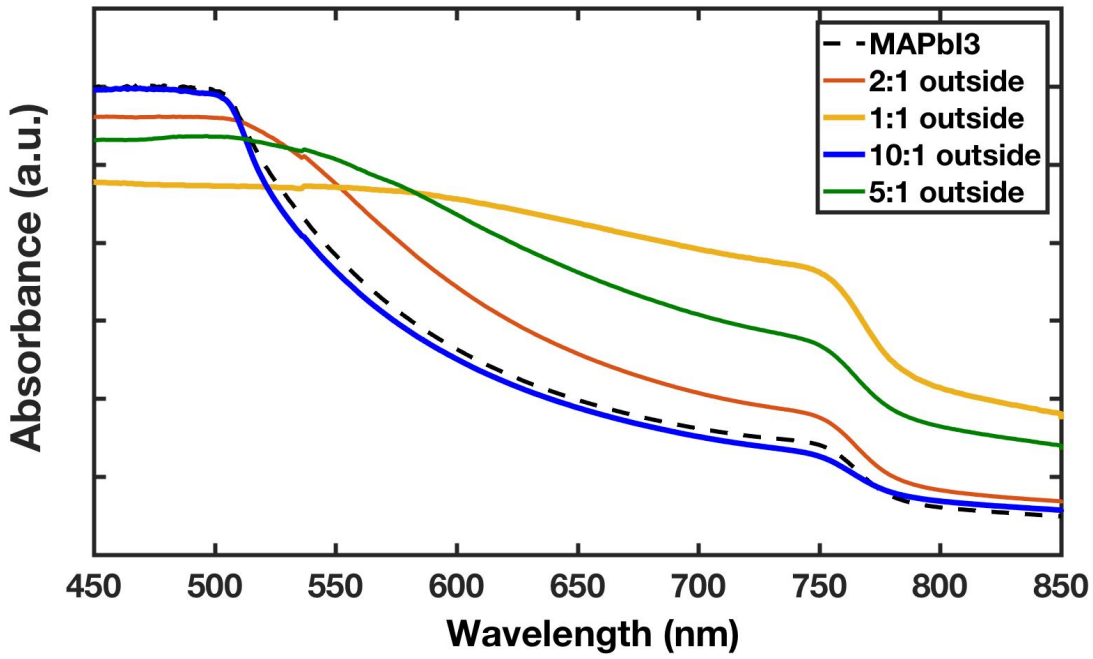

Figure 5.24: UV/Vis of melt infiltration films made in an ambient environment
Melt infiltration mixed perovskite films made in ambient conditions do not produce the same results as films made in a nitrogen environment.

Melt Infiltration Time Study

As I further experimented with the melt infiltration approach, I began to notice an interesting color change over time in some of the films. At t=0 min of the melt infiltration process, the bottom lead iodide film substrate is yellow, while the top MAI/BAI film is white. I noticed that very soon after placing the sandwiched films on the hotplate, the films began to turn black. This was not expected for all the ratios, specifically the 2:1 ratio films. From pervious experiments, I knew that the final film for the 2:1 ratio is pink. By watching as the films heated, I observed that the 2:1 ratio films first turn black but then gradually change to pink (**Figure 5.25**). Observing this gradual change suggests that for at least the 2:1 ratio, the film does not initially form n=2 layers, but instead form another species with a black color, which could be

n=3, n=4 or n=∞. Then, after forming this black species, the film then changes into the pink n=2 film. Observing this color change in the 2:1 film could also mean that the 5:1 ratio and 10:1 ratio films also form a different structure first, but the initial and final color is black so the change can't be observed by the naked eye.

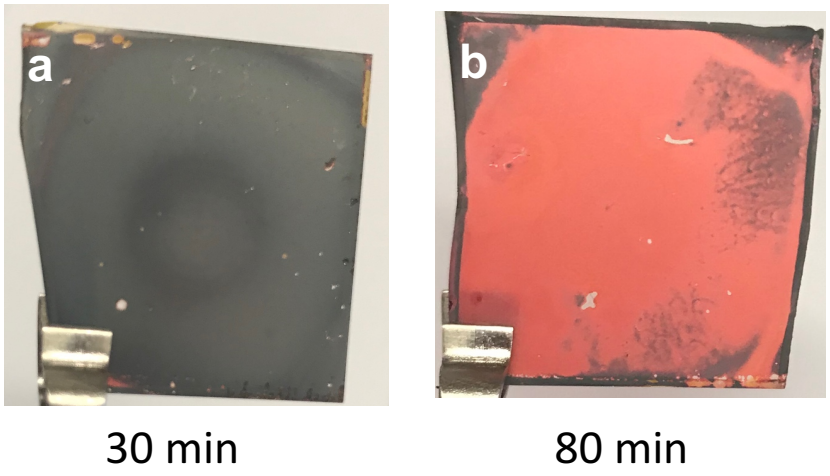

Figure 5.25: 2:1 ratio melt infiltration films after 30 and 80 minutes
a) A 2:1 ratio melt infiltration film about 30 minutes of heating. b) A 2:1 ratio melt infiltration film after 80 minutes of heating.

I initially investigated this by making two 2:1 ratio films where one was heated for 30 min and the other for 80 min. **Figure 5.25** shows that after 30 min, the 2:1 ratio film is black but at 80 min the film has changed to pink. The UV/Vis at 30 min shows a peak at 750 nm which corresponds to the n=∞ 3D $MAPbI_3$ perovskite (**Figure 5.26**). The UV/Vis at 30 minutes matches the UV/Vis of melt infiltration perovskites made with only MAI on the top film. This initial observation suggests that the MAI is more reactive than the BAI quickly forms the 3D portion of the perovskite.

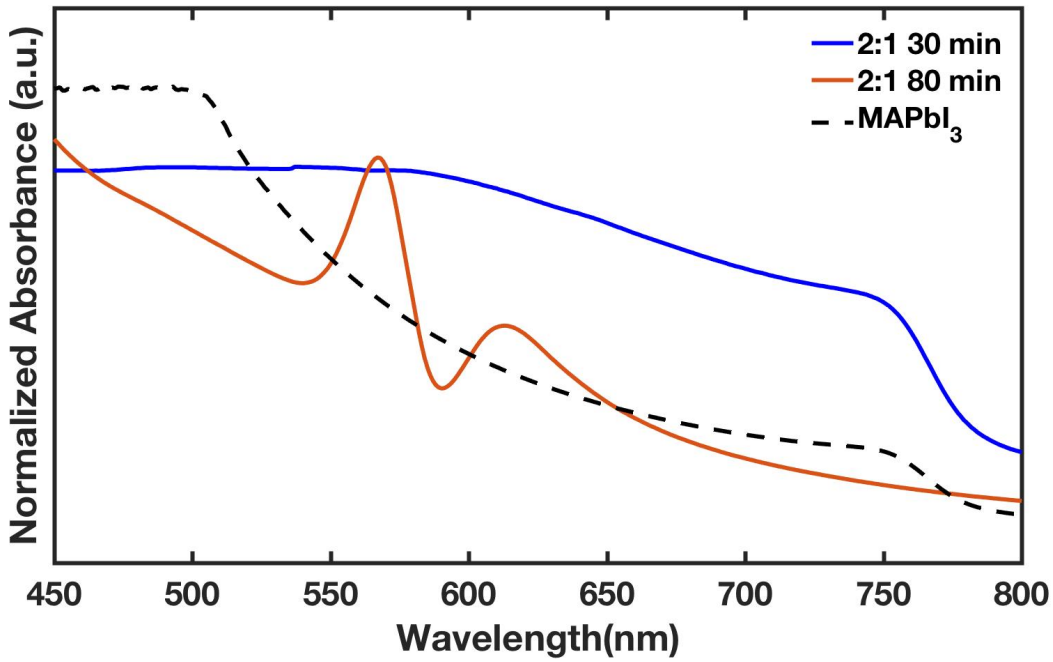

Figure 5.26: UV/Vis of 2:1 ratio melt infiltration film after heating 30 and 80 minutes
After 30 minutes of heating, the 2:1 ratio melt infiltration film has the same shoulder peak as the 3D $MAPbI_3$ perovskite. By 80 minutes, that peak disappears and the n=2 peak appears.

To further investigate this, I did a time study to observe the melt infiltration films as they formed. I made 10 different films that I stopped at the time intervals 10, 20, 30, 40, 50, 60, 70, 80, 90, and 120 minutes. The perovskite forms on the bottom slide that is initially the lead iodide film. During the time study, I analyzed the top slide that is initially the MAI:BAI mixture at every time interval to see if the ratio of MAI:BAI changes over time or if the two substances are consumed equally. Using ^{1}H NMR, I was able to measure the ratio of MAI to BAI left on the top slide after perovskite formation and compare that to the UV/Vis of the perovskite formed.

Looking at the UV/Vis every 10 minutes helps to show how the perovskite film transforms overtime. The first 10 min interval for the 2:1 ratio film has the n=∞ peak at 750 nm in the UV/Vis spectrum (**Figure 5.27**). For the next two intervals, 20 and 30 minutes, the n=∞ peak is still the only peak present. Between 10 and 30 minutes, the n=∞ peak increases in intensity which indicates an increase in the film thickness the film density of the perovskite. Overall, the first three time intervals show that the melt infiltration process forms the 3D $MAPbI_3$ perovskite after 30 minutes of heating and does not indicate that the BAI has been incorporated into the perovskite yet.

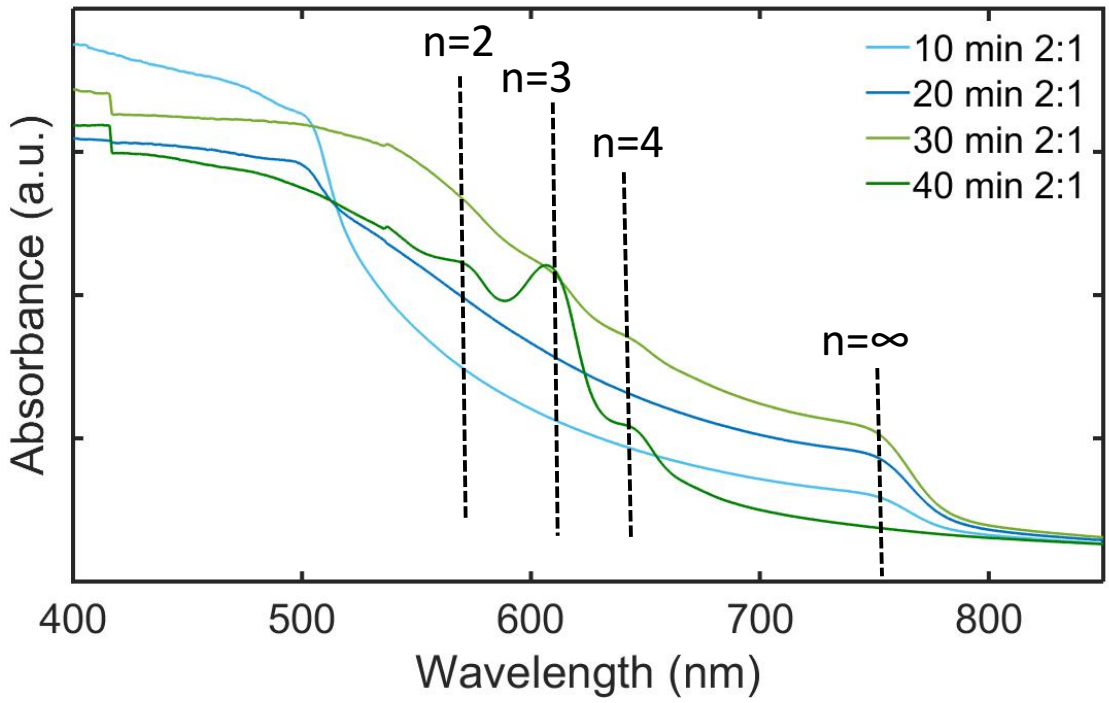

Figure 5.27: UV/Vis of 2:1 melt infiltration films after heating for 10, 20, 30, and 40 minutes
During the first 30 minutes of heating, the 2:1 ratio melt infiltration film UV/Vis shows a broad shoulder at 750 nm that corresponds to the 3D $MAPbI_3$ perovskite. After 30 minutes, peaks begin to appear that corresponds to mixed perovskite formation.

The UV/Vis spectrum abruptly changes at 40 min. The peak at 750 nm completely disappears at 40 min and beyond. After heating for around 40 min, the $MAPbI_3$ that had formed in the first 30 min begins to change to a mixed cation perovskite with BAI beginning to incorporate into the perovskite. The formation of the mixed perovskite at 40 minutes is indicated by the emergence of the n=2, n=3, and n=4 UV/Vis peaks. The n=3 peak is the most prominent at 40 min, and the n=2 and n=4 are small. For other melt infiltration films with a 2:1 ratio that have been reacted for the one hour or more, the n=2 peak is normally the most dominate. Looking at these results as a whole, 40 minutes is the approximate time for the mixed perovskite to begin to form. Before this time, the main perovskite structure in the film is

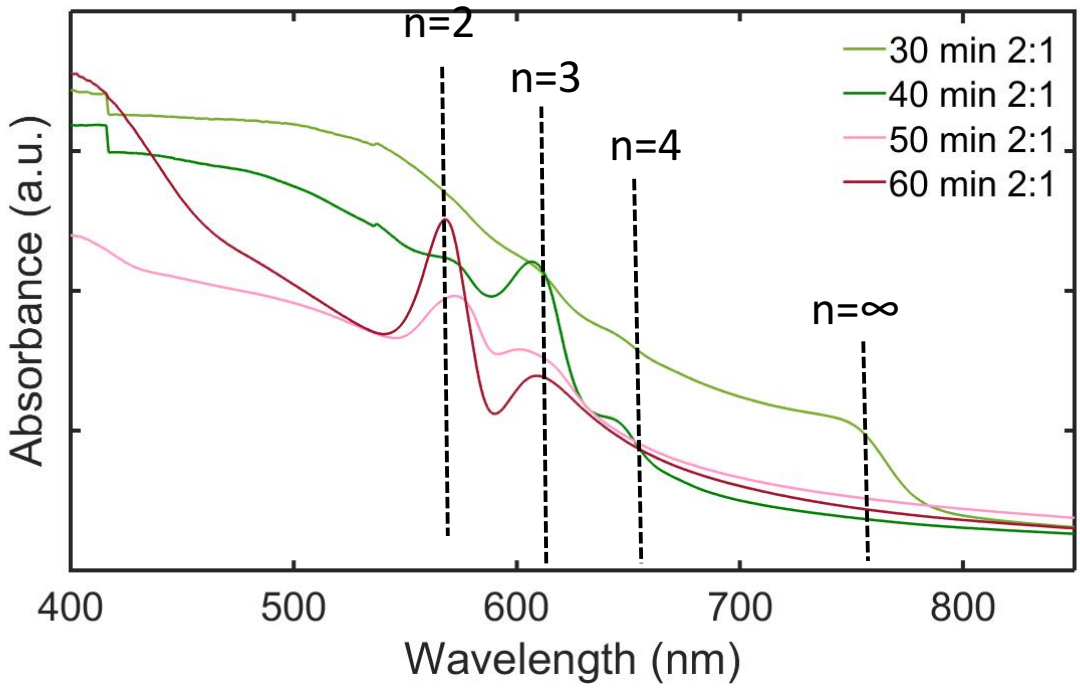

Figure 5.28: UV/Vis of 2:1 melt infiltration films after heating for 30, 40, 50, and 60 minutes
After 30 minutes, peaks begin to appear that corresponds to mixed perovskite formation but change over time. A n=4 peak is present at 40 minutes, but disappears by 50 minutes. The n=2 peak increases between 40 and 60 minutes.

the $MAPbI_3$. After 40 minutes, the BAI begins to infiltrate into the film to begin the process of the mixed perovskite formation.

The UV/Vis again shows a big change after 40 minutes. First, at the 50 minute mark and beyond, the n=4 UV/Vis peak disappears. This is similar to the disappearance of the n=∞ after 30 minutes. In addition, the n=2 peak emerges at 50 minutes and continues to grow stronger over time. This shifting of peaks suggest that as time goes on, more BAI infiltrates into the perovskite film since the n=2 perovskite has a higher ratio of BAI compared to the n=4 and n=∞ films. At 60 min, the UV/Vis spectrum has a very large n=2 peak and a smaller n=3 peak. Beyond 60 min, the UV/Vis spectra stay relatively the same which indicates that the perovskite does change much after it has formed a dominantly n=2 film.

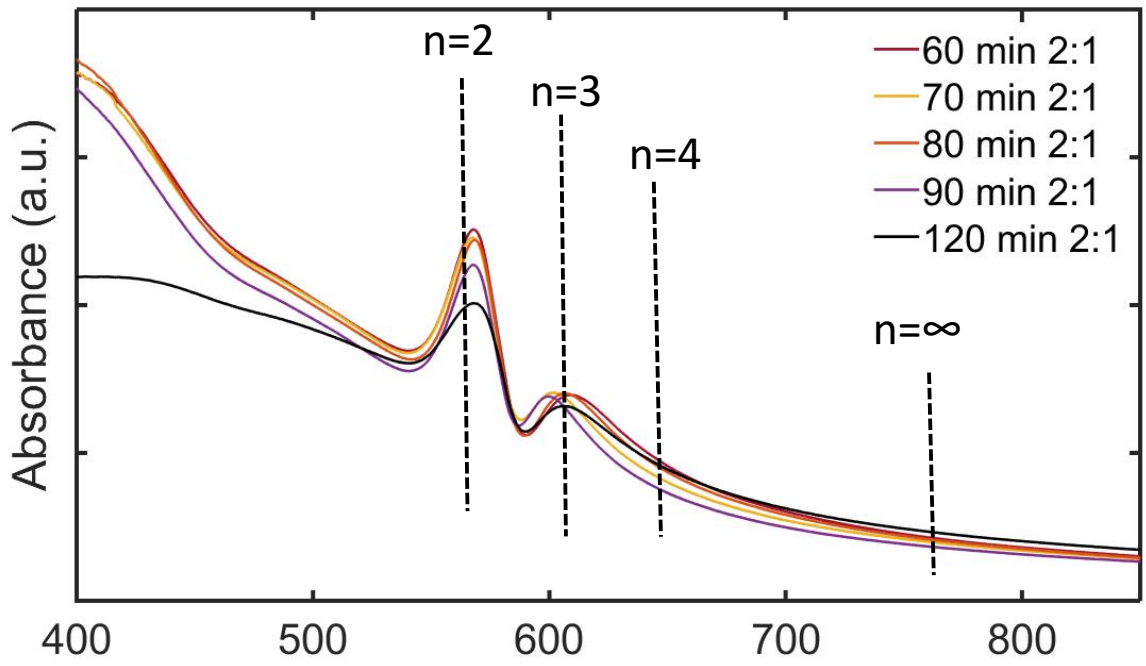

Figure 5.29: UV/Vis of 2:1 melt infiltration films after heating for 60, 70, 80, 90 and 120 minutes

After 60 minutes, the UV/Vis does not drastically change and the n=2 peak is the most prominent.

Next, ^{1}H NNR was used to analyze the ratio of MAI:BAI left on the top slide at each time interval. The measured ratio of the solution used was 2:1 MAI:BAI and the film at 0 minutes had a ratio of 1.7. Over the next 30 minutes, the ratio changes slightly but stays in between a 2:1 and a 1:1 ratio. This suggests that that MAI and BAI are infiltrating into the film at roughly the same rate, with the MAI only going slightly faster. But, the UV/Vis for 10-30 min shows only the formation of the n=∞. From the ^{1}H NMR analysis, it seems that the BAI is slowly infiltrating into the film in the first 30 min, but that formation of the $MAPbI_3$ is initially more favorable. The ratio of the of MAI:BAI begins to increase after 40 min. This indicates that the BAI is beginning to infiltrate to the bottom film more. This is matched by the emergence of n=2, n=3, and n=4 UV/Vis peaks from 40 min and onwards. After 60 min, the ratio of MAI:BAI starts becoming very large and it is assumed that almost all of the BAI has been used up. This also mirrors the UV/Vis because the large n=2 peak and small n=3 peak stay constant after 60 min. In conclusion, the melt infiltration method of perovskite formation for 2:1 ratio films is a gradual process that ultimately forms a film of n=2 perovskites.

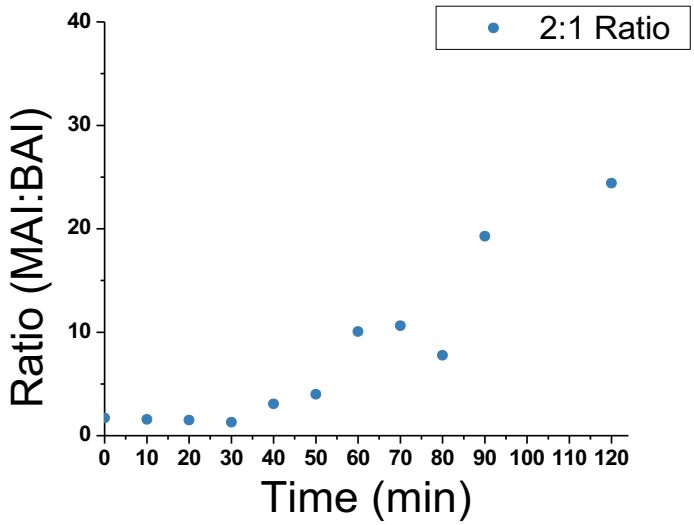

Figure 5.30: Graph of the ratio of MAI:BAI leftover on the top film after melt infiltration with a 2:1 ratio film

In the beginning, the ratio of MAI:BAI stays constant, but after 40 minutes, the ratio sharply increases over time.

Table 5.3: Table of Ratio of MAI:BAI leftover on top film after melt infiltration with a 2:1 ratio film

Time (minutes)	Ratio MAI:BAI
0	1.70
10	1.57
20	1.50
30	1.30
40	3.07
50	4.00
60	10.07
70	10.63
80	7.77
90	19.27
120	24.40

A similar time study was done using melt infiltration films made with a 5:1 ratio of MAI:BAI which were analyzed at 10 minute time intervals with both UV/Vis and ^{1}H NMR. The first three time intervals, 10, 20 and 30 minutes, look very similar to the 2:1 ratio at these intervals (**Figure 5.31**). There is a n=∞ that gradually increases between 10 and 30 minutes. The 5:1 ratio melt infiltration film initially behaves in the same way as the 2:1 ratio film with the n=∞ perovskite forming first.

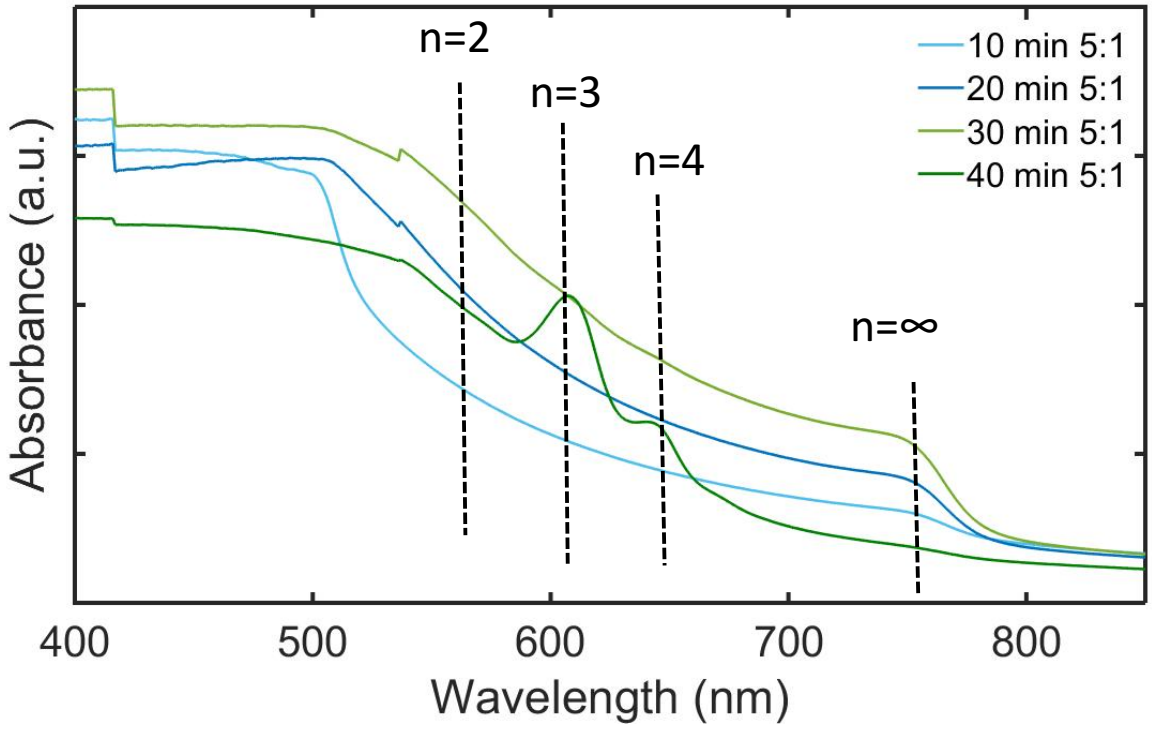

Figure 5.31: UV/Vis of 5:1 melt infiltration films after heating for 10, 20, 30, and 40 minutes
During the first 30 minutes of heating, the 5:1 ratio melt infiltration film UV/Vis shows a broad shoulder at 750 nm that corresponds to the 3D $MAPbI_3$ perovskite. After 30 minutes, peaks begin to appear that corresponds to mixed perovskite formation.

Then, the n=∞ peak disappears at 40 min and n=3 and n=4 peaks emerge. This is also similar to how the 2:1 ratio films behave. The 5:1 and 2:1 behave very similarly in the first 40 minutes. At 50 minutes and beyond, the 5:1 film UV/Vis has a large n=3 peak and a smaller n=4 peak (**Figure 5.32** and **Figure 5.33**). But, the 5:1 film does not have an n=2 peak like the 2:1 film and it does not emerge as time goes on. Therefore, the 5:1 melt infiltration film only consists of layer numbers n=3 and n=4, and is assumed to be a predominately n=3 film. Using a higher ratio of MAI:BAI will lead to a larger layer number perovskite film.

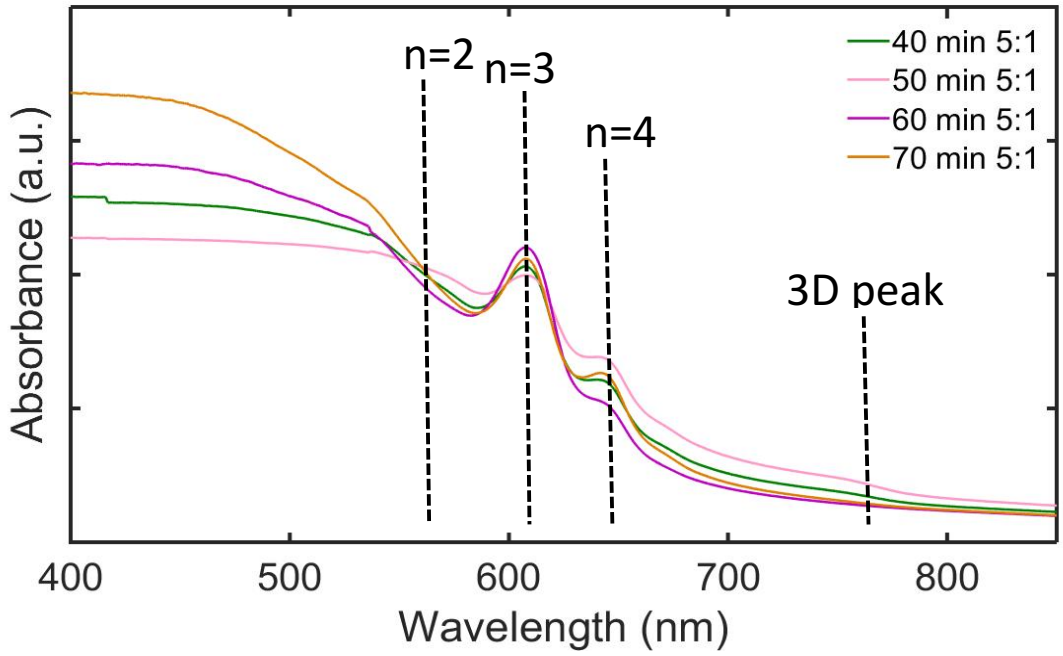

Figure 5.32: UV/Vis of 5:1 melt infiltration films after heating for 30, 40, 50, and 60 minutes After 30 minutes, the peaks stay relatively the same with a large n=3 peak and a smaller n=4 peak.

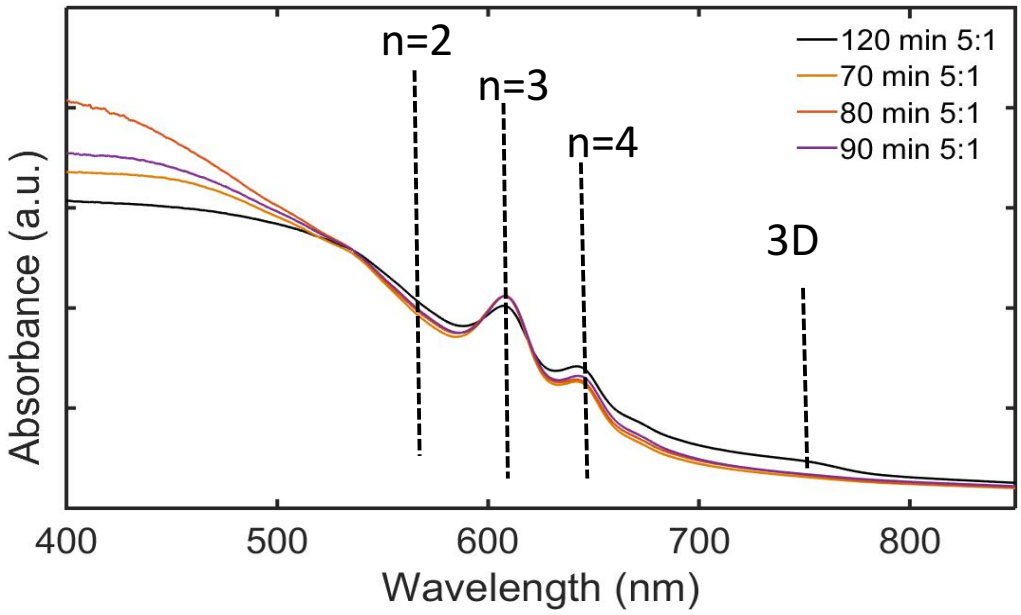

Figure 5.33: UV/Vis of 5:1 melt infiltration films after heating for 70, 80, 90, and 120 minutes The peaks do not change after 70 minutes.

The ^{1}H NMR analysis of the 5:1 ratio films does not show a clear trend but some conclusions can still be made by looking at the data. In addition to using ^{1}H NMR to look at the ratio of the MAI to BAI in the top film, I also used a TMS standard to compare the relative amounts of MAI and BAI left in the top film. First, at the beginning of the infiltration process, the ratio of MAI:BAI is between 1 and 5 for the first few time stamps. During this time period, it can be inferred that both the MAI and BAI are infiltrating into the film, but only the $MAPbI_3$ perovskite is being formed. Also, between 0 and 30 minutes, the relative amount of MAI and BAI present in the top film is decreasing at a similar rate. From 40 minutes and beyond a large change in the ratio of the MAI to BAI occurs. The ratio greatly increases while the relative amount of BAI left on the top film goes to almost zero. By 50 minutes, almost all the BAI has been infiltrated into the perovskite film. Further, after 50 minutes, the UV/Vis of the perovskite film is constant and large changes to the layer number do not occur like they do in the first 50 minutes of formation.

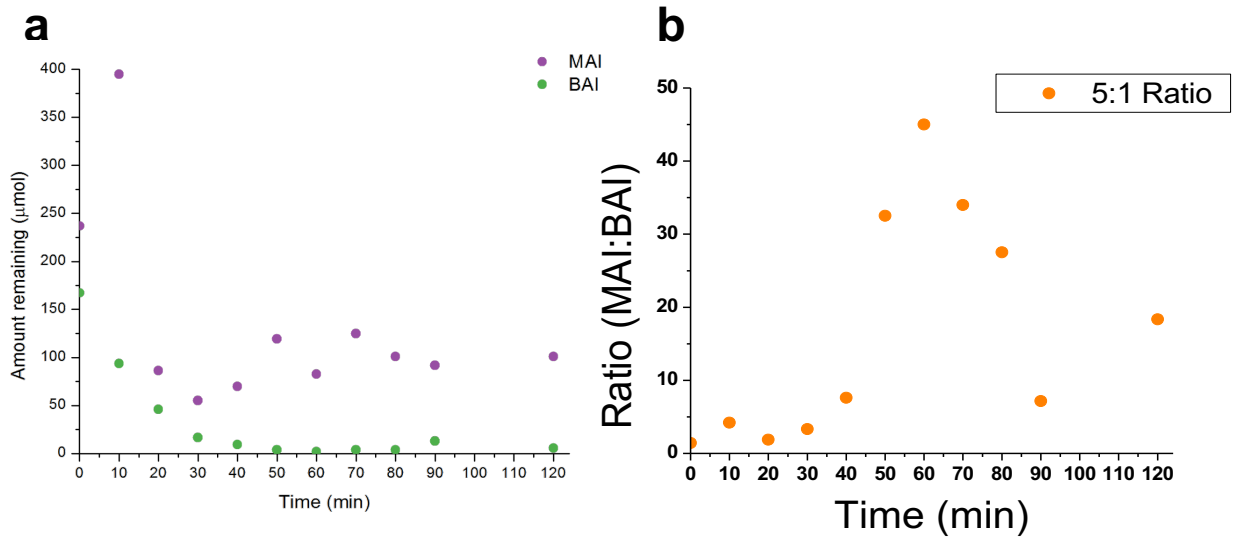

Figure 5.34: Graphs of amound of MAI and BAI leftover after melt infiltration with 5:1 ratio films

a) This graph shows the amount of MAI and BAI remaining at different time intervals during melt infiltration. b) This graph shows the ratio of MAI:BAI remaining at different time intervals during melt infiltration. After 60 minutes the amount of BAI remaining is very low, which somewhat skews the ratios.

Table 5.4: Table of Ratio of MAI:BAI leftover on top film after melt infiltration with a 5:1 ratio film

Time (minutes)	Ratio MAI:BAI
0	1.42
10	4.22
20	1.88
30	3.33
40	7.60
50	32.50
60	45.00
70	34.00
80	27.50
90	7.14
120	18.33

Concentration Effect of PbI_2 Films

The previous time study suggests that the BAI is used up more quickly than the MAI and is the limiting reagent. One possible effect that the quick usage of BAI may have on the film is that some of the PbI_2 on the bottom film may be left unreacted. All the pervious results have used a 1M concentration of PbI_2 solution to fabricate the melt infiltration films. A 1M concentration has been reported to work well with a two-step spin-coated method and was therefore chosen as a good starting point.[19]

For the next study, I lowered the concentration of PbI_2 to see how the concentration and PbI_2 film thickness changes the perovskite formation. **Table 5.5** shows the concentrations and thickness of PbI_2 used. Then, all films were used to perform melt infiltration with 2:1 ratio films of MAI:BAI. The 2:1 ratio films typically lead to n=2 layer number mixed perovskites. Since the color of these perovskites is pink, it makes it easy to see how the film changes over time.

Table 5.5: Preparation conditions for PbI_2 films used

Sample	Concentration (M)	Spin Speed/Acceleration (rpm)	Average thickness (nm)
1	0.5	3000/3000	176
2	0.5	6000/6000	153
3	1.0	3000/3000	397
4	1.0	6000/6000	308

First, I overserved all the films after 30 minutes of heating. From the previous results discussed in the chapter, at 30 min the 2:1 ratio films were mainly $MAPbI_3$ and possessed a UV/Vis peak at 750 nm. After 30 minutes, the films using 1 M PbI_2 were black, which was expected. The films using 0.5 M were pink, with small splotches of black around the edges. Further, the UV/Vis for the 1 M films has the $MAPbI_3$ peak at 750 nm (**Figure 5.36**) but the 0.5 M films do not. The 0.5 M films have a strong peak at 570 nm, which corresponds to the n=2 layer number (**Figure 5.35**). This makes sense since the films are mainly pink. The 0.5 M film UV/Vis does not have a higher wavelength n=3 peak, which has been previously seen for 2:1 ratio melt infiltration films. These initial 30 minute observations show that with a thinner PbI_2 layer, the formation timeframe of the melt infiltration perovskite shrinks. By 30 minutes, the 0.5 M film has already begun to turn pink while the 1 M film is still black.

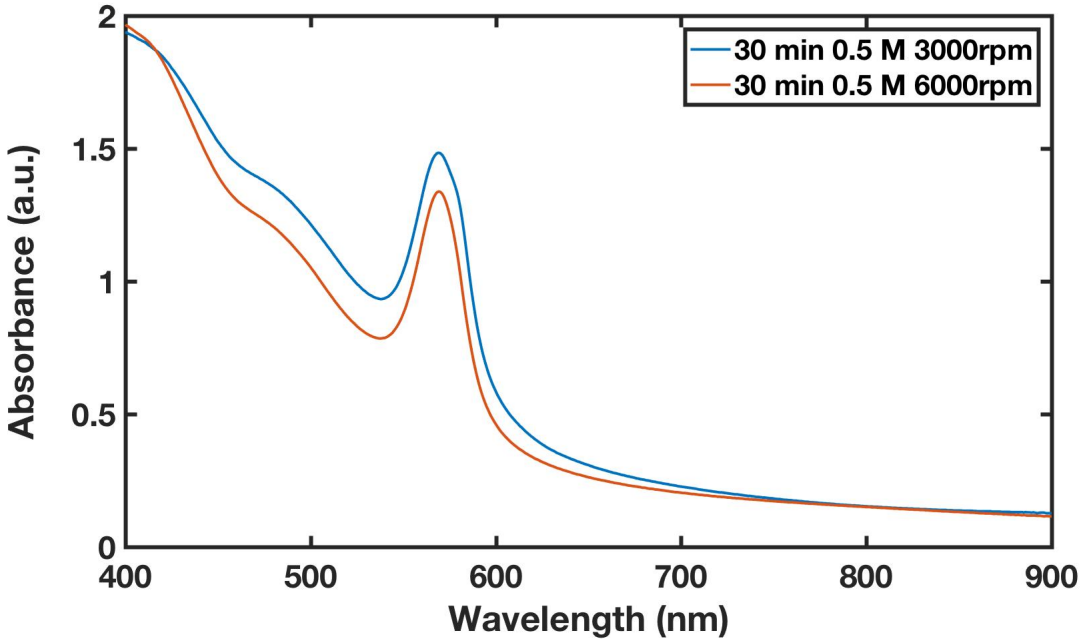

Figure 5.35: UV/Vis of 2:1 ratio melt infiltration films with 0.5 M PbI_2 after 30 minutes After 30 minutes, the films show a strong n=2 peak

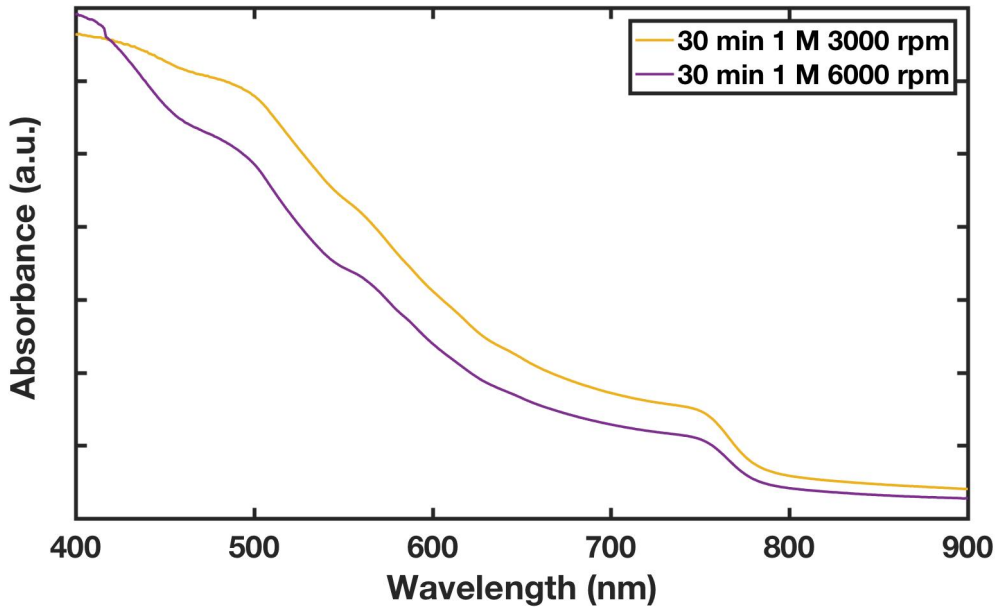

Figure 5.36: UV/Vis of 2:1 ratio melt infiltration films with 1 M PbI_2 after 30 minutes
After 30 minutes, the films show a shoulder peak at 750 nm.

Since the 2:1 ratio produces films that are pink, the reaction can be monitored by the color change of the films (**Figure 5.39**). For the 0.5 M films, they were fully pink by 60 minutes, while the 1 M films were not fully pink until 90 minutes. After observing how the 0.5 M films turned pink much quicker than the 1 M, this was expected. UV/Vis was again taken after the films had fully reacted. For the 0.5 M films, the UV/Vis still had the same n=2 peak at 60 min, and the spectrum looked very similar (**Figure 5.37**). The 1 M films were fully reacted at 90 min. The UV/Vis at 90 min has a large n=2 peak with a smaller n=3 peak (**Figure 5.38**). This is the same results seen for previous 2:1 ratio films with a 1 M PbI_2 film. The interesting difference between the fully reacted films of 0.5 M and 1 M is the absence of the n=3 peak in the 0.5 M films. This suggests that with less PbI_2 present, the 2:1 ratio of MAI:BAI only produces layer numbers of n=2. This result can hopefully lead to the tuning of the melt infiltration process to

produce films of a single layer number instead of the mixtures usually produced by the spin coating method.

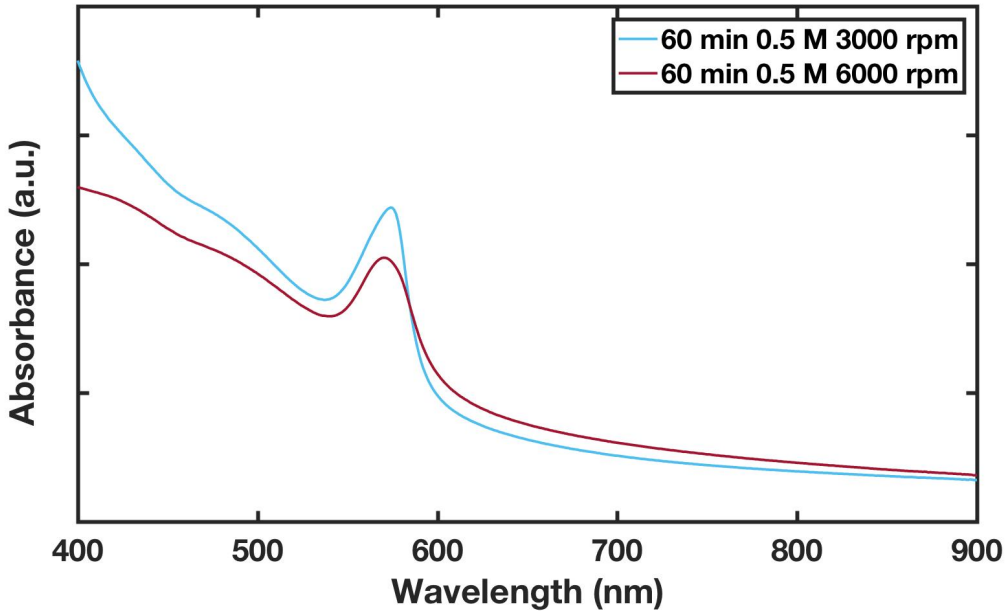

Figure 5.38: UV/Vis of 2:1 ratio melt infiltration films with 0.5 M PbI_2 after 60 minutes

After 60 minutes, the films are fully reacted and show a large n=2 peak.

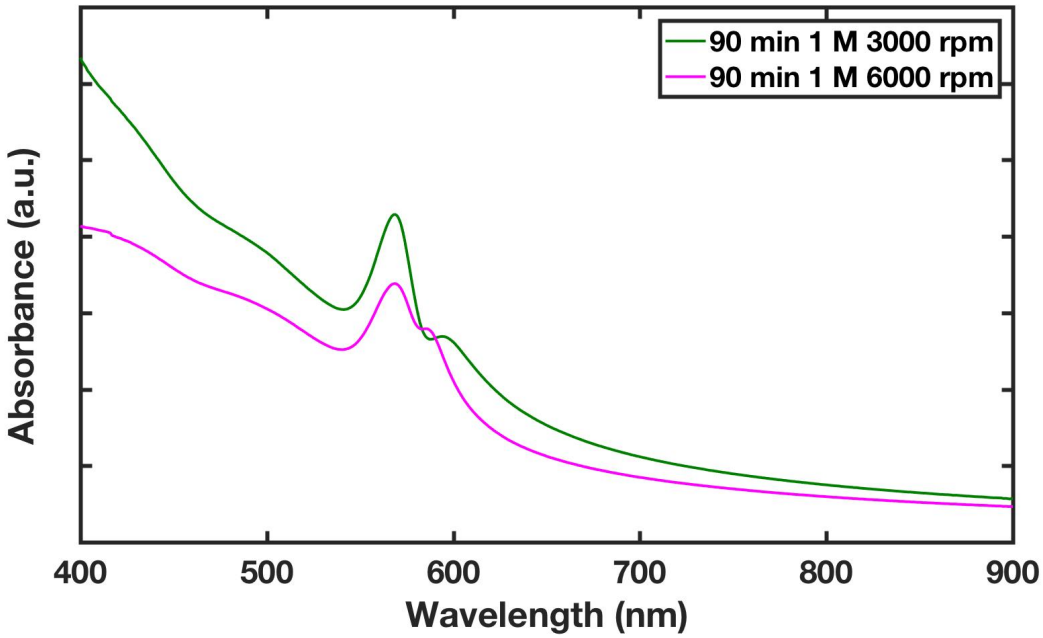

Figure 5.37: UV/Vis of 2:1 ratio melt infiltration films with 1 M PbI_2 after 90 minutes

After 90 minutes, the films are fully reacted and have a large n=2 peak and a smaller n=3 peak.

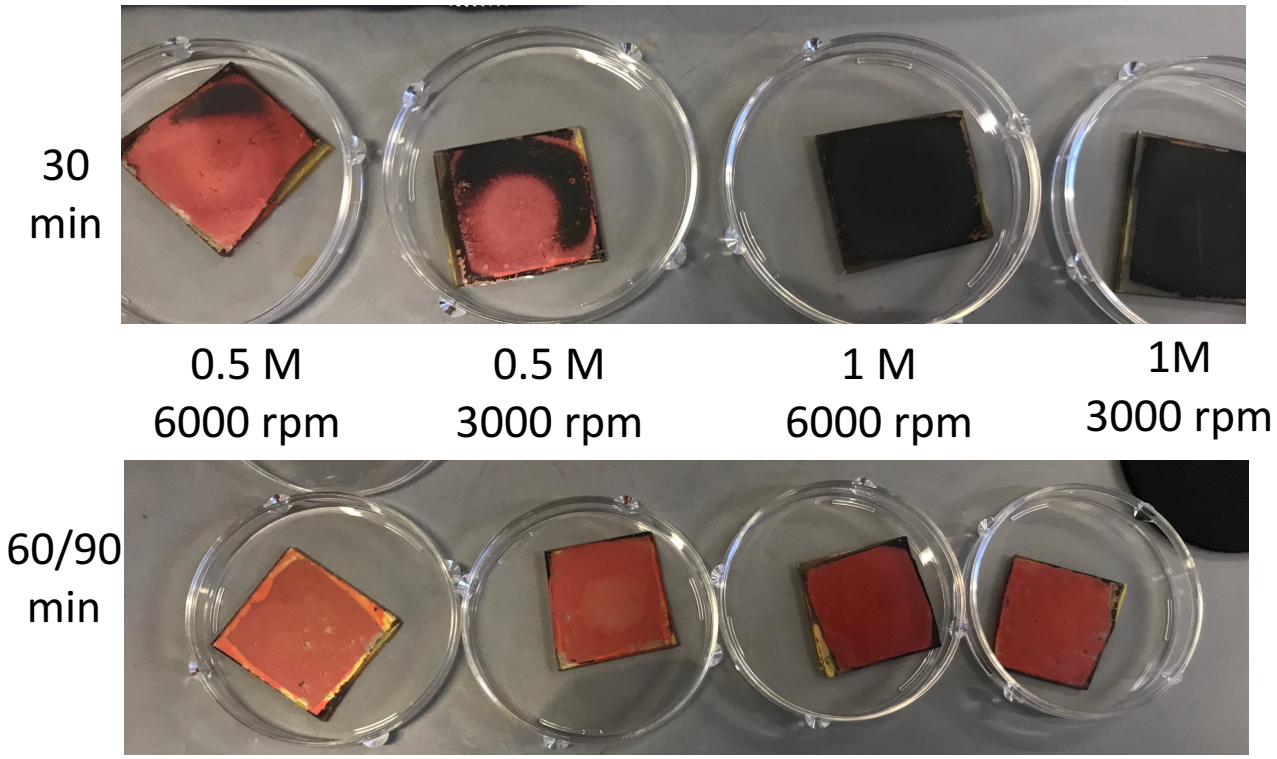

Figure 5.39: Pictures of 2:1 ratio melt infiltration films using different concentrations of PbI_2
The films using 0.5 M PbI_2 turn pink quicker than the films made using 1 M PbI_2. The 0.5 M films are finished reacting and completely pink after 60 minutes while the 1 M films take 90 minutes to turn completely pink.

Concentration Effect of MAI:BAI Films

The previous time studies showed that the BAI is used up more rapidly than the MAI. Further, the previous studies also suggest that the starting ratio of MAI:BAI determines the final layer number of the perovskite film. To further investigate this, I looked into how changing the concentration of the initial MAI:BAI film will change the final perovskite film. For this experiment, I made 3 solutions with the original amount (Sol 1), 1.5x the amount (Sol 2) and 2x the amount (Sol 3) of MAI:BAI for the initial precursor film (**Table 5.6**). Sol 1 and Sol 2 dissolved completely in IPA, while the highest concentration solution, Sol 3, did not. The film made using Sol 3 was not uniform and therefore the perovskites made using this film were not the best.

Even though the three films had a different starting concentration, the ratio of MAI:BAI for each film stay close to the wanted 2:1 ratio, as measured by ^{1}H NMR (**Figure 5.40**).

Table 5.6: Amount of MAI and BAI used for films of varying concentration

Solution #	MAI (g)	BAI (g)	Conc. MAI (M)	Conc. BAI (M)
Sol 1	0.15	0.1	1	0.5
Sol 2	0.225	0.15	1.5	0.75
Sol 3	0.3	0.2	2	1

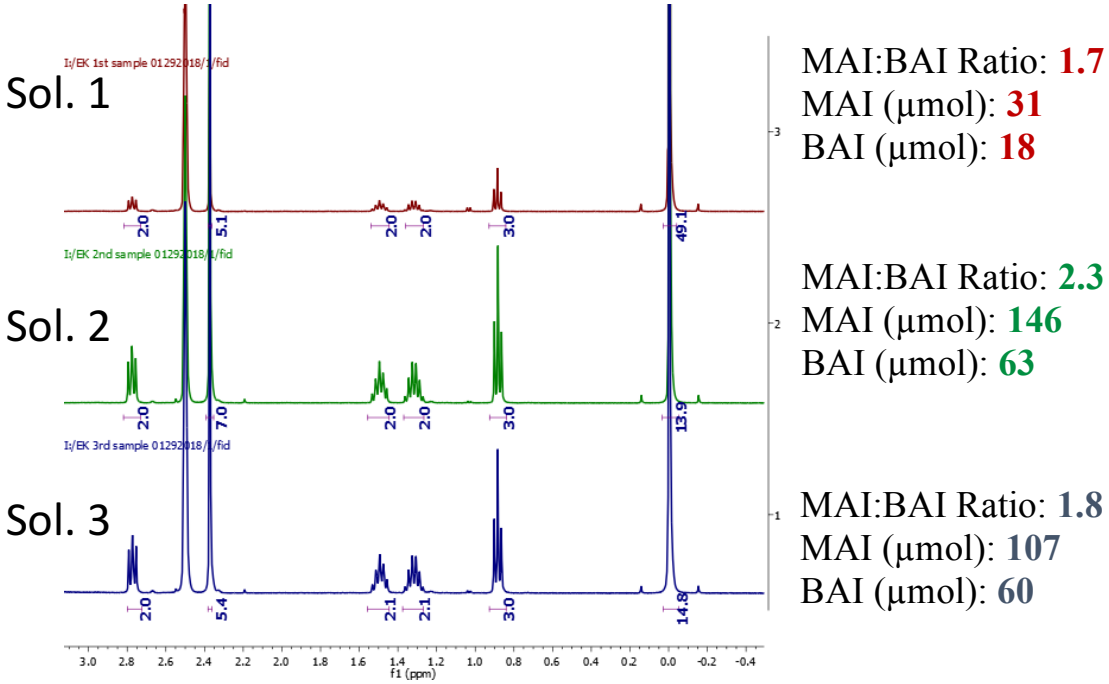

Figure 5.40: ^{1}H NMR of 2:1 ratio films made with varying concentrations
All ratios stay close to the wanted 2:1 ratio.

The films made from Sol 1 behaved the same as previously made films (**Figure 5.41**). This was expected because the same ratio was used. This also shows that there is consistency in the melt infiltration process from day to day. The Sol 1 films still first produced a black film at 30 min and had a UV/Vis peak at 750 nm which signifies the formation of the 3D $MAPbI_3$

perovskite. After, the film turns pink and the UV/Vis shows a large n=2 peak and a smaller n=3 peak.

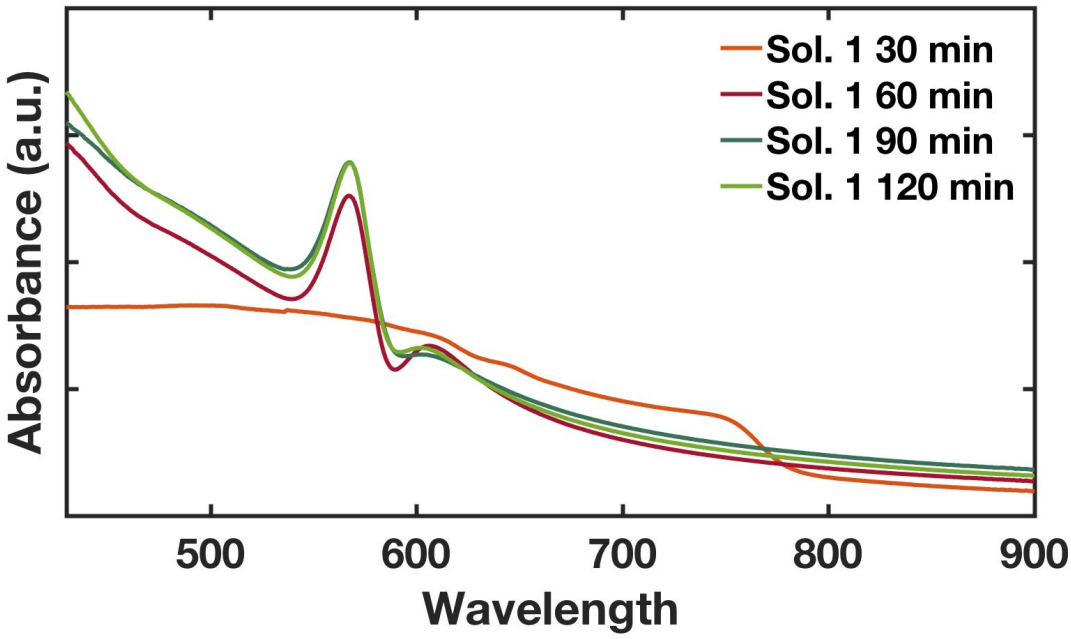

Figure 5.41: UV/Vis of film made using 2:1 ratio of MAI:BAI with a 1 M ratio of MAI

The solution used for these films was the same concentration used previously. As expected, the results were the same.

The higher concentration Sol 2 behaves in a similar way to Sol 1. The films first turned black at 30 minutes and then turned into the final pink color as time went on. Similarly, the UV/Vis for Sol 2 shows the same pattern as the UV/Vis for Sol 1. Further, Sol 3 also shows the same pattern even though the films made were not as uniform as films from Sol 1 and Sol 2. The difference for Sol 3 was that the UV/Vis peaks are not as prominent as Sol 1 and Sol 2, but this is attributed to the poor film quality.

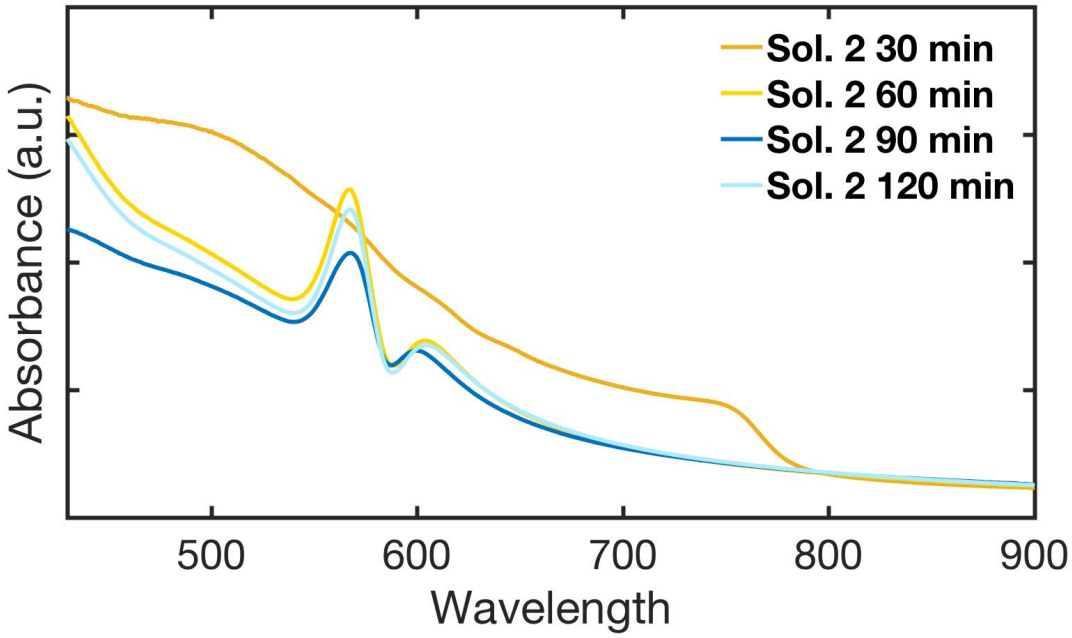

Figure 5.43: UV/Vis of film made using 2:1 ratio of MAI:BAI with a 1.5 M ratio of MAI

The films made using Sol 2 behave the same as the films made using Sol 1.

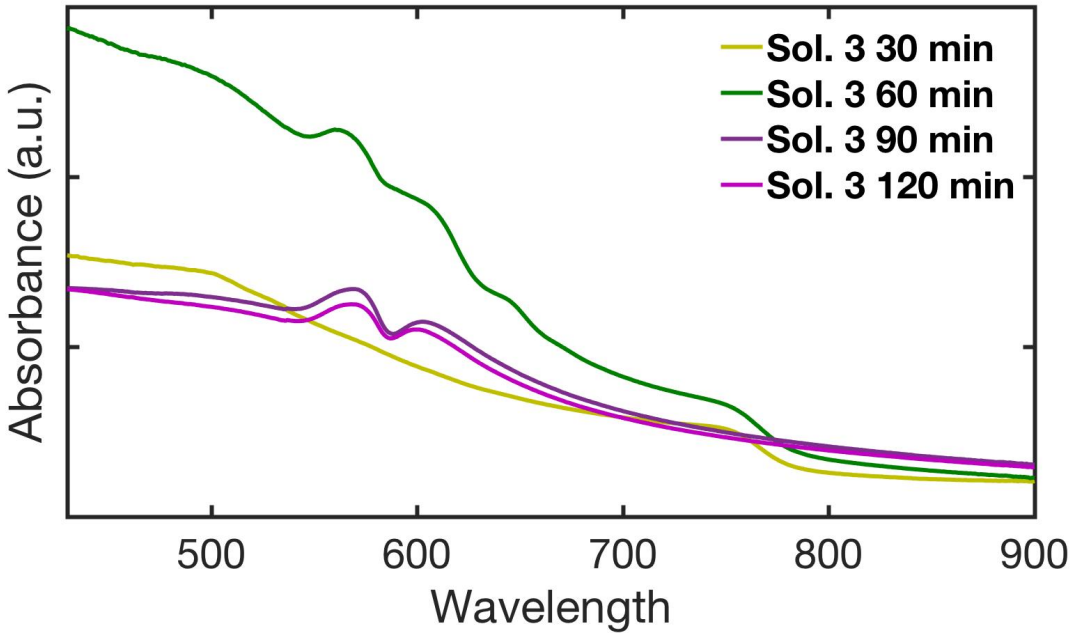

Figure 5.42: UV/Vis of film made using 2:1 ratio of MAI:BAI with a 2 M ratio of MAI

The films made using Sol 3 show the same peaks as the films made using Sol 1 and Sol 2 even though the film quality for Sol 3 was poor.

Overall, this small study reinforces the conclusion that the ratio of MAI:BAI is the most important factor when using the melt infiltration method. The concentration and thickness of the initial precursor films can change the time needed to fully react a film but do little to change the final layer number.

Conclusion

Controlling the layer number of a mixed perovskite film is not an easy task. Many spin coating methods give a mixed layer number film. The experiments in this chapter hope to give some insight into how to better control the formation of mixed cation perovskites. By controlling the ratio of MAI:BAI, I was able to make films that more closely resembled single layer number films, and with more effort and practice, this approach could be used to make single crystal structure films of mixed cation perovskites.

REFERENCES

(1) Leijtens, T.; Eperon, G. E.; Noel, N. K.; Habisreutinger, S. N.; Petrozza, A.; Snaith, H. J. Stability of Metal Halide Perovskite Solar Cells. *Adv. Energy Mater.* **2015**, *5* (20), 1–23.

(2) mindat.org and the Hudson Institute of Mineralogy. Perovskite.

(3) Green, M. A.; Ho-Baillie, A. Perovskite Solar Cells: The Birth of a New Era in Photovoltaics. *ACS Energy Lett.* **2017**, *2* (4), 822–830.

(4) Li, W.; Wang, Z.; Deschler, F.; Gao, S.; Friend, R. H.; Cheetham, A. K. Chemically Diverse and Multifunctional Hybrid Organic–inorganic Perovskites. *Nat. Rev. Mater.* **2017**, *2*, 16099.

(5) Mitzi, D. B. Synthesis, Crystal Structure, and Optical and Thermal Properties of ($C_4H_9NH_3)_2MI_4$ (M = Ge, Sn, Pb). *Chem. Mater.* **1996**, *8* (3), 791–800.

(6) Koh, T. M.; Thirumal, K.; Soo, S.; Mathews, N. Multidimensional Perovskites : A Mixed Cation Approach Towards Ambient Stable and Tunable Perovskite Photovoltaics. **2016**, 2541–2558.

(7) Tsai, H.; Nie, W.; Blancon, J.-C.; Stoumpos, C. C.; Asadpour, R.; Harutyunyan, B.; Neukirch, A. J.; Verduzco, R.; Crochet, J. J.; Tretiak, S.; Pedesseau, L.; Even, J.; Alam, M. A.; Gupta, G.; Lou, J.; Ajayan, P. M.; Bedzyk, M. J.; Kanatzidis, M. G.; Mohite, A. D. High-Efficiency Two-Dimensional Ruddlesden–Popper Perovskite Solar Cells. *Nature* **2016**, *536* (7616), 312–316.

(8) Hong, K.; Le, Q. Van; Kim, S. Y.; Jang, H. W. Low-Dimensional Halide Perovskites: Review and Issues. *J. Mater. Chem. C* **2018**.

(9) Kandjani, S. A.; Mirershadi, S.; Nikniaz, A. Inorganic–Organic Perovskite Solar Cells. In *Solar Cells - New Approaches and Reviews*; InTech, 2015; p 450.

(10) Eze, V. O.; Lei, B.; Mori, T. Air-Assisted Flow and Two-Step Spin-Coating for Highly Efficient CH 3 NH 3 PbI 3 Perovskite Solar Cells. *Jpn. J. Appl. Phys.* **2016**, *55* (2S), 02BF08.

(11) Liu, M.; Johnston, M. B.; Snaith, H. J. Efficient Planar Heterojunction Perovskite Solar Cells by Vapour Deposition. *Nature* **2013**, *501* (7467), 395–398.

(12) Mitzi, D. B.; Prikas, M. T.; Chondroudis, K. Thin Film Deposition of Organic−Inorganic

Hybrid Materials Using a Single Source Thermal Ablation Technique. *Chem. Mater.* **1999**, *11* (3), 542–544.

(13) Li, T.; Dunlap-shohl, W. A.; Han, Q.; Mitzi, D. B. Melt Processing of Hybrid Organic – Inorganic Lead Iodide Layered Perovskites. **2017**.

(14) Blancon, J. C.; Tsai, H.; Nie, W.; Stoumpos, C. C.; Pedesseau, L.; Katan, C.; Kepenekian, M.; Soe, C. M. M.; Appavoo, K.; Sfeir, M. Y.; Tretiak, S.; Ajayan, P. M.; Kanatzidis, M. G.; Even, J.; Crochet, J. J.; Mohite, A. D. Extremely Efficient Internal Exciton Dissociation through Edge States in Layered 2D Perovskites. *Science (80-.).* **2017**, *355* (6331), 1288–1292.

(15) Stoumpos, C. C.; Cao, D. H.; Clark, D. J.; Young, J.; Rondinelli, J. M.; Jang, J. I.; Hupp, J. T.; Kanatzidis, M. G. Ruddlesden-Popper Hybrid Lead Iodide Perovskite 2D Homologous Semiconductors. *Chem. Mater.* **2016**, *28* (8), 2852–2867.

(16) Green, M. A.; Ho-Baillie, A.; Snaith, H. J. The Emergence of Perovskite Solar Cells. *Nat. Photonics* **2014**, *8* (7), 506–514.

(17) Saparov, B.; Mitzi, D. B. Organic-Inorganic Perovskites: Structural Versatility for Functional Materials Design. *Chem. Rev.* **2016**, *116* (7), 4558–4596.

(18) Mitzi, D. B.; Chondroudis, K.; Kagan, C. R. Organic-Inorganic Electronics. *IBM J. Res. Dev.* **2001**, *45* (1), 29–45.

(19) Bi, D.; El-Zohry, A. M.; Hagfeldt, A.; Boschloo, G. Unraveling the Effect of PbI_2 Concentration on Charge Recombination Kinetics in Perovskite Solar Cells. *ACS Photonics* **2015**, *2* (5), 589–594.

Chapter 6: Conclusion

Introduction

This dissertation chronicles the journey I have taken over the past 5 years. What began as a study on 2D materials shifted into a study on 2D perovskites, with many ups and downs along the way. This journey did not just include doing research. Over the past 5 years I moved to a completely new area of the country, got married, traveled around the world, watched UNC lose and win a national basketball championship, did an internship at Cree and made many great friends. All aspects of this journey have helped prepare me for my future as a researcher and engineer. Through these experiments, I have learned numerous analytical techniques. I have learned that sometimes experiments just don't work but that doesn't mean to stop trying. But most importantly, I have learned how to think critically and how to learn new things. The most important take away I have from getting a Ph.D. is it helped me to learn how to learn about things I have never even heard of. I have had to teach myself how to used new equipment and new programs. I have had to shift into many different areas of chemistry and learn about new materials each time. Even if the research I completed during graduate school is forgotten, I will always have the lessons I learned to guide me through life.

Overall Conclusions

But what is a conclusion chapter without a summer of the major conclusions of the past four chapter. Following, I will lay out below the major findings of this dissertation.

MoS_2 Functionalization

Chapters 2 and 3 tell the story of a method to functionalize MoS_2. This homemade CVD method is easy to use and very versatile. I presented here how to functionalize MoS_2 with both APTMS and OTS monolayers but I believe that many other silane molecules could be used. The thickness of the monolayer is able to be tuned by changing the time and the pressure. The functionalization method does not harm the structure of the MoS_2. Also, the results shown point towards a covalent linkage between the APTMS monolayer and the MoS_2 through a Si-O-Mo bond. This bond formation can occur because of sulfur vacancies in the MoS_2. Overall, future work should include experimenting with other silane molecules and studying how the functionalization effects the transistor behavior of MoS_2.

OFET Fabrication

The preparation of films of the TES-ADT derivatives was not easy. But, after much effort, films of each were able to be prepared by either spin-coating or blade-coating. Overall, all derivatives (OO-ADT, HA-ADT, and BT-ADT) but the OT-ADT showed signs of future use in OFETs. Further, the HA-ADT mobility greatly improved when blade coating was used. Future work should include looking at how blade coating effects the mobility of the other derivatives to see if there is any improvement.

Melt infiltration of 2D Mixed Perovskites

There is still so much research to be done on perovskites. There seems to be an almost unlimited amount of different molecules that can be used to make perovskite. The melt infiltration method presented here gives a method to make perovskite that could potentially be used with many different molecules. Since the melt infiltration process causes the perovskite to

form very slowly, it gives a way to look at the perovskite formation over time. For example, it shows that the n=2 mixed perovskite first forms the 3D component and then the final 2D film. Future work on this project should include tuning the conditions to give films that are solely made up of n=3 or n=4 mixed perovskites.

The End

Thank you for reading. I hope you have a nice day!